ORIGIN, FATE, AND TRANSPORT OF DISSOLVED ORGANIC GASES IN BEDROCK AQUITARDS; SASKATCHEWAN, CANADA

A Thesis Submitted to the College of

Graduate Studies and Research

in Partial Fulfillment of the Requirements

for the Degree of Masters of Science

in the Department of Geology

University of Saskatchewan

Saskatoon, Canada

By

Adrienne Leigh Bangsund

Permission to Use Postgraduate Thesis

In presenting this thesis in partial fulfillment of the requirements for a Postgraduate degree from the University of Saskatchewan, I agree that the Libraries of this University may make it freely available for inspection. I further agree that permission for copying of this thesis in any manner, in whole or in part, for scholarly purposes may be granted by the professor or professors who supervised my thesis work or, in their absence, by the Head of the Department or the Dean of the College in which my thesis work was done. It is understood that any copying or publication or use of this thesis or parts thereof for financial gain shall not be allowed without my written permission. It is also understood that due recognition shall be given to me and to the University of Saskatchewan in any scholarly use which may be made of any material in my thesis.

DISCLAIMER

Reference in this thesis to any specific commercial products, process, or service by trade name, trademark, manufacturer, or otherwise, does not constitute or imply its endorsement, recommendation, or favoring by the University of Saskatchewan. The views and opinions of the author expressed herein do not state or reflect those of the University of Saskatchewan, and shall not be used for advertising or product endorsement purposes.

Requests for permission to copy or to make other uses of materials in this thesis in whole or part should be addressed to:

Head of the Department of Geological Sciences
114 Science Place
University of Saskatchewan
Saskatoon, Saskatchewan S7N 5E2 Canada

OR

Dean
College of Graduate Studies and Research
University of Saskatchewan
107 Administration Place
Saskatoon, Saskatchewan S7N 5A2 Canada

ABSTRACT

Dissolved gases including methane (CH_4), ethane (C_2H_6), and propane (C_3H_8) are natural components of groundwater. Knowledge of the origin, distribution, and fate of these gases is crucial for assessing the impacts of oil and gas development on shallow groundwater systems. This study provides one of the first suites of baseline profiles of dissolved CH_4, C_2H_6, and C_3H_8 through a bedrock aquitard and provides insight into their origin (using carbon (C) and hydrogen (H) stable isotopes), fate, and transport. Core samples were collected over 240 m of continuously-cored Quaternary-aged Battleford till (80 m) and underlying Cretaceous units (160 m) from an aquitard research site 140 km southwest of Saskatoon, SK, Canada. Physical properties (moisture content, density, grain size and carbon forms), stable H and oxygen isotopes of pore water (δ^2H and $\delta^{18}O$), pore water chemistry, and gas concentrations (CH_4, C_2H_6, and C_3H_8) and their stable C and H isotope values ($\delta^{13}C_{CH4}$, δ^2H_{CH4}, $\delta^{13}C_{C2H6}$, and $\delta^{13}C_{C3H8}$) were measured on these cores. Results of physical parameters and δ^2H and $\delta^{18}O$ measurements agreed with previously reported data. The high-resolution profiles extend existing data sets into the Ardkenneth aquifer, the upper layer of which contains high percentages of sand and abrupt increases in values of δ^2H, and chloride (Cl^-) and CH_4 concentrations; these peaks were likely introduced laterally from an alternate source. One-dimensional numerical modeling of the δ^2H confirms that transport across the till-shale interface occurred over ~20-30 ka Before Present (BP), and from the base of the oxidized till (~5 m below ground surface, BGS) into the till over ~10 ka BP. CH_4 concentrations through the till were below detection limit (BDL; < 5 ppmv); concentrations increase from 0.04 mg L^{-1} below the till-clay interface (at ~85 m BGS), to 49 mg L^{-1} at 240 m BGS. One-dimensional numerical modeling of the CH_4 concentration profile suggests that the timing of deposition of the till cannot be constrained using CH_4, and that a geochemical reaction impacts its transport to ~30 m below the till-clay interface. Concentrations of C_2H_6 and C_3H_8 are minor throughout the profile. Depleted ^{13}C and ^2H values of CH_4, ranging between –52 and –92‰ VPDB and –173 to –269‰ VSMOW, respectively, and the ^{13}C-depleted nature of $\delta^{13}C_{C2H6}$ (–45 to –85‰ VPDB) support a bacterial origin for the gases.

ACKNOWLEDGMENTS

I would like to thank the numerous academics that helped me in various ways to produce an outstanding data set. I am sincerely appreciative for all of those contributions. I would like to thank my supervisor, Dr. Jim Hendry, for always nudging me towards the scientific truth without giving me the answer, and for providing me with remarkable research opportunities. My co-supervisor Dr. Lee Barbour assisted in guiding me towards making this work the best that I could. It was a privilege to be mentored by these two individuals. I am thankful to the University of Saskatchewan's College of Graduate Studies and Research and the Government of Saskatchewan for scholarships. I would also like to thank the one-time landowners who donated the King site for research purposes.

I could not have persevered through this endeavour without the support and encouragement of many people. Tim Prokopiuk, Kevin Ansdell, and Joseph Essilfie-Dughan mentored me on many occasions with great kindness. I am thankful for the support of my family; my parents for helping out in any way they could; my sister for creating a special place in her own family for me and for always listening, and my brother for coming to my rescue whenever the need arose. I am grateful for the many friends and memories I made in the Geology Department. I am particularly thankful for my childhood friend Bri, for helping me solve problems outside the realm of academia, and Marjolaine, who was inspirational as she persevered through her own academic journey.

TABLE OF CONTENTS

LIST OF TABLES

LIST OF FIGURES

CHAPTER 1

INTRODUCTION

Widespread development of unconventional oil and gas reservoirs is increasing investigation into the natural distribution and controls on the transport of dissolved gases such as CH_4 and carbon dioxide (CO_2) in shallow groundwater systems (Jackson et al., 2013). Natural gases including CH_4, C_2H_6 and C_3H_8 are commonly indigenous components of groundwater. However, fugitive natural gases in the subsurface (e.g. leaking from wellbores) pose risks of contaminating shallow aquifers, damaging surrounding farmland, and explosion hazards if concentrated in poorly ventilated areas (Edwards, 1991; Rowe and Muehlenbachs, 1999; Osborn et al., 2011). Understanding the origins and transport mechanisms of, and geochemical controls on, dissolved gases in the subsurface is important for characterizing migration patterns, mitigating potential hazards, and assessing the impacts of oil and gas development.

Despite the prevalence of natural gases in groundwater, knowledge of their baseline concentrations in shallow groundwater systems is lacking, as is research on their transport and fate (Osborn et al., 2011; Vidic et al., 2013; Jackson et al., 2013). Measuring bulk gas compositions and their associated isotopes with depth prior to oil and gas development creates profiles of baseline conditions (Szatkowski et al., 2001). Gas compositional and isotopic profiles can provide insight into the origin and transport processes of gases and the fluids they are in, and the maturity of the gas, (Goth, 1985; Prinzhofer et al., 2009; Clark et al., 2015) as well as geochemical reactions controlling the fate of the gases (e.g. bacterial production or consumption) (Bernard et al., 1978; Claypool and Kaplan, 1974; Riedinger et al., 2010). Comparative relationships between the stable isotope ratios ($\delta^{13}C_{CH4}$, $\delta^{2}H_{CH4}$, $\delta^{13}C_{C2H6}$, $\delta^{13}C_{C3H8}$) of natural gases, the formation water ($\delta^{2}H_{H2O}$), and/or compositional ratios (e.g. CH_4/higher chain hydrocarbons) are indicators of various characteristics of gases: the origin (Schoell, 1983; Whiticar et al., 1986; Floodgate and Judd, 1992; Whiticar, 1999), the diagenetic stage of the sediments and the maturity of a gas (Prinzhofer and Huc, 1995; Whiticar, 1999), and mixing of thermogenic and bacterial gases (Prinzhofer and Huc, 1995; Prinzhofer and Pernaton, 1997).

The measurement of dissolved gases and their isotopes offer great potential in characterizing geochemical conditions in shallow groundwater systems.

Diffusion is a known transport mechanism of dissolved gases in the pore waters of low hydraulic conductivity (*K*) sediments (i.e. aquitards) (Leythauser et al., 1982; Jacops et al., 2013). The transport of CH_4 in groundwater, however, may be complicated by microbial consumption, or production via various pathways (Mechalas, 1974; Martens and Berner, 1977; Prinzhofer et al., 2009). Concentration-depth diffusive profiles of dissolved gases (predominantly CH_4 and CO_2) in shallow soils and soft marine and freshwater sediments (< 16 m) are prevalent in the literature. These profiles are used to identify origin of the gases, calculate rates and contributions of production or consumption, define geochemical boundaries within a system (e.g. depth of atmospheric penetration, sulphate reducing zone), determine diffusion coefficients, calculate fluxes, and explore effects of transport processes (e.g. diffusion-induced isotopic fractionation) (Reeburgh and Heggie, 1974; Barnes and Goldberg, 1976; Martens and Berner, 1977; Bernard et al., 1978; Bernard, 1979; Martens, 1982; Goth, 1985; Prinzhofer and Pernaton, 1997; Borowski et al., 1996; Kruse et al., 1996). In contrast, profiles of CH_4 in aquitards are few, are of low-resolution, and profiles of higher chain hydrocarbons (e.g. C_2H_6, C_3H_8; denoted as C_{2+}) are extremely rare (Simpkins and Parkin, 1993; Keller, 1991; Prinzhofer et al., 2009).

In aquitards, conservative groundwater constituents, such as the stable isotopes of pore waters (δ^2H and $\delta^{18}O$) and chloride (Cl^-), are transported by diffusion. Vertical profiles of these constituents are used to define the paleo-hydrogeology of sediments, estimate groundwater age, interpret climate records, and as the basis for solute transport modeling (Desaulniers et al., 1981; Remenda et al., 1994; Hendry and Wassenaar, 1999; Koroleva et al., 2011; Hendry et al., 2013). Generating and interpreting high-resolution vertical profiles of dissolved gases in conjunction with conservative groundwater constituents would provide insight into their origin, transport, and fate in the subsurface.

Baseline data of dissolved gas concentrations and their isotopic values in shallow groundwater systems are scarce in the literature, despite the amount of information that is extracted from their measurement. The Cretaceous clay-Quaternary till aquitard system examined in this study represents a common juxtaposition of sediments across much of southern Saskatchewan; this provides the opportunity to correlate transport mechanisms and geochemical

conditions over a large geographic region (Hendry et al., 2011, 2014, 2016 (b)). The pore waters and sediments within this aquitard system are well-characterized at the study site (referred to as the King site), located approximately 140 km southwest of Saskatoon, Saskatchewan, Canada (Figure 1.1; UTM coordinates: 13N 365972E 5663279N). Physical properties of the sediments and pore water chemistry data previously collected at the King site and numerical modeling of that data were used to confirm the results of this study.

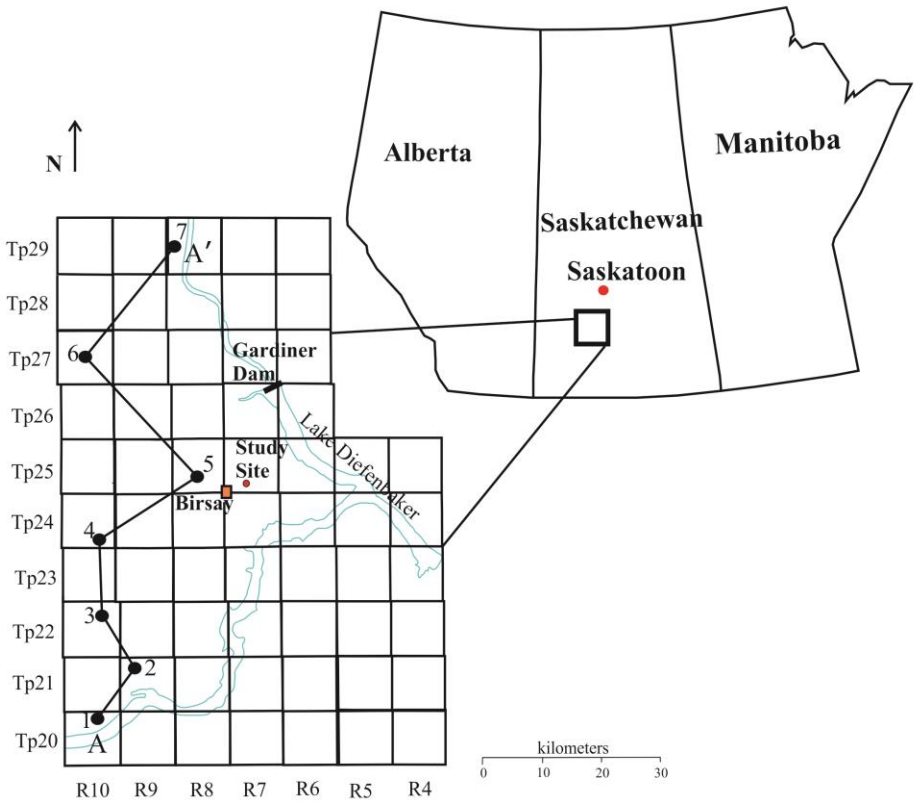

Figure 1.1. Geographic location of the King study site (modified after Shaw, 1997). Figure 4.1 shows the stratigraphic cross section of line A–A'.

The objectives of this study were to identify the origin, mode of transport, and fate of dissolved gases in the aquitards at the study site. This was achieved by measuring a number of physical parameters of the sediments, characterizing the distribution of the stable isotopes of pore waters (δ^2H and $\delta^{18}O$), dissolved chloride (Cl^-) and CH_4, C_2H_6, C_3H_8 and their stable

isotopes with depth. The timing of development of the δ^2H-depth profile was estimated using one-dimensional numerical modeling. Geochemical controls on the transport of CH_4 were investigated with one-dimensional numerical modeling.

CHAPTER 2
LITERATURE REVIEW

2.1 Principles of solute transport

Three main physical processes govern the transport of dissolved solutes in groundwater: advection, mechanical dispersion, and diffusion. Advection is movement of solutes at the same velocity as the groundwater. In one dimension, advection is determined by (Ingebritsen and Sanford, 1999):

$$\frac{\partial C}{\partial t} = -v\frac{\partial C}{\partial x} \quad \text{(Eq. 2.1)}$$

where C is concentration (mass volume^{-1}), t is time, v is average linear groundwater velocity (length time^{-1}), and x is distance (length). The natural heterogeneities in sediments cause local spatial variations in v. This results in spreading of solutes driven by advection, referred to as mechanical dispersion (Ingebritsen and Sanford, 1999).

Solute transport via diffusion is driven by concentration gradients and occurs under low groundwater velocities. By diffusion, solutes travel from regions of high concentration to those of low concentration (Ingebritsen and Sanford, 1999). The diffusive mass flux rate (J_d; moles of solute length^{-2} time^{-1}) of mass in water is described by Fick's first law as (Hendry et al., 2011):

$$J_d = -n_e D_e \frac{\partial C}{\partial x} \quad \text{(Eq. 2.2)}$$

where D_e is the effective diffusion coefficient of the solute (length^2 time^{-1}), n_e is effective porosity (unitless) and C and x are as previously defined. The negative sign indicates that the mass flux travels in the opposite direction of the concentration gradient. The D_e of a solute takes into account transport within sediment, which is complicated by tortuous pathways caused by the porosity of the medium. Measured D_e and the diffusion coefficient of the solute in water (D_w) can be used to calculate the apparent tortuosity factor (τ_a) of sediment by (Shackelford and Daniel, 1991):

$$D_e = D_w \tau_a \quad \text{(Eq. 2.3)}$$

Mechanical dispersion and diffusion can be combined into one coefficient, *D*, the dispersion coefficient (Ingebritsen and Sanford, 1999). *D* is defined by (Freeze and Cherry, 1979):

$$D = D_e + \alpha v \quad \text{(Eq. 2.4)}$$

where α is dispersivity (length) and $v = q/n_e$ (q = Darcy velocity (volume time^{-1} area^{-1}). In hydrogeologic systems in which diffusion is the dominant mode of solute transport, *v* is negligible, and *D* simply equals D_e (Hendry and Wassenaar, 1999). Several studies conclude that diffusion is the dominant mode of solute transport in the hydrogeologic system at the King site (Shaw and Hendry, 1998; Hendry and Wassenaar, 1999; Wassenaar and Hendry, 1999; Hendry et al., 2011).

The following partial differential equation is applicable to one-dimensional modeling of the transport of a non-reactive solute through a homogeneous saturated porous media (Gillham and Cherry, 1982):

$$\frac{\partial C}{\partial t} = D_e \frac{\partial^2 C}{\partial x^2} - v \frac{\partial C}{\partial x} \quad \text{(Eq. 2.5)}$$

where the parameters D_e, C, x, v, and t are as previously defined. Eq. 2.5 is modified to include a term for transport of a reactive solute (Gillham and Cherry, 1982):

$$\frac{\partial C}{\partial t} = D_e \frac{\partial^2 C}{\partial x^2} - v \frac{\partial C}{\partial x} - R \quad \text{(Eq. 2.6)}$$

The *R* term relates to the process causing the change in concentration of the solute (e.g. production, consumption or sorption). The form of *R* is dependent on the process involved, but it is the rate at which that process occurs (mass volume^{-1} time^{-1}) (Gillham and Cherry, 1982).

2.2 Natural groundwater tracers

Non-reactive solutes commonly measured for interpretation of the paleo-hydrogeology of groundwaters include the stable isotopes of pore water (δ^2H and δ^{18}O), dissolved halogens (e.g. Cl^- and bromide (Br^-)), and noble gases (e.g. helium) (Hendry et al., 2000; Hendry and Wassenaar, 2000; Hendry et al., 2005; Hendry et al., 2011; Koroleva et al., 2011; Mazurek et al., 2011; Hendry et al., 2013). Conservative solutes are useful for tracing the hydrogeologic history of groundwater because they do not react with the surrounding sediments or other components of the groundwater (Desaulniers, 1981). The transport mechanisms of numerous conservative solutes have been investigated at the King site; to facilitate integration of existing data sets, this study will focus on δ^2H and Cl^-.

While non-reactive, stable isotopes are subject to processes that impact their composition by way of fractionation. Kinetic isotope effects occur due to the difference in the translational velocities (v_t) of lighter (e.g. ^{16}O) and heavier (e.g. ^{18}O) isotopes. This is the result of the difference in mass (m); the kinetic energy ($K.E.$) of a molecule is the same regardless of the isotopes in the molecule. By the following equation (Sharp, 2007):

$$K.E. = \frac{1}{2}mv_t^2 \quad \text{(Eq. 2.7)}$$

as mass increases, v_t must decrease to maintain $K.E.$ In response, lighter molecules have greater v_t and travel preferentially during diffusive or evaporative processes over heavy molecules. This fractionation leaves the remaining substance enriched in the heavier isotope (Sharp, 2007). Biologically-mediated processes cause similar kinetic fractionations. Bonds of lighter isotopes are easier to break and doing so is more energy efficient, therefore light molecules are preferentially involved in, for example, production or consumption reactions. Biological reactions leave the remaining substrate or residual gas enriched in the heavier isotopes, and the products are isotopically lighter than the substrate or the source gas (Kendall and Doctor, 2005). Other processes that cause changes in isotopic compositions are known as equilibrium fractionation effects. These occur in closed systems, between two phases (e.g. liquid-solid), and are temperature dependent (Dansgaard, 1964).

Fractionation effects impart distinct signatures on molecules, and therefore offer insight into the origin, recharge rates, transport, and paleo-hydrogeology of pore waters in regionally extensive aquitard systems (Desaulniers et al., 1981; Fortin et al., 1991; Remenda et al., 1994; Kendall and Caldwell, 1998; Hendry and Wassenaar, 1999, 2009; Hendry and Woodbury, 2007; Stumpp and Hendry, 2012; Hendry et al., 2011, 2013). Fractionation processes affect isotopes of liquids, gases, and solids (Sharp, 2007).

The standard method of reporting isotope values is in delta (δ) notation (Sharp, 2007):

$$\delta = \left(\frac{R_x - R_{std}}{R_{std}}\right) \times 1000 \quad \text{(Eq. 2.8)}$$

In this notation, R represents the ratios of the heavy isotopes (e.g. ^{18}O) to the light isotopes (e.g. ^{16}O) in the sample (x) and the standard (std). The ratio for H isotopes is $^{2}H/^{1}H$, and is $^{13}C/^{12}C$ for C isotopes. The standards are internationally recognized values and are referred to as VSMOW (Vienna Standard Mean Ocean Water) for H and O isotopes and VPDB (Vienna Pee Dee

Belemnite) for C isotopes. Isotopic values are given in parts per thousand, or per mil (‰) (Sharp, 2007).

Cl^- concentrations in pore waters are useful groundwater tracers due to the conservative nature of the ion; Cl^- does not adsorb to or react with sediments, and is only a minor component in common minerals (Hendry et al., 2000; Patriarche et al., 2004). Concentrations of this ion can be used to determine its mode of transport and the origin of pore waters, and Cl^--depth profiles are commonly used as a basis for transport modeling (Hendry et al., 2000; Koroleva et al., 2011 Mazurek et al., 2011).

2.3 Dissolved organic gases in groundwater

2.3.1 Origins of organic gases

Gases in the subsurface originate from a number of processes: degradation of organic matter, either by microbes or thermal influences, volcanic activity, hydrothermal vents, or mantle emissions. The bulk composition of a gas relates to the pathway of origin, but may include primarily CH_4 with CO_2, C_2H_6, C_3H_8 and higher-chain hydrocarbons, and hydrogen sulfide (H_2S) in lesser quantities (Claypool and Kaplan, 1974; Floodgate and Judd, 1992). This study will focus on quantifying and characterizing the distribution and origin of CH_4, C_2H_6, and C_3H_8, and the transport and fate of CH_4.

In the subsurface, CH_4 is the product of either biogenic or abiogenic processes, and can be further categorized as bacterial or thermogenic in origin (Schoell, 1988; Whiticar, 1999). Bacterial CH_4 is produced by one of two primary pathways:

1) CO_2 reduction (Schoell, 1980):

$$CO_2 + 4H_2 \rightarrow CH_4 + 2H_2O \qquad \text{(Eq. 2.9)}$$

where CO_2 reacts with molecular hydrogen (H_2), producing one CH_4 and two water molecules (H_2O). All four of the hydrogen atoms in the CH_4 molecule are sourced from the surrounding water (Whiticar et al., 1986).

2) Acetate fermentation (Whiticar et al, 1986):

$$CH_3COOH \rightarrow CH_4 + CO_2 \qquad \text{(Eq. 2.10)}$$

In this case, one entire methyl group (CH_3) is used for the CH_4 from the hydrogen acetate (CH_3COOH) and the additional hydrogen atom for the CH_4 molecule is sourced from the surrounding water (Whiticar et al., 1986). The dominant pathway is dependent on the

surrounding environment; acetate fermentation occurs primarily in freshwater while CO_2 reduction prevails in marine sediments (Whiticar, 1999). The pathway is partially determined by the bacterial community in the environment. Bacteria that produce methane, methanogens, are out-competed for substrates by sulfate-reducing bacteria (SRB). SRB use the same substrates for energy as methanogens do, but do so more efficiently, and methane production is restricted to depths below which sulfate is no longer available. Methanogens cannot compete with SRB for available acetate in marine settings, so in this environment, CO_2 reduction is the primary pathway of CH_4 production. In freshwater environments low in sulfate, CH_4 production by acetate fermentation dominates (Whiticar, 1999). The presence of CH_4 in shallow sediments marks the zone of anaerobic activity, typically observed below the sulfate-reducing zone (Claypool and Kaplan, 1974). Both pathways of CH_4 production can occur concurrently, and in a multitude of anoxic environments (Schoell, 1980; Whiticar et al., 1986).

The decomposition of organic matter at high temperatures results in thermogenic gases (Schoell, 1988). These gases may develop in conjunction with oil, or as a result of post-oil-formation processes (Schoell, 1983). Thermogenic processes will produce greater concentrations of C_{2+} gases than bacterial pathways (Schoell, 1983; Taylor et al., 2000). Few studies report bacterial production of ethane and propane in conjunction with bacterial methane production in shallow groundwater environments (Oremland, 1981; Oremland et al., 1988; Prinzhofer and Huc, 1995; Taylor et al., 2000; Schloemer et al., 2016).

Abiogenic CH_4 is formed by inorganic processes and is rare, predominantly found in mid-ocean ridge-type environments (Schoell, 1988; Floodgate and Judd, 1992). Most CO_2 in the subsurface originates from the decay of organic matter and plant root respiration in the soil zone; minor contributions are produced by the reduction of sulfate and nitrate and dissolution of carbonates (Reeburgh and Heggie, 1974; Freeze and Cherry, 1979; Keller, 1991).

2.3.2 Characterizing the origin of organic gases

Key to the genetic classification of natural gases are the $\delta^{13}C$ and $\delta^{2}H$ isotope values. Figure 2.1 shows the wide range $\delta^{13}C$ has for many carbonaceous materials (Fuex, 1977). Compared to the higher-chain hydrocarbons, CH_4 spans the broadest range of values. Figure 2.1 defines ranges of $\delta^{13}C$ values for different types of CH_4 and while some of the categories overlap, shallow, bacterial CH_4 and deep-sourced CH_4 are distinct.

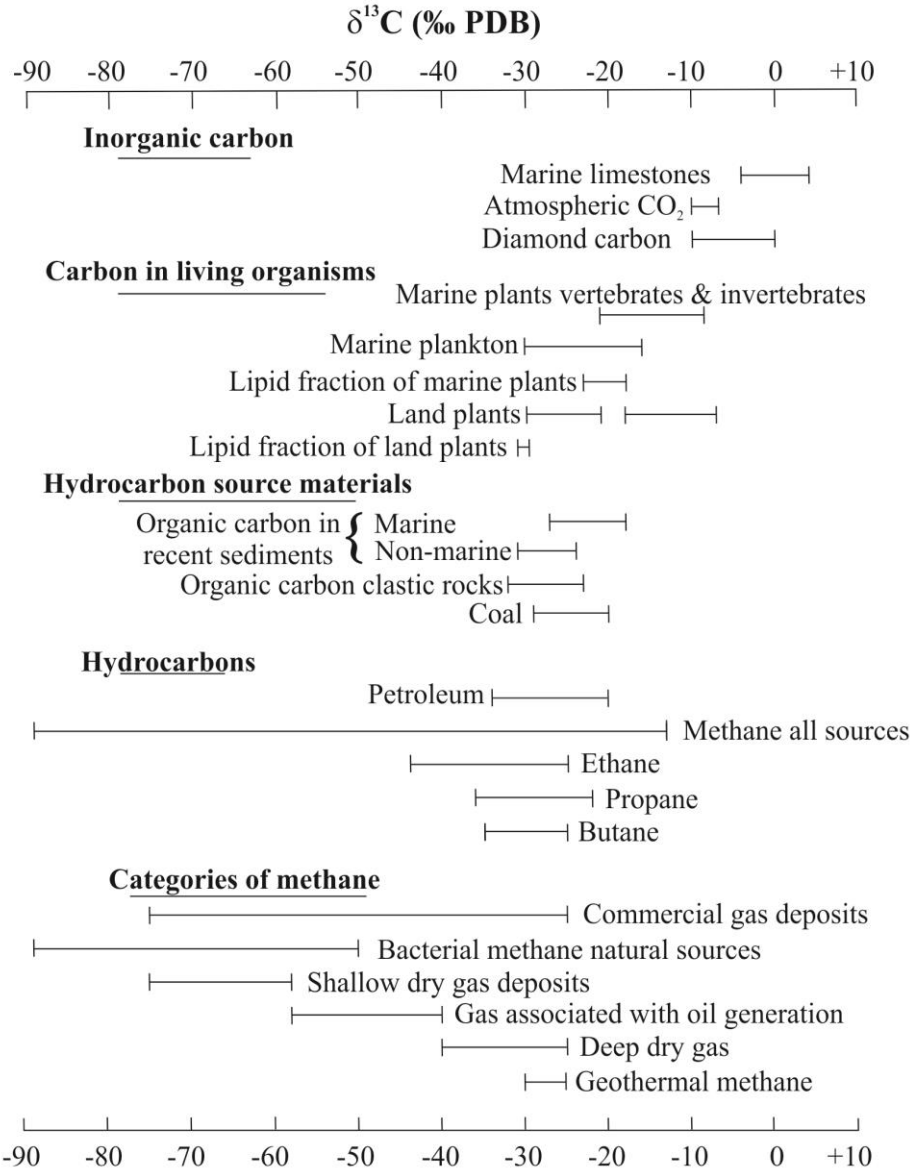

Figure 2.1. Range of $\delta^{13}C$ values of numerous carbonaceous materials (‰ PDB) (after Fuex, 1977).

Akin to the isotopes of pore waters, the isotopes of organic gases are susceptible to kinetic isotope effects (Kotelnikova, 2002). These effects impart distinct signatures and enable determination of source, production pathway, and transport processes. The use of isotopes for genetic characterization of natural gases is based on the assumption that isotopic signatures are a result of formational processes (Schoell, 1983). However, mixing, diffusive, and bacterial

processes reportedly induce fractionation that can alter the original signature of a gas (Coleman et al., 1981; Prinzhofer and Pernaton, 1997). As described previously, molecules containing lighter isotopes (e.g. ^{12}C) travel more readily than those with the heavier isotopes (e.g. ^{13}C), leaving the remaining gas isotopically heavier than the source (Whiticar, 1999). This effect is observed in diffusion-dominated systems, as CH_4 migrates away from its source, it becomes isotopically lighter (Stahl, 1977; Prinzhofer and Huc, 1995).

The $\delta^{13}C_{CH4}$ of a gas is reflective of the environment in which it was produced, the source of organic matter, and the maturity of the gas (Schoell, 1980; Whiticar et al., 1986; Chanton et al., 2004). Differentiating between thermogenic and bacterial CH_4 can be done using ^{13}C isotopes; the former is typically enriched in ^{13}C with respect to the latter (Whiticar, 1999). An isotopic boundary delineates CH_4 produced in marine or freshwater environments; $\delta^{13}C_{CH4}$ produced in freshwater is > –60‰ while CH_4 of marine origin is more depleted in ^{13}C (Whiticar et al., 1986). The type of organic matter from which CH_4 is derived is also reflected in $\delta^{13}C_{CH4}$ values. CH_4 produced from decaying C_3 plant matter is lighter (more positive) compared to that produced by decaying C_4 plants (Chanton et al., 2004).

During production, the H in the CH_4 molecules may be sourced from either the decomposing organic matter or the surrounding water (Schoell, 1980). The transfer of H which occurs in Equations 2.9 and 2.10 causes fractionation of the H isotopes, and therefore δ^2H_{CH4} is useful for distinguishing between CH_4 produced in freshwater or marine environments and production pathway (Whiticar, 1999). CH_4 produced in freshwater has very low δ^2H_{CH4} values, nearing –300‰ SMOW and marine δ^2H_{CH4} is heavier, closer to –190‰ SMOW (Whiticar et al., 1986). This distinction is owed to the difference in δ^2H values of oceanic versus continental waters (Schoell, 1983).

The relationship between $\delta^{13}C_{CH4}$ and δ^2H_{CH4} establishes characteristic regions of the production pathways and origin of CH_4 (Figure 2.2; Schoell, 1980; Whiticar et al., 1986). This relationship also estimates the maturity of a gas; both δ^2H_{CH4} and $\delta^{13}C_{CH4}$ concentrations increase with increasing maturity (Schoell, 1980). Thermogenic CH_4 has heavier δ^2H (-75 to -105‰) due to the high temperatures of the surrounding water in which it is produced.

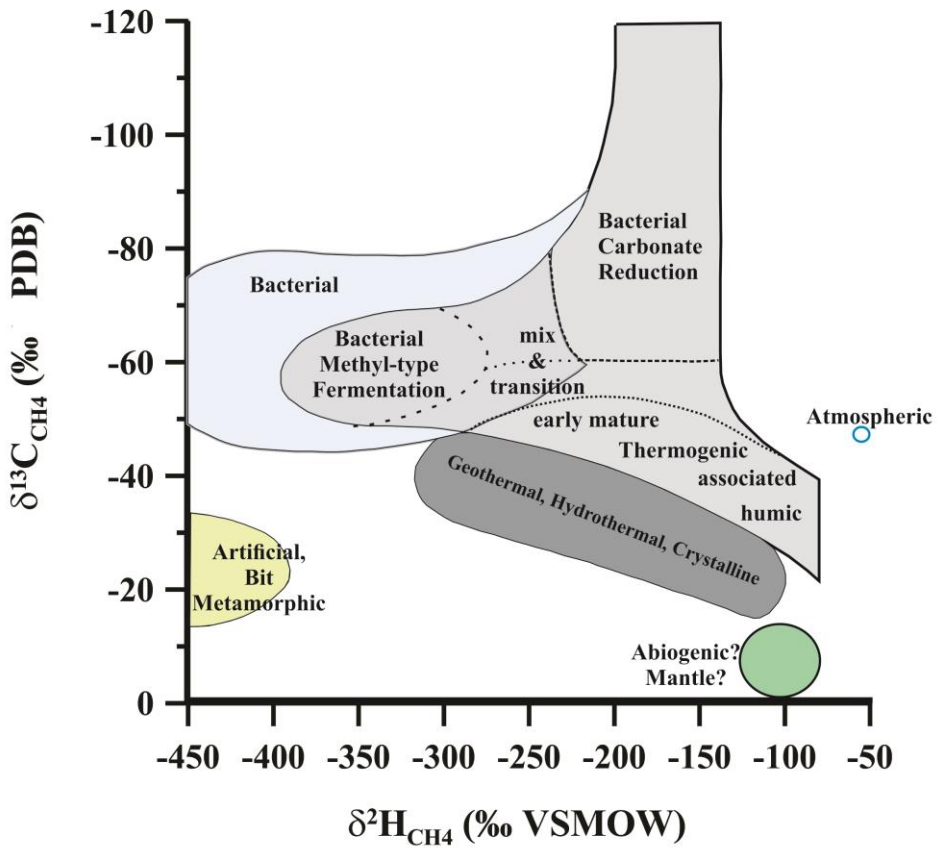

Figure 2.2. A natural gas characterization plot developed by Whiticar (1999), which defines regions of isotopic values of $\delta^{13}C_{CH4}$ and $\delta^{2}H_{CH4}$ of CH_4 produced by various pathways (after Whiticar, 1999).

Comparing the ratio of the concentrations of C_{2+} gases to the concentration of CH_4 (C_1) in a gas is a method of genetic characterization of natural gases. C_{2+} is calculated by (Schoell, 1983):

$$C_{2+} = \left(1 - \frac{C_1}{\Sigma C_n}\right) \times 100 \qquad \text{(Eq. 2.11)}$$

where C_n represents CH_4, C_2H_6, C_3H_8, normal butane (n-C_4H_{10}) and normal pentane (n-C_5H_{12}). Concentrations of C_{2+} gases are highest under optimal oil-generating temperature and pressure conditions, and decrease as gases mature (Schoell, 1983). For this reason, CH_4 in combination with greater than trace concentrations of C_{2+} is not considered to be of bacterial origin (Schoell, 1980; Whiticar et al., 1986). When C_{2+} is plotted against $\delta^{13}C_{CH4}$, categories of bacterial and

thermogenically-sourced gases are evident (Figure 2.3); $\delta^{13}C_{CH4}$ increases with the content of C_{2+} gases. The maturity of the gas, effects of mixing, migration, or bacterial oxidation can be detected by this relationship (Schoell, 1983; Faber and Stahl, 1984). In contrast, $\delta^{2}H_{CH4}$ decreases as C_{2+} concentrations of a gas increase (Schoell, 1983). The relationship between $\delta^{13}C_{C2H6}$ and $\delta^{13}C_{CH4}$ is also used to define genetic groupings of gases and distinguish between thermogenic and bacterial gases (Schoell, 1983; Taylor et al., 2000). In co-genetic gases, C_2H_6 is characteristically enriched in ^{13}C by up to 10‰ over the $\delta^{13}C_{CH4}$ of the gas. When $\delta^{13}C_{CH4}$ are plotted against $\delta^{13}C_{C2H6}$, data that falls outside of the defined genetic fields may be representative of mixed gases (Schoell, 1983).

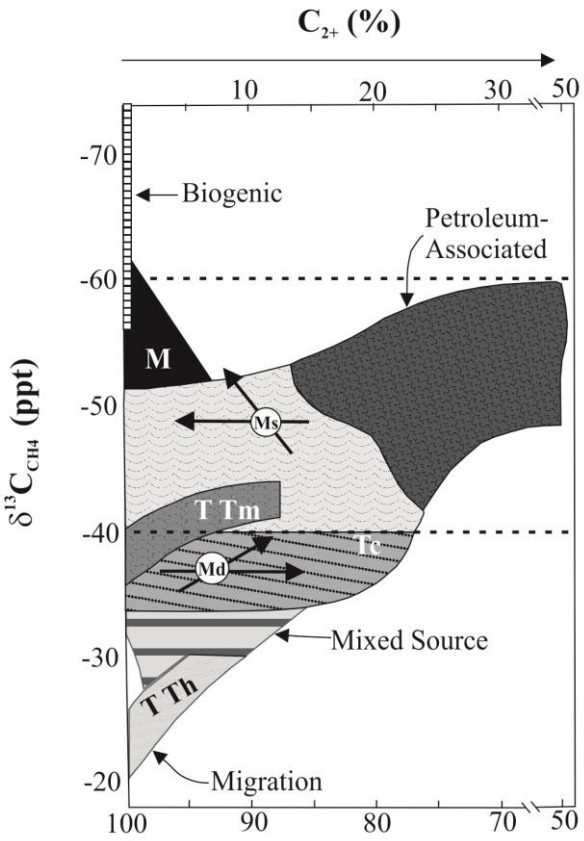

Figure 2.3. A plot developed by Schoell (1983) of $\delta^{13}C_{CH4}$ versus C_{2+} concentrations to define genetic groupings of natural gases. 'M' represents mixing of gases, and the arrows indicate the direction migration will change the composition of a gas in deep (M_d) and shallow (M_s) settings. 'T_c' are gases associated with condensates while the 'TT' groups are non-associated gases sourced from different types of organic matter: sapropelic liptinitic (TT_m), and humic (TT_h) (after Schoell, 1983).

2.3.3 Fate of organic gases in the subsurface

CH_4 is consumed by bacterial oxidation, upon entering oxic zones or zones of sulfate reduction (Whiticar et al., 1986; Chanton et al., 2004). Methanotrophs initially consume CH_4 composed of lighter isotopes and the left over gas is heavier in $\delta^{13}C_{CH4}$ and $\delta^{2}H_{CH4}$, thus, enriched values of ^{13}C and ^{2}H in CH_4 isotopes may be indicative of bacterial activity (Chanton et al., 2004). Bacteria consume CH_4 preferentially over C_{2+} gases and, as a result, the residual gas becomes enriched in those compounds. Hence the $CH_4/\sum C_{2+}$ ratio is another indicator of bacterial activity. However, CH_4 may not be entirely consumed if the influx is greater than the consumption rate (Whiticar, 1999).

As opposed to consumption, when dissolved CH_4 concentrations reach saturation in groundwater, a gas phase forms (Martens, 1982). The bubbles may travel by ebullition to surface. In some marine environments, the bubbles will not escape if the overlying hydrostatic pressure is greater than the gas pressure (Barnes and Goldberg, 1976).

2.4 Study site

In 1996, the King site was established to define the hydrogeology and solute transport mechanisms in thick clay-rich aquitards. Since its establishment, more than 15 refereed scientific publications have been prepared on aspects of reactive and conservative solute transport in aquitards. Some of the papers (and their key findings) relevant to the current study are presented below.

Shaw and Hendry (1998) measured numerous index and hydrogeologic parameters, installing 22 piezometers and collecting cores to a depth of 80 m BGS. That study defined the geology at the site as ~3-4 m of oxidized and ~77 m of unoxidized Battleford till, and ~76 m of Cretaceous Snakebite clay to the base of exploration, which was the top of the Ardkenneth aquifer. The *K* of the unoxidized till was determined to be between 2.4-5.3 x 10^{-11} m s^{-1}, and *K* of the clay between 2.3-4.3 x 10^{-12} m s^{-1}. Shaw and Hendry (1998) also estimated the downwards *v* to be between 0.5-0.8 m/10 ka.

While data from Shaw and Hendry (1998) defined the index properties of the unoxidized till and Snakebite clay to be relatively homogeneous, a few studies at the site revealed the heterogeneous nature of the till across the site (Hendry and Wassenaar, 2009; Stumpp and Hendry, 2012). Hendry and Wassenaar (2009) presented transport modeling of shallow (< 20

m), high-resolution δ^2H profiles which demonstrate the impact that small heterogeneities such as sand lenses have on solute transport. Stumpp and Hendry (2012) used very shallow (< 6 m) δ^2H profiles to assert the variability of the unoxidized till and the impacts of seasonal water events. Harrington et al. (2007) used mathematical models of Cl^- transport to investigate the influence that circular or elliptical-shaped sand deposits have on solute transport in the till.

Various transport models of concentration-depth profiles of δ^2H, $\delta^{18}O$, ^4He, and Cl^- from the King site agree that the Battleford till was deposited between 20-30 ka BP and that the climate change over the Holocene occurred over 7.5-12 ka BP (Hendry and Wassenaar, 1999; Hendry et al., 2000; Hendry et al., 2005; Hendry and Woodbury, 2007). Modeling in all of these studies confirmed that diffusion is the dominant solute-transport mechanism in the King site aquitards. Most recently, a δ^2H profile from the King site was used in a regional comparison of solute and groundwater transport in aquitards (Hendry et al., 2011).

The pore water chemistry at the King site has been used to define chemical zonations, observe mixing processes, and confirm that solute transport is dominated by diffusion (Hendry and Wassenaar, 2000; Vengosh and Hendry, 2001). Hendry and Wassenaar (2000) distinguished the oxidized till from the unoxidized till using the pore water chemistry and determined that geochemical reactions (e.g. carbonate dissolution/precipitation, ion exchange, CO_2 degassing) do not control solute transport in the till. The distribution of pore water compositions in the King site sediments has been defined as: low Cl^- concentrations in the top of the unoxidized Battleford till (< 80 mg L^{-1}), peaks in sand lenses ~13 and 22 m BGS from an alternate source (~190 mg L^{-1}), the glacial meltwater with low Cl^- concentrations between 20-60 m BGS (< 60 mg L^{-1}), and the high Cl^- concentrations (~960 mg L^{-1}) of the Cretaceous units (Hendry et al. 2000). The chemistry of the pore waters in the Snakebite clay indicated mixing has occurred between the aquifer water and glacial waters over time (Vengosh and Hendry, 2001).

An investigation into bacterial populations in the till and clay at the King site concluded that what little bacterial activity was present below the oxidized till was not homogeneously distributed (Lawrence et al., 2000). A zone of increased bacterial presence was noted at 82 m BGS which was identified as a “disturbed zone” at the till-clay interface caused by glaciation. That study determined that bacteria do not impact the composition of the pore waters and bacterial populations are low in part due to low temperatures in the sediments (Lawrence et al.,

2000). A thermal profile was measured and modeled by Hendry and Woodbury (2007) which showed temperature in the till and clay varies between 4-8 °C.

The King site is well suited to an investigation into the behaviours of dissolved gases in groundwaters as the geology, index properties, and hydrogeologic conditions are well defined by, and correlated between, numerous proxies.

CHAPTER 3

MATERIALS AND METHODS

3.1 Study area

The King site is in the mixed prairie/dry mixed prairie region of the province of Saskatchewan. This region is characterized by mid-short grasses, limited tree cover, and a semi-arid climate. The annual mean temperature is ~2-3 °C, and the region receives ~350 mm of precipitation and ~1000 mm of snowfall annually (1961-1990 data; Fung et al., 1999).

The elevation at the King site is ~576 m above sea level (masl). Alternating moraines and valleys construct the topography of the region, and the nearest topographic high is the Missouri Coteau to the west (700-800 masl; Fung et al., 1999). The South Saskatchewan River, as it flows into Lake Diefenbaker (Figure 1.1), is located ~18 km to the east of the King site. Small sloughs exist on the site, and a 20 km^2 salt lake, Luck Lake, is located ~10 km southwest of the site (Schmutz, 2002).

The geologic formations of interest at the King site are thick, argillaceous units that are laterally extensive across much of southern Saskatchewan. Approximately 80 m of Saskatoon Group glacial till unconformably overlies a thick sequence of Cretaceous-aged Bearpaw marine clays and sands (Caldwell, 1968). The till and uppermost Cretaceous member, the Snakebite clay, form a two-tiered aquitard system. The dominant groundwater flow through the system is vertically downward at extremely low velocities (0.5-0.8 m/10 ka based on hydraulic considerations, Shaw and Hendry, 1998; 0.75-1.0 m/10 ka based on isotopic profiling, Hendry and Wassenaar, 1999).

3.2 Coring and sampling of solids

Drilling and sample collection was conducted at the King site between September 18-21, 2013. Cross Borders Drilling (Pilot Butte, Saskatchewan) performed the drilling with a truck-mounted top drive coring rig and Christensen wire-line core retrieval system. This method required contemporaneous circulation of drill fluids, for which a surface water source ~4 km south of the site was used (13N 366527E 5660221N).

During drilling, core was recovered in 3.05 m lengths from PVC tubes inside the core barrels (PVC tube – 75 mm inner diameter (I.D.)). The final depth of the hole was 240 m BGS (336 masl). Core recovery varied between 0-100% through each formation; the average recovery per geologic unit was: Battleford till, 67%; Snakebite clay, 70%; Ardkenneth aquifer, 79%; Beechy clay, 85%. The length of core recovered per run was removed from the PVC tubes at surface and samples (100 mm long x 75 mm I.D. PVC tube) were immediately cut, and the outer ~10 mm of each core removed with a kitchen knife (to minimize core contamination by drill fluid) prior to storage for the analyses detailed in Table 3.1.

Table 3.1. Summary of core samples collected for each analysis, including the frequency of, and depth intervals over which, samples were collected and the total numbers of samples analyzed.

Analysis	Sampling Frequency	Depth Intervals (m)	Number Analyzed
$\delta^{18}O$ and $\delta^{2}H$ of pore water via vapour equilibration	1 meter	0-240	193
$\delta^{18}O$, $\delta^{2}H$ and major dissolved ions via pore water squeezing	1 meter	0-240	66
Physical hydrogeology: gravimetric water content, density, porosity, grain size	3 meters	0-240	77
Solid carbon forms	1 meter	0-15	77
	3 meters	15-240	
Dissolved gas concentrations (CH_4, C_2H_6, C_3H_8, CO_2, N_2, O_2)	1 meter	0-15	82
	3 meters	15-240	
$\delta^{13}C$ of CO_2	1 meter	0-15	82
	3 meters	15-240	
$\delta^{13}C$ and $\delta^{2}H$ of CH_4, $\delta^{13}C$ of C_2H_6, and C_3H_8	1 meter	0-15	57
	3 meters	15-240	

Samples for pore water isotope, mechanical squeezing, physical hydrogeology, and solid carbon analyses were placed in medium-sized Ziploc® bags (1.4 L), the atmospheric air squeezed out of the bags, and the zipper lock sealed. These samples were placed in large Ziploc® bags (4 L), air squeezed out of the bags, and the bags sealed (Hendry et al., 2013). All samples were stored in coolers at surface temperature until they were transported to the University of Saskatchewan (U of S) where they were kept in coolers at room temperature until analysis.

Core samples collected for analysis of dissolved gas concentrations and $\delta^{13}C_{CH4}$, $\delta^{2}H_{CH4}$, $\delta^{13}C_{CO2}$, $\delta^{13}C_{C2H6}$, and $\delta^{13}C_{C3H8}$, were placed in 650 mL IsoJars® after trimming (Clark et al., 2010). Prior to sampling, vacuum grease was applied to the rim of each IsoJar® to prevent leakage of gases during storage. After each core sample was placed in an IsoJar®, a polypropylene tube connected to a tank of nitrogen (N_2) was placed inside the IsoJar® and the lid of the jar placed on top. The N_2 was flushed through the jar for 10 s to displace atmospheric air, the tube was quickly removed and the lid sealed (Clark et al., 2010). All IsoJars® were stored in cardboard boxes at surface temperature on site prior to transport to the U of S and remained in the cardboard boxes at room temperature in the laboratory prior to analysis.

To identify possible core-contamination by drilling fluid, the drill fluid was spiked with 99.9% deuterium oxide; 125 mL D_2O per 9000 L water tank (Hendry et al., 2013). A sample of the source water was collected at each refilling of the water tank (n = 3), and the drill fluids were sampled every 2 h during drilling (n = 26). The source water and drill fluid samples were stored in a cooler at surface temperature prior to transport to the U of S where they were stored at room temperature prior to analysis.

3.3 Laboratory analyses of core samples

3.3.1 Physical hydrogeology

Core samples for physical hydrogeology measurements were split widthwise into three subsamples for determination of: 1) gravimetric moisture content (θ_g); 2) wet density (ρ_m); and 3) grain size distribution. The θ_g was measured according to ASTM D2216-05 (ASTM, 2005). That subsample of core was weighed prior to, and after, oven-drying at 110 °C for 48 h. The difference in mass yielded the mass of water that was in the subsample.

The ρ_m was determined following ASTM D7263-09 (ASTM, 2009). These subsamples were weighed then dipped in hot paraffin wax several times to create a seal. The wax-coated subsample was then weighed in air and weighed submerged in water. The wax was removed and the subsample weighed in air again. The ρ_m was calculated using (ASTM, 2009):

$$\rho_m = \frac{M_t}{\left[\left(\frac{(M_c - M_{sub})}{\rho_w}\right) - \left(\frac{(M_c - M_t)}{\rho_p}\right)\right]} \quad \text{(Eq. 3.1)}$$

where
M_t = mass of the wet subsample (g)
M_c = mass of the wax-coated subsample in air (g)
M_{sub} = mass of the wax-coated subsample in water (g)
ρ_w = density of the water the wax-coated sample was submerged in (assumed to be 998.2 kg m^{-3} @ 20 °C (Petrucci et al., 2002))
ρ_p = density of the paraffin wax; 850 kg m^{-3} (Honeywell, 2004)

Measured values for ρ_m and θ_g were used to calculate dry density, (ρ_d; kg m^{-3}) using (ASTM, 2009):

$$\rho_d = \frac{\rho_m}{\left(\frac{1+\theta_g}{100}\right)} \quad \text{(Eq. 3.2)}$$

Total porosity (n_T, unitless) was calculated using the ρ_d calculated by Eq. 3-2 according to (Fetter, 2001):

$$n_T = \left[1 - \left(\frac{\rho_d}{s_g}\right)\right] \times 100 \quad \text{(Eq. 3.3)}$$

where a value of 2650 kg m^{-3} was assumed for specific gravity (s_g), due its limited range amongst sediment types (Das and Sobhan, 2014). Void ratio (e) was then calculated using (Fetter, 2001):

$$e = \frac{n_T}{1 - n_T} \quad \text{(Eq. 3.4)}$$

The volumetric water content (θ_v) was calculated according to (Fetter, 2001):

$$\theta_v = \left(\frac{\rho_b}{\rho_w}\right)\theta_g \quad \text{(Eq. 3.5)}$$

Grain size distribution was determined by two methods. Sixteen of the subsamples were analyzed via hydrometer: five from the Battleford till (23, 58, 62, 68, and 74 m BGS), five from the Snakebite clay (85 (x2), 104, 121, and 145 m BGS), four from the Ardkenneth aquifer (159, 162, 165, and 174 m BGS), and two from the Beechy member (206 and 212 m BGS). Between 300-500 g of the subsamples were oven-dried for 48 h at 110 °C, then crushed with a mortar and pestle. Eight of the hydrometer tests were conducted at the U of S Geotechnical Laboratory (23,

85, 159, 162, 165, 174, 206, and 212 m BGS) and the other eight at the U of S Cameco Chair Geochemistry Laboratory (58, 62, 68, 74, 85, 104, 121, and 145 m BGS) according to ASTM D422-63 (ASTM, 2007). By this standard, grain sizes larger than 0.075 mm are separated through a series of sieves while the fraction smaller than 0.075 mm are measured in a hydrometer. This method will be referred to as the hydrometer method throughout the thesis.

Grain size distribution of 82 subsamples were measured with a Malvern Mastersizer 2000™ laser diffraction unit paired to a Malvern Hydro2000MU wet sample dispersion accessory, similar to Sperazza et al. (2004) at the U of S Cameco Chair Geochemistry Laboratory. These subsamples were oven-dried and hand-crushed with a mortar and pestle. Less than 3 g of the sediment was placed in a 1000 mL glass beaker containing 800 mL of deionized (DI) water, to obtain obscuration between 5-15%. The sediment was sonicated for one min in the Hydro2000MU before analysis. Pump speed on the Hydro2000MU was 2200 rpm during analysis, and values of the index of refraction and absorption were 1.55 and 0, respectively. This will be referred to as the particle size analyzer method.

The core samples collected for total carbon (TC) and total organic carbon (TOC) analysis (n = 77) were cut widthwise into two subsamples (on occasion, three subsamples) and air-dried. The subsamples were weighed on a daily basis until no change in mass was measured (typically 3-4 d). All subsamples were then pulverized into a fine powder in a carbide swing mill. For TOC analysis, an acid fumigation method was applied to remove carbonates (Harris et al., 2001). In this method, 0.2 g of the pulverized sediment was measured into a ceramic boat and wetted with 1 mL of deionized (DI) water. The boats were placed inside a vacuum desiccator containing three to six vials of 30 mL of hydrochloric acid (HCl). The desiccators were sealed for 48 h in a fume hood. The boats were then removed from the desiccators and the sediment fumigated inside the fume hood for another 48 h. Finally, the boats were placed in an oven at 105 °C for 24 h directly prior to analysis. For measurement of TC, 0.2 g of the air-dried and pulverized sediment was weighed into a ceramic boat and directly analyzed. Carbon solids analysis was conducted at the U of S Soil Science Analytical Laboratory on a Leco® L632 Carbon analyzer (Wang and Anderson, 1998). During analysis, both TOC and TC samples were combusted at 1100 °C for two min. Total inorganic carbon (TIC) was calculated as the difference between TC and TOC.

To test the variability and heterogeneity of the sediments using the above method, replicate samples were selected approximately every 20 m (n = 15). Of the initial 77 core samples, eight had a sufficient mass of sediment to be cut into a third subsample. In seven cases, not enough sediment was available for three subsamples, and another core from a nearby depth was selected. After air-drying 400-500 g of each subsample, the subsamples were split into three portions of equal weight by manually breaking with a mortar and pestle. Each portion was separately pulverized into a powder using the carbide swing mill. The aforementioned methods for TOC and TC were followed on each of the three portions (n = 45). Using the three replicate values, and including values from the initial analysis where available, the sample mean (μ) and standard deviation (σ) values of TOC and TC for each set of replicates were calculated.

3.3.2 Stable isotopes of pore water via the vapour equilibration method

The $\delta^{18}O$ and $\delta^{2}H$ of the pore waters were determined using the vapour-core equilibration method (Wassenaar et al., 2008). Preparation required inflation of the medium Ziploc® bags containing the core samples with H_2O-free air. Atmospheric air was forced through a canister containing DRIERITE® desiccant to remove external moisture while filling the bags. Once inflated, the medium Ziplocs® were resealed and placed back inside the original large Ziploc® bags which were also resealed. Samples equilibrated at room temperature for three d. The $\delta^{18}O$ and $\delta^{2}H$ of the vapour were analyzed on a Picarro Cavity Ringdown Spectrometer L2120-*i* (precision ± 0.7‰ $\delta^{2}H$, ± 0.3‰ $\delta^{18}O$) at the U of S Cameco Chair Geochemistry Laboratory. During analysis, two water standards with known isotopic values bracketing those expected of the King site pore waters were analyzed with every four core samples (Hendry et al., 2013). Thirty-three percent of the samples were analyzed as replicates. Error on the vapour samples is ± 2.25‰ $\delta^{2}H$ and ± 0.53‰ $\delta^{18}O$, based on duplicate analysis of 67 samples. Analyses commenced within one week of drilling completion and were finalized within 41 d. Vapour equilibration isotope results are reported in δ-‰ notation with reference to VSMOW as in Eq. 2.8.

3.3.3 Squeezing of cores for pore water stable isotopes and geochemistry

Pore water samples were squeezed from the cores using the method described in Hendry et al. (2013). Given the intensive equipment demands of the squeezing process, a limit of five

samples could be processed at a time. Cores remained in the Ziploc® bags in the coolers prior to squeezing. The first cores were squeezed 61 d after collection and the final samples were squeezed within 263 d. All core samples were trimmed in the laboratory to fit the 50.6 mm I.D. of the stainless steel squeezing apparatus (Figure 3.1). When possible, cores were left intact and were not fragmented to fit into the cylinder. A 0.45 µm stainless steel filter was positioned in the bottom of the squeezing cylinder, the core sample was placed on top of the filter, and a brass piston placed on top of the core. A metal frame was used to hold a PowerFist™ 12-ton low profile bottle jack on a table top and the cylinder sat on top of the jack. Finally, a spacer was placed between the piston and the top of the metal frame. Manual force was used to pump the hydraulic jacks, which provided a maximum of 53 MPa to force the piston down onto the sample (Bangsund et al., 2012). Pore water was expelled through a sampling port on the base of the cylinder. A polypropylene tube was connected to the sampling port at one end and to a three-way valve on the other. The pore water collected in a sterile 60 mL luer-lok syringe attached to the valve. Cores were squeezed until a sufficient volume (~10 mL) of pore water was expelled. These samples were used to analyze for $\delta^{18}O$ and $\delta^{2}H$, cations (Na^{+}, Ca^{+2}, Mg^{+2}), anions (Cl^{-}, Br^{-}, SO_4^{-2}), and pH. The length of time a sample was squeezed to collect the necessary amount of pore water varied by lithology: (on average) oxidized tills and sand, 6 d; unoxidized tills, 7 d; thick clay, 11 d; mudstone/claystone, 14 d. In between squeezing of individual cores, the cylinder, base, piston, polypropylene tube and three-way valves were washed with tap water, rinsed with DI water a minimum of three times, and air-dried. The stainless steel filters were rinsed with DI water several times, placed in a beaker of DI water on a stirring plate with a magnetic stirring bar for 60 min, and oven or air-dried. Syringes were rinsed with DI water three times before and after being placed in a 10% nitric acid (HNO_3) acid bath for 2 h, followed by a DI water bath for 2 h, a final rinsing with DI water, and air-drying.

Once squeezing of a core was complete, the pore water was separated into three aliquots for isotope, cation, and anion analysis. Of the total pore water extracted per sample, 2 mL was filtered through a 0.45 µm disposable polyethersulfone filter into a 2 mL polypropylene bottle for isotope analysis. Once capped, each bottle was wrapped in parafilm and refrigerated until analysis on a Picarro L2130-*i* (precision ± 1.0‰ $\delta^{2}H$, ± 0.15‰ $\delta^{18}O$) at the U of S Cameco Chair Geochemistry Laboratory using the method of Lis et al (2008). Where enough pore water was available, an additional bottle was prepared as a duplicate; 11% of the samples submitted were

duplicates. Squeezed pore water isotope results are reported in δ-‰ notation with reference to VSMOW, as in Eq. 2.8.

For cation analysis, 4 mL of the squeezed pore water was acidified with 70% HNO_3 (~114 µL HNO_3 per 4 mL sample) to prevent chemical reactions (Herzog et al., 1991) and refrigerated until analysis. When excess pore water was available from a sample, an additional 4 mL was collected and used for quality control in the laboratory; 12% of samples were submitted in duplicate. Samples were analyzed at the U of S Cameco Chair Geochemistry Laboratory on a Perkin Elmer® NexION® 300D inductively coupled plasma mass spectrometer (precision ± 5%).

The leftover aliquots of pore water were used to measure pH and anions (Cl^-, Br^-, and SO_4^{-2}). A Fisher Scientific™ accument™ gel-filled pH combination electrode was inserted into each sample to measure pH. Anion analysis was conducted on a Thermo Scientific™ Dionex™ ICS-2100 Ion Chromatography instrument (precision ± 5%) at the U of S Cameco Chair Geochemistry Laboratory. When possible, 4 mL duplicates were measured and submitted to the laboratory (12% of total submitted). With the exception of Cl^-, the pore water chemical analyses and pH are not discussed in the thesis. For completeness, the chemistry data are presented in Appendix A.

Figure 3.1. The apparatus used to squeeze pore water from core samples.

3.4 Dissolved gases

3.4.1 Headspace analysis

Samples collected in IsoJars® for dissolved gas analysis were allowed to equilibrate at room temperature for 65 d. Hendry et al. (2016) suggest equilibration is reached in IsoJars® within 10-30 d. Ten mL of headspace gas from each IsoJar® was withdrawn and injected into a 7890B Agilent Technologies Gas Chromatography (GC) system (precision ± 10%). The 7890B consisted of four columns: two ultimetal (0.5 m, 3.2 mm outer dia (O.D.); 1.8 m, 3.2 mm O.D.) columns packed with HayeSep® porous polymers; a 2.4 m, 3.2 mm O.D. stainless steel column with molecular sieve 5A packing; and a 60 m x 0.25 mm x 1.0 µm CP-Sil 5 CB capillary column. A thermal conductivity detector measured CO_2, O_2, and N_2, and a flame ionization detector measured CH_4, C_2H_6, and C_3H_8. The initial oven temperature was held constant at 50 °C for five min, after which the temperature was ramped up 10 °C per min until 100 °C was reached (10 min). Carrier gas pressures in the system were as follows: hydrogen – 55 psi, zero air – 70 psi, and N_2 – 42 psi. The CO_2 concentrations are presented in Appendix C, but will not be discussed.

The dissolved concentration of CH_4 in the pore water of the cores was calculated from the concentration measured in the headspace by the method of Kampbell and Vandegrift (1998), as follows. The mole fraction of CH_4 (x_g; unitless) was calculated using the form of Henry's law:

$$x_g = \frac{p_g}{H} \quad \text{(Eq. 3.6)}$$

where p_g was the partial pressure of the gas (ppm) and *H* was Henry's Law constant (unitless) calculated at 21 °C according to (Green and Perry, 2008):

$$\ln x = A + \frac{B}{T} + C \ln T + DT \quad \text{(Eq. 3.7)}$$

$$H = \frac{1}{x} \quad \text{(Eq. 3.8)}$$

where A = -338.217; B = 13282.1; C = 51.9144 ; D = -0.0425831 (no units) and T is temperature, in Kelvin (K). The mole fraction of a gas (x_g) is defined as (Kampbell and Vandegrift, 1998):

$$x_g = \frac{n_g}{(n_g + n_w)} \quad \text{(Eq. 3.9)}$$

where n_g and n_w represent the moles of gas and moles of water, respectively. The moles of gas were found by rearranging Eq. 3.9 (Kampbell and Vandegrift, 1998):

$$n_g = x_g(n_g + n_w) \quad \text{(Eq. 3.10)}$$

Kampbell and Vandegrift (1998) assumed the pore water has a density of 1.00 g mL^{-1} and that 1 L of water contains 55.5 moles, therefore:

$$n_g = x_g(n_g + 55.5) \quad \text{(Eq. 3.11)}$$

The assumption was also made that $n_g x_g << n_g$, and Eq. 3.11 becomes (Kampbell and Vandegrift, 1998):

$$n_g \approx x_g(55.5) \quad \text{(Eq. 3.12)}$$

Substituting Eq. 3.6 into Eq. 3.12 for x_g gives (Kampbell and Vandegrift, 1998):

$$n_g = 55.5\left(\frac{p_g}{H}\right) \quad \text{(Eq. 3.13)}$$

Subsequently, the saturation concentration of the gas was calculated using (Kampbell and Vandegrift, 1998):

$$C = n_g \times (MW) \times \left(\frac{1000\ mg}{1\ g}\right) \quad \text{(Eq. 3.14)}$$

where MW is the molecular weight of CH_4 = 16.04 g. The latter term is a conversion for g to mg. Then the volume of CH_4 in the headspace (A_h; mL) was determined using (Kampbell and Vandegrift, 1998):

$$A_h = (vol\ headspace) \times (p_g) \quad \text{(Eq. 3.15)}$$

The volume of headspace was determined for each IsoJar® by subtracting the volume of the core from the known volume of the IsoJar® (650 mL). The volumes of the cores were determined by taking the known mass of an empty IsoJar® from the total mass of the IsoJar® and the core. The measured density of the nearest core sample was then used to calculate the volume (v) of the core ($v = mass/\rho$).

The mass of CH_4 dissolved in the pore water (A_l; mg) was calculated using (Kampbell and Vandegrift, 1998):

$$A_l = \left(\frac{A_h}{V_w}\right) \times D \times \left(\frac{1000\ mg}{1\ g}\right) \times \left(\frac{1\ L}{1000\ mL}\right) \quad \text{(Eq. 3.16)}$$

where V_w was the volume of water in the core (θ_v x the volume of the core), and D was a correction for density of CH_4 at the temperature of the lab in which CH_4 concentrations were measured (21 °C or 294.15 K) (Kampbell and Vandegrift, 1998):

$$D = \frac{MW}{(22.4\ L\ mole^{-1}) \times \left(\frac{294.15K}{273K}\right)} \quad \text{(Eq. 3.17)}$$

This density correction is required due to the ideal gas law which states that at 0 °C (273 K), the volume of one mole of gas is 22.4 L (McQuarrie et al., 2011). Finally, the total concentration of CH_4 (TC; mg CH_4 L^{-1}) was determined (Kampbell and Vandegrift, 1998):

$$TC = A_l + C \quad \text{(Eq. 3.18)}$$

To investigate whether desorption or production of CH_4 occurred in the IsoJars® over time, additional analyses were conducted on seven IsoJar® samples. Three samples of the Battleford till (54, 63, and 79 m BGS), one sample of the Ardkenneth sand (162 m BGS) and three of the Snakebite and Beechy member clays (148, 219, and 234 m BGS) were selected for testing. Dissolved gases were measured in each sample by the previously described method at 10 months from the collection date, and then flushed with N_2 for ~20 s (1st flush). Samples were analyzed on approximately 1, 2, 5, 10, 20 and 30 d after flushing by withdrawing 5 mL of headspace and injecting into the GC. The 30 d maximum was based on the time required for CH_4 concentrations to reach equilibration after flushing determined by Hendry et al. (2016) on similar sediments. This procedure was followed two subsequent times (2nd and 3rd flush).

3.4.2 Isotopes of dissolved organic gases

IsoJars® containing core samples were shipped to Isotope Tracer Technologies Inc., Waterloo, Ontario, Canada for $\delta^{13}C_{CH4}$, $\delta^{13}C_{C2H6}$, $\delta^{13}C_{C3H6}$, $\delta^{13}C_{CO2}$ and $\delta^{2}H_{CH4}$ analyses. The gas samples were removed from the headspaces of the IsoJars® (after equilibrating for ~280 d) and injected into a Delta^{Plus}XL, Thermo Finnigan Isotope Ratio Mass Spectrometer (IRMS) coupled to an Agilent 6890 GC and a combustion system for $\delta^{13}C$, and a pyrolysis system for $\delta^{2}H$. The GC was equipped with a GS-Carbon plot capillary column for compound separation after which all compounds were converted to CO_2 (or H_2) before being directed to the IRMS for isotopic measurement. Accuracy and precision was better than ± 0.5‰ for $\delta^{13}C$ and ± 5‰ for $\delta^{2}H$ based on laboratory standards and duplicate sample analysis. Gas isotope results are reported in δ-‰ notation with reference to VPDB for $\delta^{13}C$ and VSMOW for $\delta^{2}H$ as in Eq. 2.8. The $\delta^{13}C_{CO2}$ values measured on the King site sediments are presented in Appendix C. These data will not be discussed.

CHAPTER 4

RESULTS AND DISCUSSION

4.1 Geology

The local Cretaceous geology in the vicinity of the King site is illustrated in cross section A–A' (Figure 4.1; after Caldwell, 1968), the location of which appeared in Figure 1.1. Stratigraphy at the site includes, from oldest to youngest, the Lea Park, Oldman, and Bearpaw formations. The Cretaceous is overlain by glacial drift (not completely detailed in the cross section). The bedrock units were deposited in a sequence of transgression-regressions through the Late Campanian to Early Maastrichtian stages.

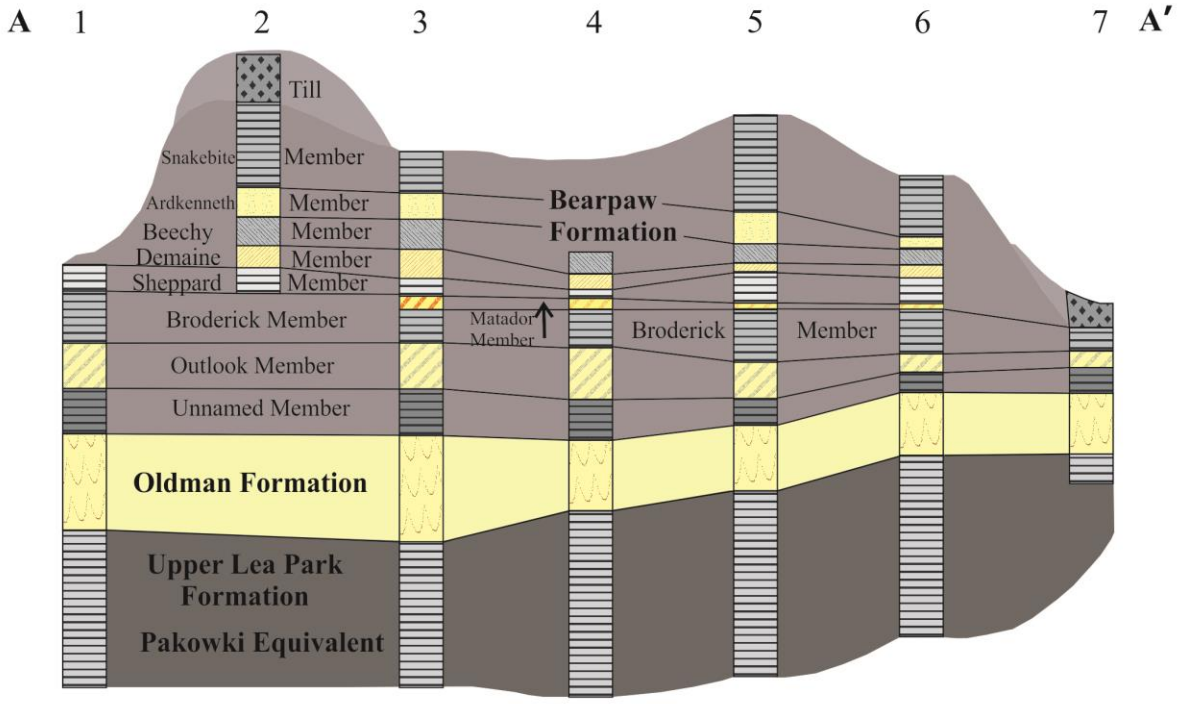

Figure 4.1. Cross section A–A' (location shown in Figure 1.1) portraying the Late Cretaceous stratigraphy near the King study site. Borehole 5 is a location closest to the King site (after Caldwell, 1968).

The Lea Park formed during a marine transgression in the mid-Campanian (Leckie et al., 1994). This unit is highly plastic, composed of fine-grained mudstones and siltstones, and is dark brown to grey in colour. The Lea Park can be over 175 m thick in west-central Saskatchewan (Dawson et al., 1994; Sauer and Christiansen, 1996). The top of the Lea Park is gradational into the bottom of the non-marine Oldman Formation, also called the Belly River or Judith River Formation (Caldwell, 1968; Dawson et al., 1994).

The Oldman Formation is an extensive aquifer in Saskatchewan, and is composed of very fine-to-medium grained sand, silt and clay (Simpson, 1998). This formation can be up to 100 m thick in the region around the King site (Dawson et al., 1994).

The Bearpaw Formation can be up to 350 m thick in the South Saskatchewan River valley and is divided into 11 members (from oldest to youngest): an unnamed basal unit, and the Outlook, Broderick, Matador, Sherrard, Demaine, Beechy, Ardkenneth, Snakebite, Cruikshank, and Aquadell members. The units are alternating layers of silty clays and sands; the sandy units are the Outlook, Matador, Demaine, Ardkenneth and Cruikshank (Caldwell, 1968). The Beechy, Ardkenneth, and Snakebite members were encountered during the 2013 drilling. The Beechy member is documented as dark grey to greyish brown, poorly consolidated, fine-grained sand, silt and clay. The sand of the Ardkenneth aquifer is reportedly poorly indurated, medium to dark grey with lenses of silt and clay. The Snakebite member is dark grey to dark brownish grey, silty clay (Caldwell, 1968). These formations were deposited during the Maastrichtian stage in a shallow seaway (Caldwell, 1968).

The glacial till at the site was confirmed to be the Battleford till, deposited ~20-30 ka (Christiansen, 1967) by Shaw and Hendry (1998). The Battleford Formation is a till within the Saskatoon Group, which can be up to 100 m thick in the surrounding area (Simpson, 1998). This till is reported to be soft, massive, with no iron staining, dark olive grey in colour, and contains localized sand lenses (Christiansen, 1968; Sauer and Christiansen, 1996; Shaw and Hendry, 1998).

A stratigraphic log of the borehole drilled in 2013 at the King site is depicted in Figure 4.2. Where oxidized, the till is light brown and contains organic material. The contact between the oxidized and unoxidized till is not well defined in the 2013 core due to poor core recovery in the upper 10 m. Using distinct colour transitions and the depth of identifiable fractures in the oxidized till, previous studies at the King site placed the oxidized-unoxidized till contact at 3-4 m

BGS (Shaw and Hendry, 1998; Stumpp and Hendry, 2012). In the current study, the first occurrence of dark grey till (unoxidized) is at 5 m BGS. That depth was assumed to be the location of the contact for these two units. The unoxidized till is soft, dark grey, reacts vigorously to 10% HCl where tested (n = 3), and contains varying amounts of pebble-sized, and smaller, rock fragments (< 64 mm; Wentworth, 1922).

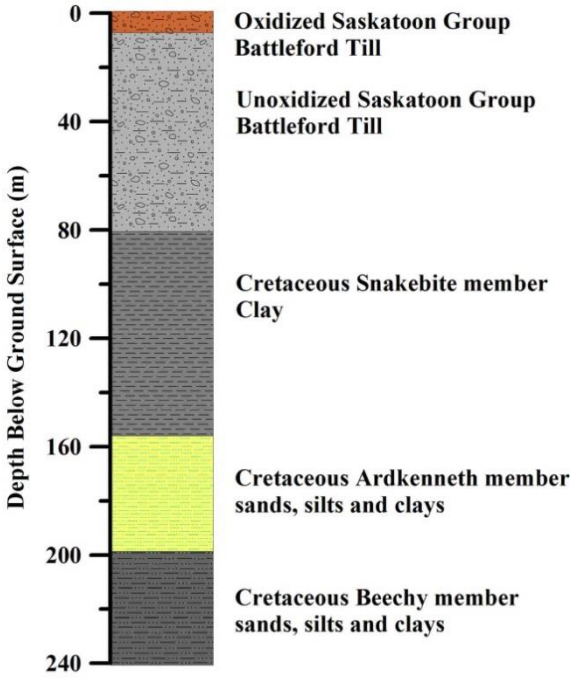

Figure 4.2. Stratigraphic log at the King site based on field logging of core samples.

The Snakebite clay is dark grey to black, with occasional lenses of grey silt and is fissile in some sections. The Snakebite is underlain by the Ardkenneth aquifer. The contact was at 159 m BGS. The Ardkenneth consists of well-sorted, sub-angular, green-grey, unconsolidated sand extending to a depth of 197 m BGS. From there to the base of exploration (240 m BGS), the Beechy member contains mottled-to-occasionally laminated light grey silt and sand and dark grey clay and has varying degrees of lithification.

4.2 Physical properties of the sediments

The geotechnical properties measured on the 2013 King site core are plotted versus depth BGS in Figure 4.3 (a-c) and are summarized for each geologic unit in Table 4.1. The θ_g and θ_v

profiles with depth (Figure 4.3 (a)) are uniform from surface to 80 m BGS, where a large increase occurs. Both θ_g and θ_v decrease through the top 20 m of the Snakebite and remain more or less constant to ~159 m BGS. Through the Ardkenneth and Beechy members, θ_g and θ_v are variable. The ρ_b and ρ_d profiles through the Battleford in Figure 4.3 (b) display a similar level of homogeneity as the θ_g and θ_v profiles. In contrast, ρ_b and ρ_d decrease at the till-clay contact, increase to ~100 m BGS and remain consistent to the top of the Ardkenneth. Through the Ardkenneth, ρ_b and ρ_d decrease and increase to the top of the Beechy, thereafter remaining more or less constant through to the base of exploration. The shape of the n_T and e profiles (Figure 4.3 (c)) mimic those of the θ_g and θ_v. Given the unlithified nature of these sediments, the n_T values are consistent with other sedimentary materials (Schwartz and Zhang, 2003).

The dramatic shift in physical parameters at 80 m BGS delineates the well-defined till-clay contact. Shaw (1997) noted an increase in moisture content and decrease in density at the till-clay contact at a similar depth (Figure 4.3). Shaw suggested this shift to be the result of glacial shear. Shearing of overconsolidated clay causes dilation of the pores, leading to increased moisture content and decreased density (Sauer et al., 1990). In a study on glacial shear of bedrock sediments in Saskatchewan, Sauer et al. (1990) noted that gouge zones present in Cretaceous clays, caused by glacial disturbance, have moisture contents between 28-45%. The θ_g in the top 5 m of the Snakebite in the 2013 King site core is 27%, consistent with moisture contents reported in gouge zones, however, no disturbed zone was visually confirmed in the 2013 King site core. At a site approximately 20 km southwest of the King site, Powell (2010) noted an increase in θ_g at the Battleford till-Snakebite clay interface, consistent with the findings of the current study. This locally consistent feature may indicate that the upper portion of the Snakebite was disturbed by glacial activity in the region.

The propagation of measurement errors through calculations of the geotechnical properties is small; the error for each property (θ_g, θ_v, ρ_b, ρ_d, n_T, and e) are summarized by geologic unit in Table 4.1. However, these errors do not encompass all possible sources. Engler (2010) notes that n can be underestimated by up to 10% between different methods of measurement. The θ_g, ρ_b, ρ_d, n_T, and e measured in this study are consistent with those reported by Shaw (1997), which are plotted in Figure 4.3 along with the 2013 data. Based on this consistency, it was assumed that the data collected from the 2013 core are representative of the physical properties at the King site.

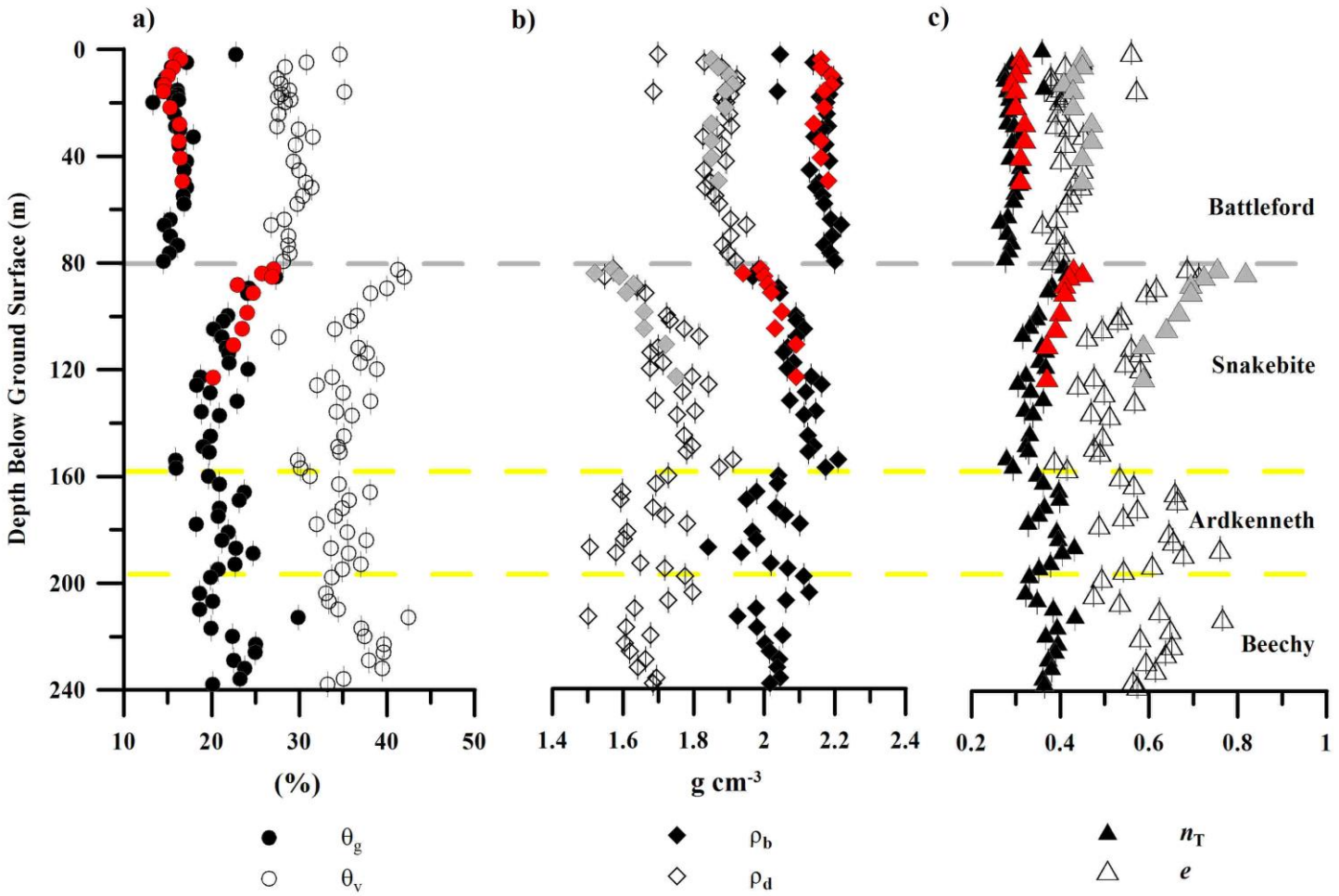

Figure 4.3. Physical properties measured on solid samples of core (black and white symbols) from the King site (2013) for (a) gravimetric (θ_g) and volumetric (θ_v) moisture content, (b) bulk (ρ_b) and dry (ρ_d) density, and (c) total porosity (n_T) and void ratio (e). Red and grey symbols represent data collected by Shaw (1997).

Table 4.1. Summary of the mean (μ) and standard deviation (σ) of the geotechnical properties measured in the 2013 King site core. Error is that from measurement and propagated through calculations.

		θ_g (%)			θ_v (%)			ρ_b (g cm^{-3})			ρ_d (g cm^{-3})			n_T			e		
Geologic Unit	**n**	**μ**	**σ**	**error**	**μ**	**σ**	**error**	**μ**	**σ**	**error**	**μ**	**σ**	**error**	**μ**	**σ**	**error**	**μ**	**σ**	**error**
Battleford	28	16	2	<0.11	29	2	<0.17	2.09	0.07	<0.01	1.76	0.09	<0.002	0.29	0.02	<0.001	0.42	0.05	<0.002
Snakebite	23	21	3	<0.09	36	4	<0.14	2.10	0.06	<0.001	1.74	0.08	<0.002	0.34	0.03	<0.001	0.53	0.08	<0.001
Ardkenneth	14	22	2	<0.07	35	2	<0.11	2.01	0.07	<0.001	1.66	0.08	<0.001	0.37	0.03	<0.001	0.60	0.08	<0.001
Beechy	12	22	3	<0.06	37	3	<0.09	2.02	0.05	<0.001	1.65	0.07	<0.001	0.38	0.03	<0.0004	0.60	0.07	<0.001

Grain size distribution (Figure 4.4 and Appendix B) is relatively constant throughout the Battleford till. The percentage of sand-sized particles (0.075–4.75 mm) decreases while clay-sized particles (< 0.005 mm) increases in the Snakebite and the opposite occurs in the Ardkenneth and into the Beechy, which are dominated by sand and silt. The data from the current study are consistent with those of Shaw (1997) (Figure 4.4). The high-resolution of the 2013 geotechnical profiles display relative homogeneity through the Battleford and Snakebite sediments, and increasing heterogeneity in the Ardkenneth and Beechy members.

The grain size distributions measured by the hydrometer and particle size analyzer methods have a strong correlation (Figure 4.5). Duplicate samples (n = 9) analyzed by both methods have R^2 values > 0.90 in all but two cases (not shown). The sample depths and R^2 values are summarized in Table 4.2. The strong correlations indicate that the methods produce the same results.

Table 4.2. Summary of the correlation coefficients between grain size distributions of samples measured by both the hydrometer and particle size analyzer methods on duplicates of core samples from the 2013 King site core.

Sample depth (m BGS)	R^2
23	0.86
59	1.00
63	0.99
69	1.00
74	0.94
159	0.99
163	1.00
166	0.64
174	1.00

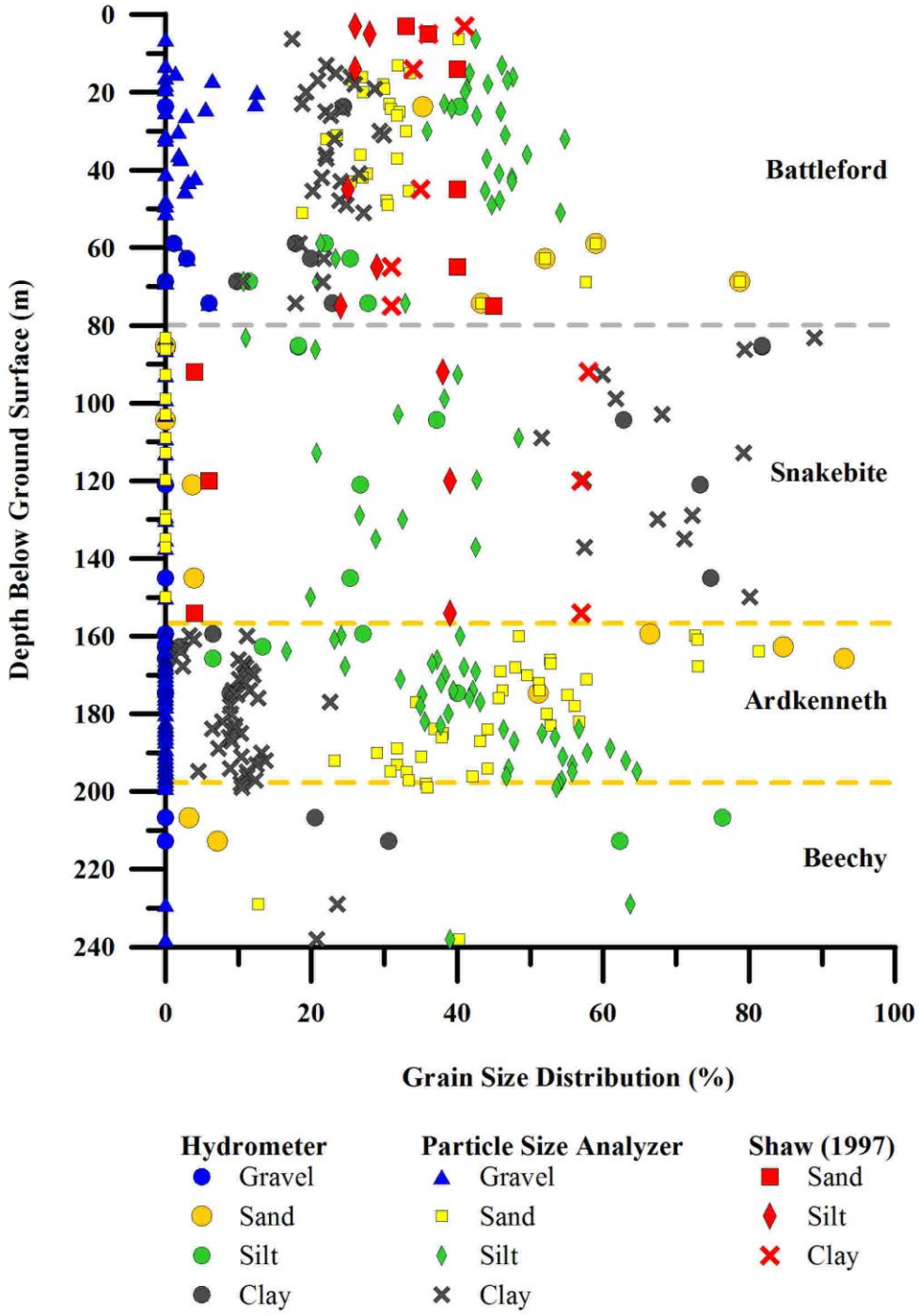

Figure 4.4. Grain size distribution versus depth from the 2013 King site core and Shaw (1997; red symbols). The legends reflect grain size percentages of the total sample. The size distributions are as follows: gravel = 2-4.75 mm; medium and fine sand are grouped together in the figure as sand: medium sand = 0.425-2 mm, fine sand = 0.075-0.425 mm; silt = 0.005-0.075 mm; clay < 0.005 mm. The Shaw (1997) data is in agreement with the 2013 data.

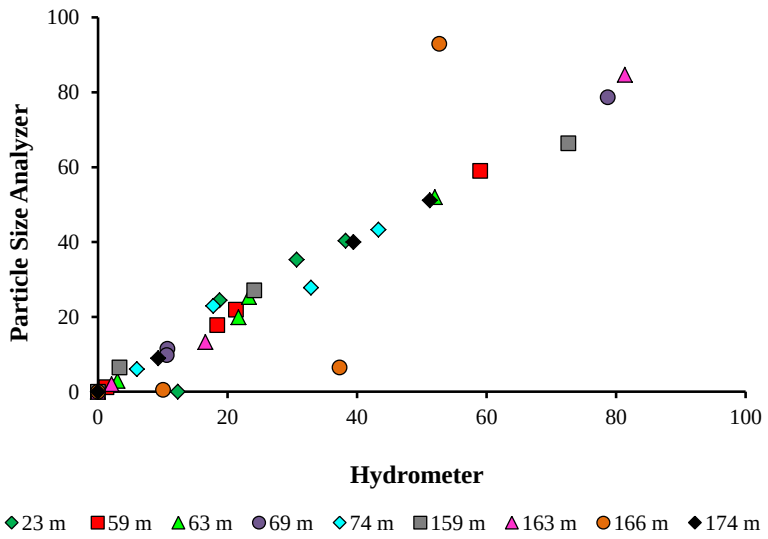

Figure 4.5. Grain size distributions measured on duplicate samples of the 2013 King site core by the hydrometer and particle size analyzer methods. The R^2 values (regression lines not shown) for the individual sample correlations are summarized in Table 4.2.

The TC, TOC, and TIC versus depth are presented in Figure 4.6. TOC is low throughout the Battleford with a μ of 0.62 ± 0.16% while TIC has a μ of 0.98 ± 0.26% (n = 36). The TOC increases across the till-clay boundary to a μ of 0.95 ± 0.15% while TIC decreases to a μ of 0.03 ± 0.04%. Through the Ardkenneth, TOC decreases to a μ of 0.56 ± 0.25% (n = 20), but increases at the inferred Beechy contact through to the base of the profile, with a μ of 0.81 ± 0.19% (n = 19) in the Beechy sediments. The μ TIC in the Ardkenneth and Beechy sediments is 0.002 ± 0.01% and 0.03 ± 0.05%, respectively (n = 20, n = 19). Shaw (1997) also notes a decrease in TIC at the till-clay boundary and low TIC through the Snakebite at the King site and attributes that to its low carbonate content. The measured values of the Cretaceous sediments from the 2013 King site core are all < 2% TOC. This is consistent with the TOC of Cretaceous Lea Park sediments at a site approximately 130 km north of the King site, which are reported to be between 0.7–2.0% (Whittaker et al., 1988).

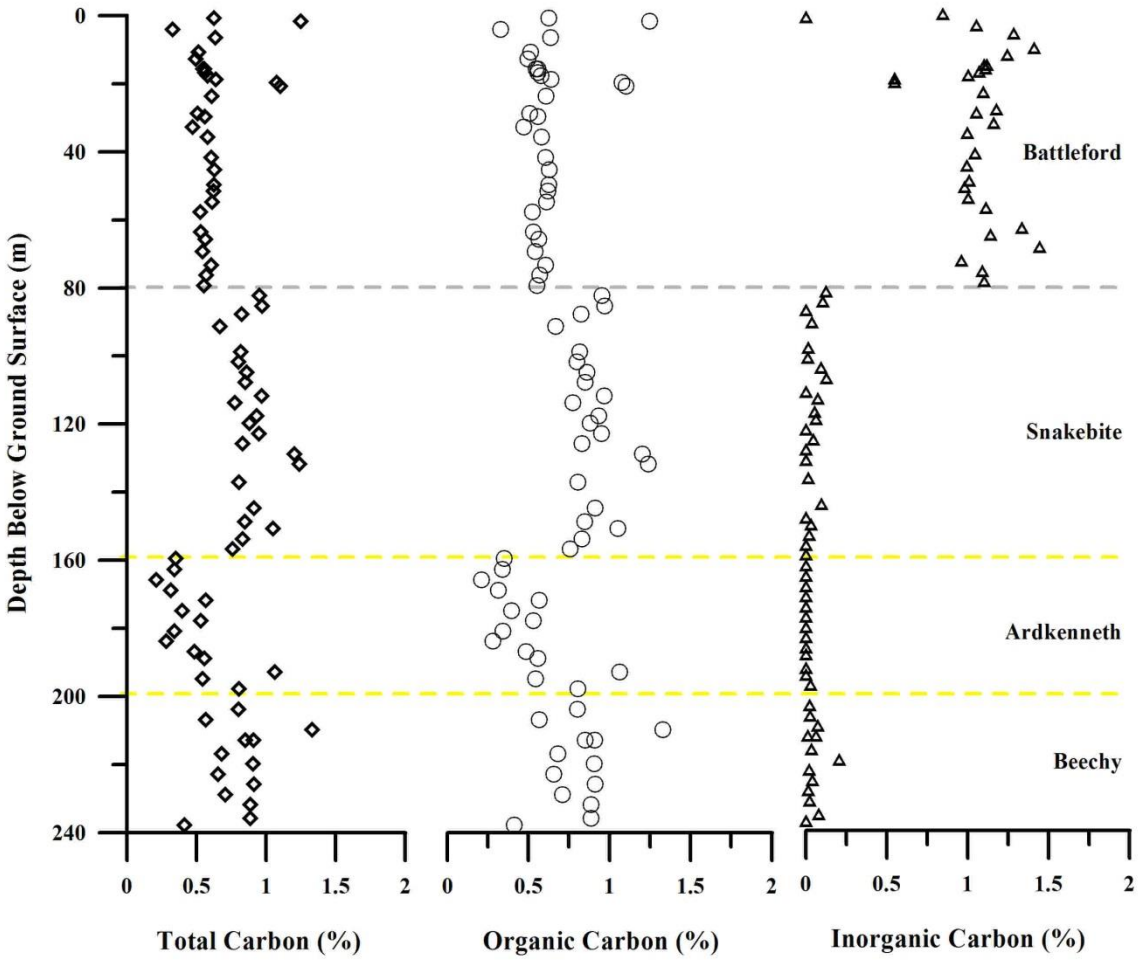

Figure 4.6. Carbon forms versus depth of core samples collected at the King site in 2013.

4.3 Stable isotopes of pore water

The $\delta^{18}O$ and $\delta^{2}H$ depth-profiles from the core samples collected at the King site in 2013 are presented in Figure 4.7. The μ and σ of the vapour equilibration samples and the squeezed samples for each unit are summarized in Table 4.3. Samples that lie outside the local trends within the profile, discussed below, are not included in the calculation of the μ and σ in Table 4.3. Both the $\delta^{18}O$ and $\delta^{2}H$ profiles follow the same trends with depth: the isotope values are variable from surface to the oxidized-unoxidized till contact at ~5 m BGS, and are consistent with modern precipitation in central Saskatchewan which is, on average approximately –130‰ VSMOW (Environment Canada, unpublished data, 1999–2008). The values decrease from ~5 to ~20 m BGS and remain relatively constant from ~20 m to ~50 m BGS. The isotope values

increase in a steep-linear fashion from ~50 m BGS across the till-clay interface to ~100 m BGS, below which the values increase in a near linear trend to the base of exploration at ~240 m BGS.

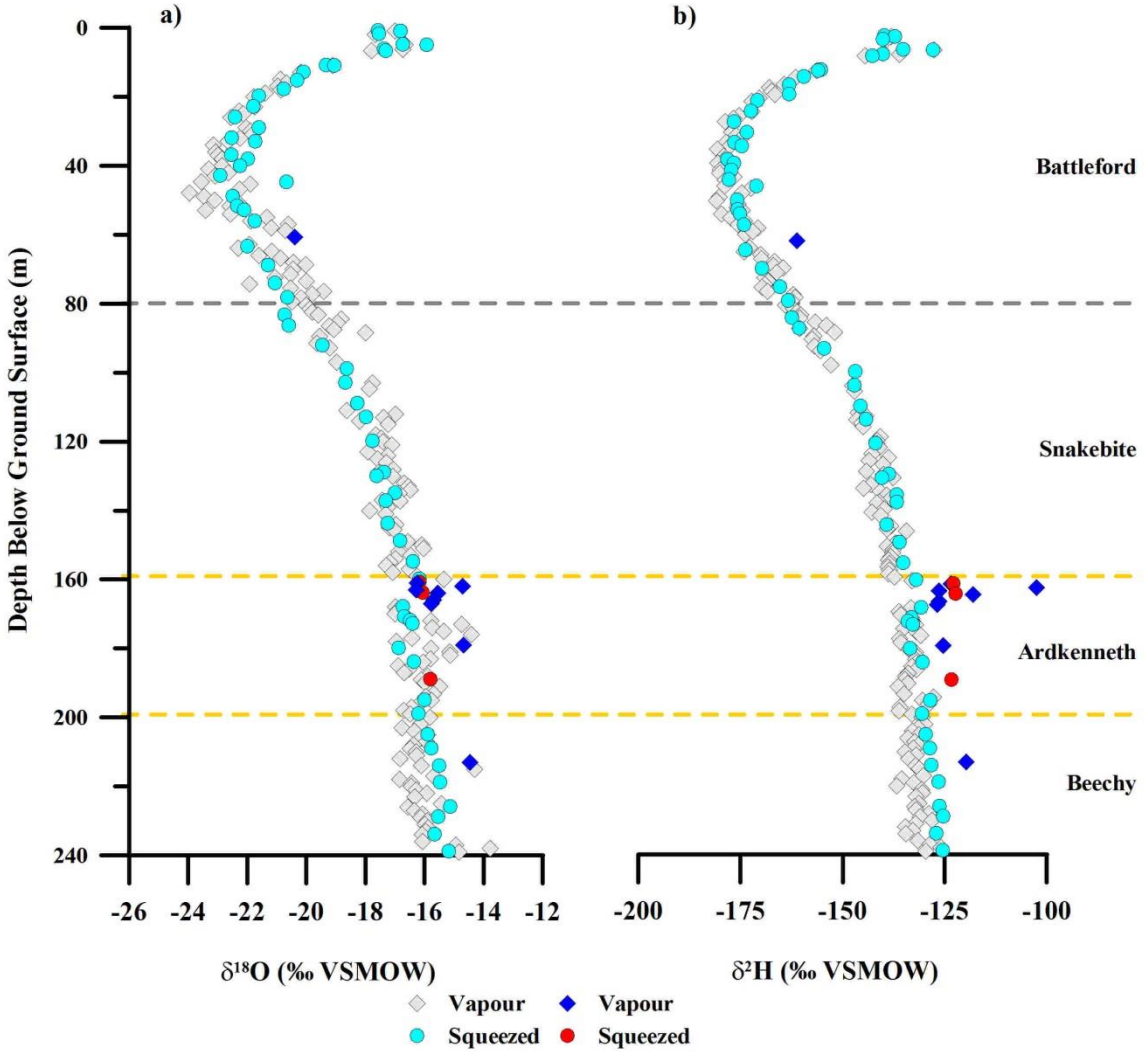

Figure 4.7. Pore water (a) $\delta^{18}O$ and (b) $\delta^{2}H$ measured using the vapour equilibration method (grey symbols) and on squeezed (light blue symbols) pore waters versus depth from the King site 2013 core. The dark blue and red symbols are vapour and squeezed samples, respectively, that deviate from the local trends within the profile. These deviations could be the result of contamination, evaporation during storage, or in the case of the values in the upper Ardkenneth, lateral groundwater flow from an external source.

Table 4.3. The μ and σ of the pore water δ^2H and $\delta^{18}O$ values measured by the vapour equilibration method and on squeezed pore waters from core samples collected at the King site in 2013.

	Vapour					Squeezed				
Unit	**n**	**δ^2H μ**	**δ^2H σ**	**$\delta^{18}O$ μ**	**$\delta^{18}O$ σ**	**n**	**δ^2H μ**	**δ^2H σ**	**$\delta^{18}O$ μ**	**$\delta^{18}O$ σ**
Oxidized Till	2	-139	1	-17	< 1	4	-138	2	-17	< 1
Unoxidized Till	60	-171	10	-21	2	27	-167	13	-21	2
Snakebite	54	-145	8	-18	1	15	-144	9	-18	1
Ardkenneth	32	-133	2	-16	1	9	-132	2	-16	< 1
Beechy	35	-132	2	-16	1	8	-127	2	-16	< 1

The results from both the vapour equilibration and squeezing methods are compared in Figures 4.8 (a) and (b). The δ^2H results have a slope of 1.00 and a R^2 value of 0.98 (Figure 4.8 (a)), and the $\delta^{18}O$ values have a slope of 0.91 and an R^2 value of 0.93 (Figure 4.8 (b)). The predicted values of squeezed δ^2H and $\delta^{18}O$ were calculated using the regression equations in Figures 4.8 (a) and (b) and plotted against the observed values in Figures 4.8 (c) and (d); these plots have high R^2 values as well. The residuals (observed squeezed values – predicted squeezed values) were calculated. Even distribution of residual values around 0 and lack of any pattern in a residual plot indicate that the variance between two methods is constant and that the model is valid (Yan, 2009). The plots of the predicted squeezed values versus the residuals for δ^2H and $\delta^{18}O$ shown in Figures 4.8 (e) and (f) demonstrate low residual values, the data cluster closely around 0, and there is no obvious pattern, indicating that the vapour and squeezed methods produce consistent results.

The data from all of the $\delta^{18}O$ samples are within the analytical error of the two methods. Seventeen of the 58 samples were outside of the combined analytical error for δ^2H of the two methods (± 3.25‰). In all but one of the samples, the δ^2H are heavier in the squeezed samples than the vapour samples. One thought on this difference is the length of time the squeezed samples were in storage prior to processing. These 17 samples were squeezed between 61 and 263 d post-collection. Meanwhile the vapour samples were all analyzed within 41 d of sample

collection. This issue may be worth further investigation, yet the overall conclusion of this study is that the two methods of measuring pore water isotope values yielded the same results.

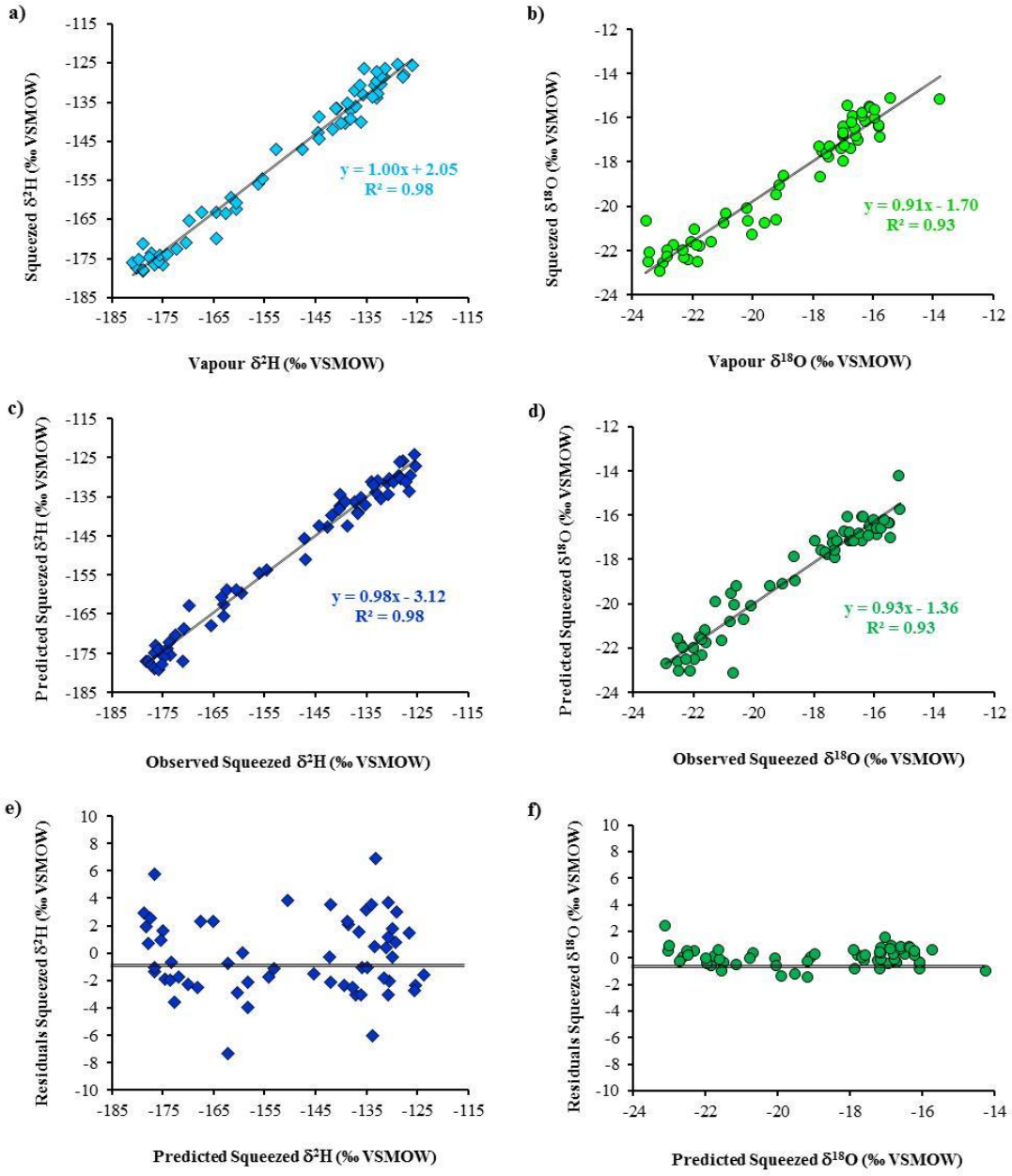

Figure 4.8. (a) δ^2H and (b) $\delta^{18}O$ cross-plots of the pore waters produced by squeezing and measured by the vapour equilibration method on the King site 2013 core samples. (c) δ^2H and (d) $\delta^{18}O$ cross-plots of the squeezed data and the values predicted by the regression equations in (a) and (b). (e) and (f) show predicted values of δ^2H and $\delta^{18}O$ versus the residuals of both, respectively.

The $\delta^{18}O$ and $\delta^{2}H$ data from the King site 2013 core plot on the Saskatoon Meteoric Water Line (SMWL) (Figure 4.9; Environment Canada, unpublished data, 1999–2008). This correlation is in keeping with results of previous studies at the King site (Hendry and Wassenaar, 1999; Hendry and Wassenaar, 2009). A strong correlation of $\delta^{18}O$ and $\delta^{2}H$ to a local MWL confirms that: the isotopic values were not impacted by evaporation or isotopic exchange between the pore waters and minerals within the sediments; that the shape of the isotope profiles are attributable to mixing of isotopically distinct pore waters; and that the pore waters are largely meteoric in origin (Hendry and Wassenaar, 1999; Hendry et al., 2011). Evaporation can disturb this correlation because $\delta^{18}O$ is more susceptible to that kinetic isotope effect (Dansgaard, 1964). The $\delta^{2}H$-$\delta^{18}O$ correlation coefficients for the vapour and squeezed data are 0.98 and 0.99, respectively (not shown). Given these strong correlations and since the 2013 data plot along the SMWL, it will be assumed that the samples were not affected by evaporation or exchange processes and are representative of in-situ pore water isotope values. As evaporation is not of concern, the interpretations into either of the profiles should be synonymous; what is interpreted from the $\delta^{2}H$ data can to be applied to the $\delta^{18}O$ profile (Hendry and Wassenaar, 1999; Hendry and Woodbury, 2007). Hendry and Wassenaar (2009) opted to interpret the $\delta^{2}H$ profile at the King site because the analytical error was lower with respect to the range of $\delta^{2}H$ values over that profile than for $\delta^{18}O$. For comparison to previous studies, specifically for the purpose of the transport modeling, the $\delta^{2}H$-depth profile will be the focus of subsequent interpretations.

The dark-coloured symbols in Figure 4.7 are 12 samples that deviate outside of the local trends within the pore water isotope profiles. These deviations are less noticeable in the $\delta^{18}O$ profile perhaps due to the greater spread in values compared to the $\delta^{2}H$ profile. Other than one vapour equilibration sample at 60 m BGS and one squeezed sample at 213 m BGS, the majority of the deviations occur in the Ardkenneth aquifer: vapour equilibration samples from 161, 162, 163, 164, 166, 167, and 179 m BGS and squeezed samples from 160, 163, and 188 m BGS. Initially these samples were considered contaminated by drill fluid, sample collection or handling error, or evaporation during storage. However, when these 12 samples were isolated on the SMWL (Figure 4.10), they plot on the line, aside from one sample (162 m BGS) which plotted slightly above the line, perhaps towards the values of the drill fluid (Figure 4.9). If these samples were contaminated by drill fluid, the $\delta^{2}H$ of the pore waters should trend towards the

spiked δ^2H values of the drill fluids. As the samples plot on the SMWL, evaporative and exchange processes can be ruled out.

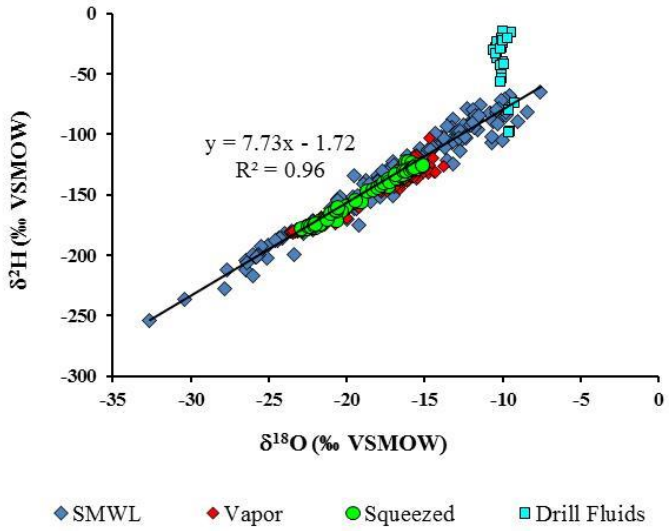

Figure 4.9. δ^2H versus $\delta^{18}O$ of pore waters measured on the King site core in 2013, the isotopes of deuterium-spiked drill fluids collected throughout drilling, and values of precipitation in Saskatoon, SK (Saskatchewan Meteoric Water Line (SMWL); Environment Canada 1999 – 2008, unpublished data, and associated linear equation).

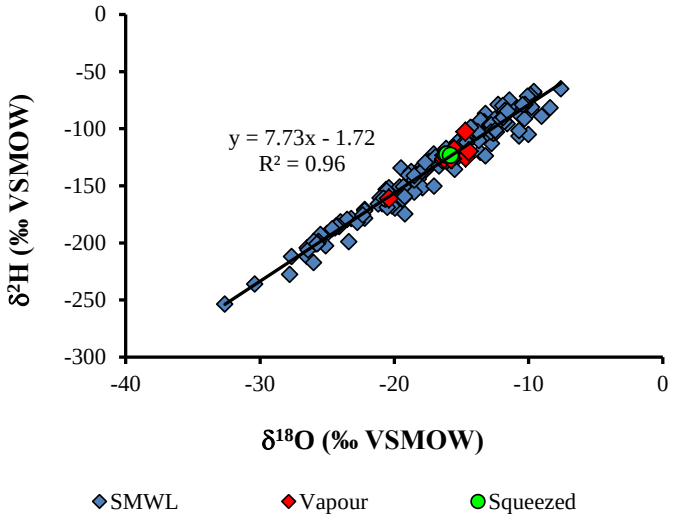

Figure 4.10. δ^2H versus $\delta^{18}O$ of the SMWL data (Environment Canada, unpublished data, 1999–2008), shown in Figure 4.9, along with the 12 isotope samples from the King site 2013 data that deviate outside of local trends within the profiles. The data plots directly on the SMWL, indicating that these samples were not affected by evaporative or exchange processes.

Deviations from the δ^2H profiles previously reported at the King site are attributed to geologic heterogeneities such as sand layers which increase *K* (Harrington et al., 2007; Hendry and Wassenaar, 2009). The grain size distribution (Figure 4.4) indicates that the samples from 160-188 m BGS are from an interval of high sand content (50–93%). The deviations in the δ^2H profile across this interval could be the result of this high sand content creating a zone of increased *K*, enabling a component of lateral flow. Harrington et al. (2007) used transport modeling to suggest that anomalous trends in solute data at the King site are the result of sand deposits creating preferential pathways for lateral solute transport by advection. A peak in the δ^2H profile occurs in the top 10 m in the Ardkenneth and does not appear to affect samples in the Snakebite. Due to the possibility of lateral advective transport occurring in the Ardkenneth, the δ^2H values from the 160-188 m BGS interval were not included in the one-dimensional transport modeling conducted for this study. Similar deviations appear in other parameters measured in this study and will be discussed further on.

Figure 4.11 features the δ^2H profile of the 2013 data, along with δ^2H data collected at the site between 1995 and 2004 (Hendry and Wassenaar, 1999; Hendry and Wassenaar, 2009). The good agreement between these data sets demonstrates the reliability of the methods used to procure the data and that solute transport mechanisms in the aquitards have not changed over the time frame between measurements. The increased resolution of the 2013 data set confirms that the trends displayed by the low-resolution data sets represent in-situ conditions.

The decrease the δ^2H values from ~5 to ~20 m BGS reflects mixing of precipitation with ^2H-depleted pore waters at depth in the till over the last 10-12 ka. The isotopic value of precipitation is enriched in ^2H due to warming of the climate over the Holocene (Hendry and Wassenaar, 1999; Hendry et al,. 2011).

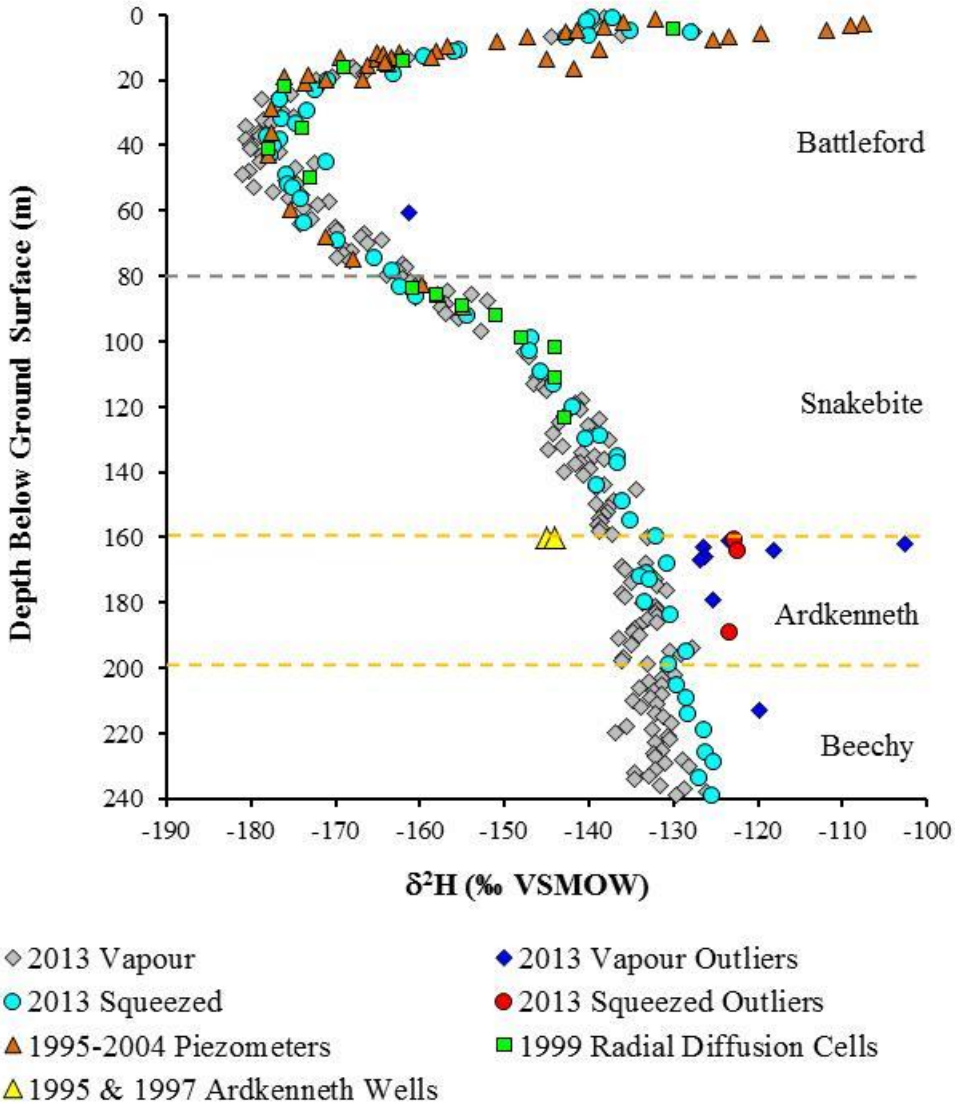

Figure 4.11. Pore water δ^2H data collected at the King site by various methods versus depth: 2013 vapour and 2013 squeezed – this study; 1995-2004 piezometers – Hendry and Wassenaar, 1999 and Hendry and Wassenaar, 2009; Radial Diffusion Cells – Hendry and Wassenaar, 1999; 1995 and 1997 domestic wells in the Ardkenneth – Hendry and Wassenaar, 1999.

Between ~20 and ~50 m BGS, δ^2H values are low (μ = –177‰ VSMOW) and relatively constant (± 3‰). Hendry and Wassenaar (1999) and Hendry et al. (2011) attribute these ^2H-depleted values to pore waters emplaced by the glacier during deposition of the Battleford till (20-30 ka BP). The $\delta^{18}O$ of a large glacial lake that covered much of present-day Manitoba and parts of Saskatchewan and Ontario between 11.7-7.7 ka BP, Lake Agassiz, is reported to have

been –24 to –25‰ VSMOW (Remenda et al., 1994; Birks et al., 2007). The corresponding δ^2H values calculated via the SMWL are –187 to –195‰ VSMOW. The μ $\delta^{18}O$ and δ^2H values of –23‰ and –177‰ measured between 20 and 50 m BGS on the 2013 King site core are consistent with isotopic values of glaciogenic surface waters in the Canadian prairies (Ferguson and Jasechko, 2015).

The hydraulic conditions at the King site further support the conclusion that the pore waters in the 20-50 m depth interval in the Battleford till are glaciogenic. The measured *K* and hydraulic gradient (*i*) of the unoxidized till are reported as 3.2×10^{-11} m s^{-1} and 0.014, respectively (Shaw and Hendry; 1998). The thickness of the Battleford at the King site (80 m), the lack of observed fractures throughout that unit, and the low vertical *v* calculated for the unoxidized till at the site (0.5–0.8 m/10 ka), are conditions conducive for a long residence time of pore waters. Furthermore, the curvilinear shape of the δ^2H profile is typical of groundwater systems in which diffusion is the dominant transport mechanism (Hendry et al., 2011). The King site δ^2H profile is in keeping with results of a δ^2H profile in an older glacial till in Saskatchewan about 160 km north of the King site. Numerical transport modeling of that data set confirmed that diffusion was the main transport mechanism through the Sutherland Group till at that site (Remenda et al., 1996; Hendry and Wassenaar, 2004).

The δ^2H profile across the till-clay interface (50–100 m BGS) is the result of diffusive mixing; the ^2H-depleted glacial water has, over geologic time, mixed with the ^2H-enriched pore waters of the upper Snakebite (Hendry and Wassenaar, 1999; Hendry and Woodbury, 2007). Although the Cretaceous sediments were deposited in a marine setting and the δ^2H values of the seas covering the region in the Upper Cretaceous are reported to be between 0 to –70‰ (Cadrin et al., 1995), the δ^2H values measured on the pore waters of the Cretaceous sediments at the King site are depleted in ^2H by comparison (–147 to –125‰ VSMOW). This discrepancy suggests that the in-situ pore waters are not representative of connate waters (Hendry and Wassenaar, 1999; Wassenaar and Hendry, 1999). Below the till-clay interface, the linear increase in δ^2H with depth is similar to isotopic profiles collected in Cretaceous sediments elsewhere in Saskatchewan. Hendry et al. (2013) measured pore water isotopes that increase linearly over hundreds of meters of depth through the Cretaceous clays and shales in southwestern Saskatchewan. That trend is attributed to long-term mixing of meteoric waters with brines located deep in the Williston Basin.

4.4 Pore water chemistry

The Cl^- and Br^- concentration-depth profiles presented in Figure 4.12 (a) and (b) are similar; concentrations increase from ~1 to ~12 m BGS, then decrease and remain relatively constant through the till to the till-clay contact. Below this contact, the concentrations gradually increase, peaking just below the top of the Ardkenneth, and decrease to the bottom of the Ardkenneth. Concentrations increase through the Beechy with maximum values encountered at the base of exploration.

In the oxidized till (0-5 m BGS), Cl^- ranges between 37-53 mg L^{-1}. Through the unoxidized till (5-80 m BGS), the minimum Cl^- is 22 and maximum is 113 mg L^{-1}. The μ Cl^- in the Snakebite, Ardkenneth, and Beechy members are 364 (± 200; n = 14), 953 (± 100; n = 12), and 1423 (± 433; n = 10) mg L^{-1}, respectively.

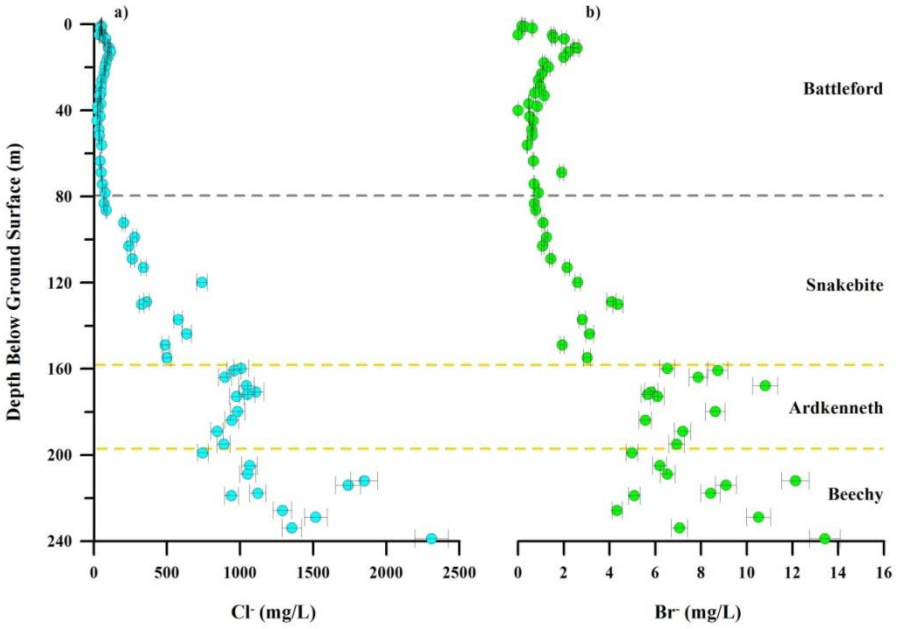

Figure 4.12. Pore water (a) Cl^- and (b) Br^- concentrations of squeezed pore waters from the 2013 King site core versus depth. Error bars represent the ± 5% analytical error.

While the shapes of the Cl^- and Br^- profiles are similar, the Br^- concentrations are, on average, nearly 200% less than the Cl^- concentrations. This difference is typical of pore waters at the site, and the Cl^-/Br^- ratios are in consistent with previous data (Hendry et al., 2000). The μ

Br^- in the oxidized till is 0.3 mg L^{-1} (± 0.3; n = 4), increasing to a μ of 1 mg L^{-1} (± 0.7; n = 25) through the unoxidized till. From a μ of 2 mg L^{-1} (± 1; n = 14) in the Snakebite, the μ Br^- increases to 7 mg L^{-1} (± 2; n = 12) in the Ardkenneth and to 8 mg L^{-1} (± 3; n = 10) in the Beechy.

Figure 4.13 includes the King site data from Figure 4.12 along with Cl^- and Br^- concentrations of water samples collected from piezometers at the King site and from two domestic wells completed in the Ardkenneth (~160 m BGS) ~2 km south of the site. These samples were collected on several occasions between 1995 and 1998 (Hendry et al., 2000; Vengosh and Hendry, 2001). Where the depths of samples were within < 1 vertical m, concentrations of Cl^- and Br^- from the piezometers were plotted against the squeezed concentrations (Figure 4.14 (a) and (b)). Both the Hendry et al. (2000) and Vengosh and Hendry (2001) piezometer data sets show strong correlations to the 2013 squeezed data ($R^2 > 0.80$). The good agreement indicates that the squeezed concentrations are representative of in-situ pore water concentrations. The highest concentrations of Cl^- and Br^- are the samples from the domestic water wells in the Ardkenneth ~2 km south of the King site. (The data points in Figures 4.13 and 4.14 are the average of the two samples.) The distance away from the King site may account for the variability between the wells and squeezed data.

Notable in the data sets presented in Figure 4.13 are the peaks in concentrations between ~11-15 and ~160-170 m BGS. The previous studies attributed the peak between ~11-15 m BGS to the presence of permeable sand streaks introducing pore waters from an alternate source via lateral migration (Hendry et al., 2000; Vengosh and Hendry, 2001). A similar peak in Cl^- was measured in the Battleford till at a site ~10 km southwest of the King site (Powell, 2010). At that site, Cl^- values increased to 200 mg L^{-1} between ~8-12 m BGS, then declined through the unoxidized till. This indicates that the presence of sand layers is prevalent in the Battleford till in this region. Noteworthy is the lack of a peak at ~8-12 m BGS in the δ^2H data set. Hendry et al. (2000) noted this discrepancy and concluded that the Cl^- and Br^- were transported from an unknown external source. This would suggest that the δ^2H of the source water would be similar to that of the pore water at the King site. The consistency between the peaks in Cl^-, Br^- and δ^2H in the upper Ardkenneth (between ~160-170 m BGS), however, suggests that those pore waters

are from another source (with a slightly different δ^2H value), which are transported laterally due to increased *K*.

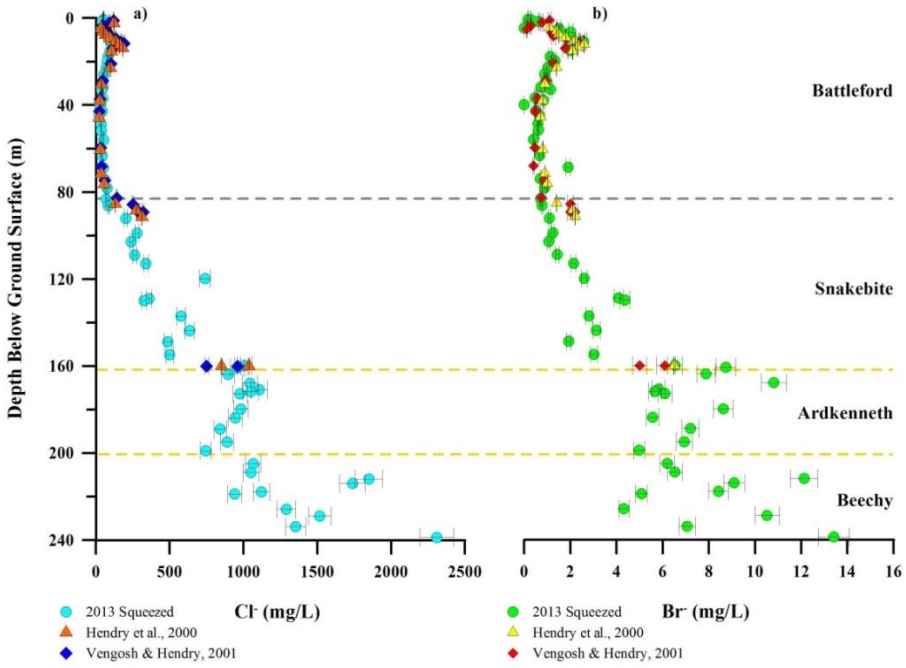

Figure 4.13. Pore water (a) Cl^- and (b) Br^- concentration profiles of squeezed pore waters from the 2013 King site core versus depth including previously published data (Hendry et al., 2000; Vengosh and Hendry, 2001). Analytical error is ± 0.5% on Hendry et al. (2000) data and ± 6% (Br^-) and ± 2% (Cl^-) for the Vengosh and Hendry (2001) data.

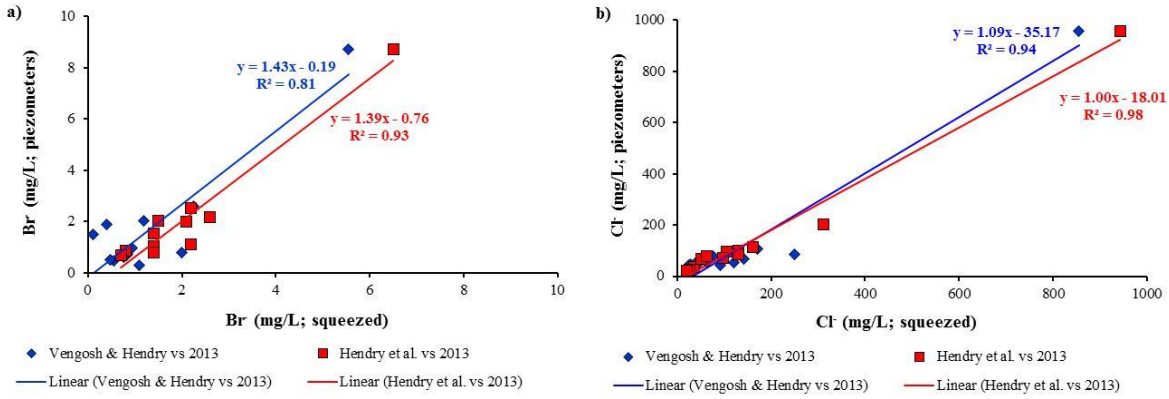

Figure 4.14. Cross-plots of (a) Br^- and (b) Cl^- data from previous studies (Hendry et al., 2000; Vengosh and Hendry, 2001) versus squeezed pore waters from the 2013 King site core.

The Ardkenneth aquifer extends as far south as Swift Current, SK (~200 km from Birsay, SK), ranging in thickness from 3-70 m (Maathuis and Simpson, 2007). This aquifer outcrops or is very near surface in southern SK, and is hydraulically connected to the Quaternary-aged Empress Group sediments and Lake Diefenbaker. Reported *K* is variable throughout the Ardkenneth, ranging from 2.3 x 10^{-05} to 1.1 x 10^{-08} m s^{-1} (Maathuis and Simpson, 2007). In a study over an area ~150 km^2 around the Birsay – Luck Lake – South Saskatchewan River region, Christiansen (1990) reported Cl^- concentrations ranging from 4 to 993 mg L^{-1} in the Ardkenneth. The variability in *K* and Cl^- concentrations as well as the regional extent of this aquifer and connectivity to numerous water-bearing units offers a number of possibilities for an alternate source. The most recent hydraulic perturbation in the area was the damming of the South Saskatchewan River into Lake Diefenbaker, starting in 1965. That event is reported to have increased water levels and reversed water flow direction in the Ardkenneth by 1966 (Van Everdingen, 1967). By the equation (Schulz and Zabel, 2013):

$$L = \sqrt{2D_e t} \qquad \text{(Eq. 4.1)}$$

the distance a solute has diffused (*L*, length) over an amount of time (*t*) can be calculated. Using a value of 1.6 x 10^{-10} m^2 s^{-1} for the D_e of Cl^- in the Snakebite clay (Hendry et al., 2000) and the time frame of 48 years, diffusion across the Snakebite-Ardkenneth interface is ~ 0.7 m. Using a D_e of 1.7 x 10^{-10} m^2 s^{-1} for δ^2H (Hendry and Wassenaar, 1999) in Eq. 4.1, L is ~ 0.7 m. The sample spatial resolution of the Cl^- and δ^2H profiles over the Snakebite-Ardkenneth interface (1 m or greater) cannot demonstrate this diffusion length into the Snakebite. However the lack of a response in the Snakebite greater than 1 m coincides with timing of the event and it seems plausible that the filling of the reservoir could be the cause of the perturbations in the Cl^- and δ^2H profiles.

Hendry et al. (2000) propose that the source of the low Cl^- concentrations through the till is the same glacial water that imparted the depleted ^2H signature. Further evidence that the pore water in the Cretaceous sediments is not connate water is found in the Cl^- data. The average concentration of Cl^- in seawater is ~19, 000 mg L^{-1} (Kresic, 2006); yet the Cl^- is notably lower in the Cretaceous sediments at the King site, suggesting that those pore waters are not representative of the original marine waters deposited with the sediment. Hendry et al. (2000) propose that the Cl^- diffused upwards out of the marine sediments into layers of the Snakebite

and glacial deposits over the past 1.8 Ma which were eventually eroded. It has also been suggested that the original pore waters have been replaced by recharge that entered these sediments since deposition (Hendry and Wassenaar, 1999; Wassenaar and Hendry, 1999).

Vengosh and Hendry (2001) suggest that the Snakebite pore waters are a result of mixing of the Cretaceous waters with the glacial water. A cross-plot of the Br^--Cl^- data (Figure 4.15(a)) supports a mixing hypothesis, given the distinctive groupings of the till pore waters and the Ardkenneth-Beechy pore waters. The Snakebite pore waters are located between these two end members. This relationship between Br^- and Cl^- was noted in older Cretaceous shales about 350 km to the southeast, near Weyburn, Saskatchewan (Hendry et al., In progress). These older sediments display a linear trend in the Br^--Cl^- data (Figure 4.15 (b)). The agreement between these data sets suggests transport of pore water through the Cretaceous sediments may be consistent over hundreds of kilometers.

A few of the King site 2013 Br^--Cl^- data points from the Ardkenneth aquifer plot above the mixing line that is inferred between the samples representing the till end member and the remaining samples representing the Ardkenneth-Beechy end member. This observation is consistent with the waters in the depth interval ~160-170 m BGS believed to have originated from an external source.

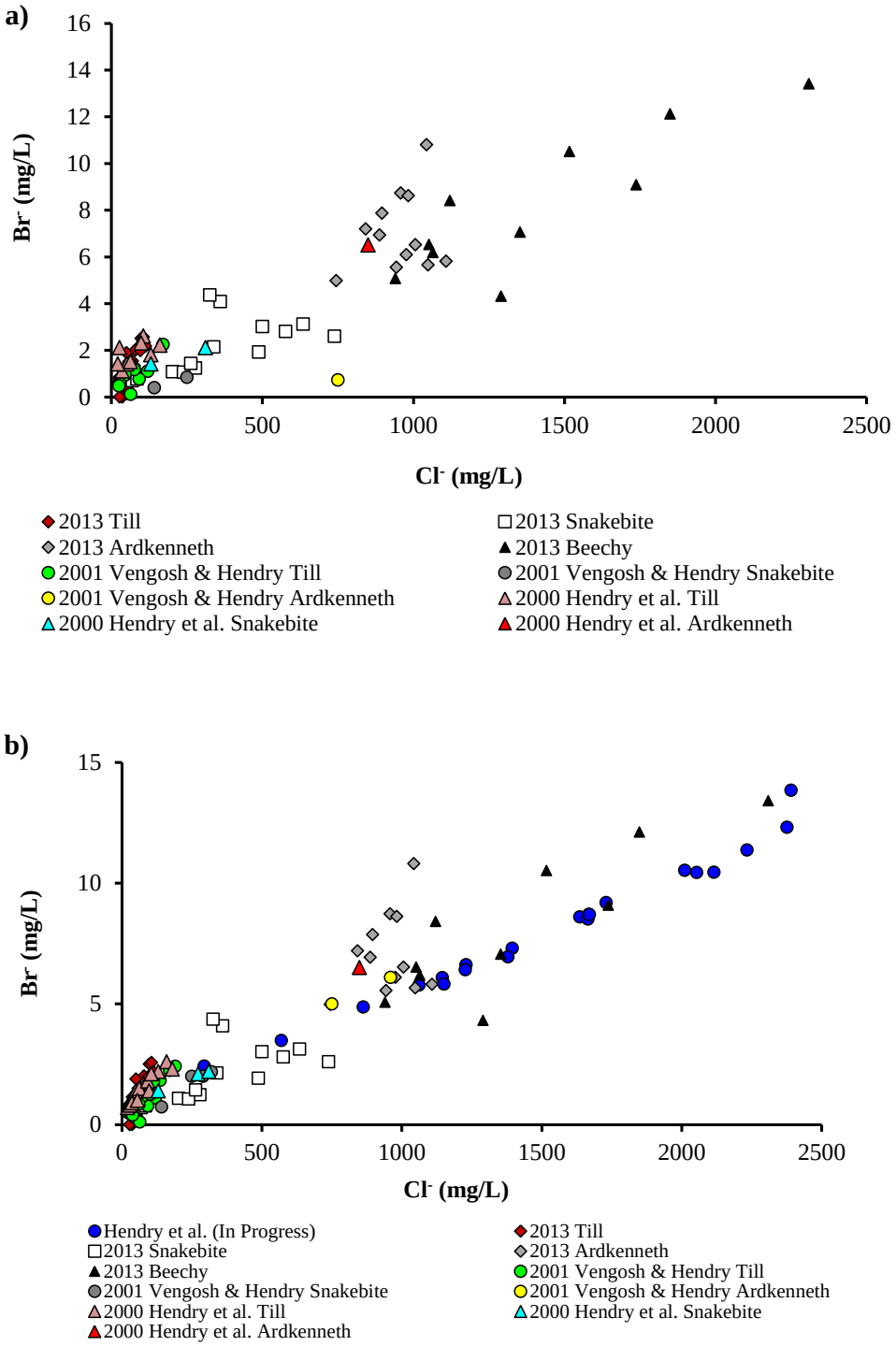

Figure 4.15. Dissolved Cl^- versus Br^-: (a) pore waters from squeezed cores (2013) and piezometers at the King site and a domestic well nearby (Hendry et al., 2000; Vengosh and Hendry, 2001) and (b) data from (a) plus pore water Cl^- and Br^- concentrations from a site in southeastern Saskatchewan squeezed from till and Cretaceous shales (Hendry et al., In progress).

4.5 Dissolved organic gases

The concentrations of dissolved CH_4 versus depth from the 2013 King site core are presented in Figure 4.16. Gases from IsoJars® containing > 2 mole % O_2 were considered to have leaked and likely reflect a considerable degree of atmospheric contamination. A total of 16 of the 82 samples analyzed experienced ingress of O_2 likely due to poor seals and these outliers will not be discussed further. The measured CH_4 concentrations at three, seven, and 10 months post-collection are within the ± 10% analytical error of the GC. This indicates that the CH_4 concentrations in the IsoJars® reached equilibrium within the initial three months, and that leakage did not occur between the three and 10-months measurements.

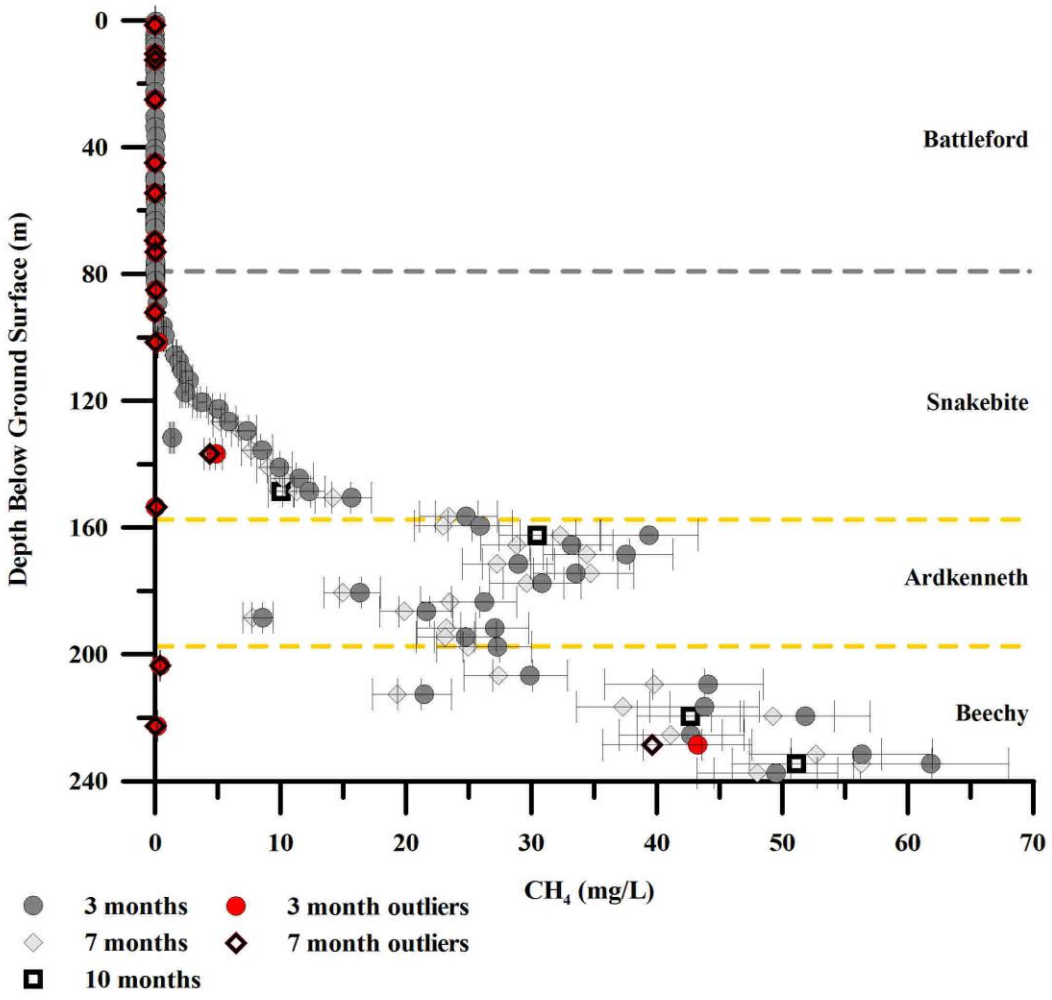

Figure 4.16. CH_4 concentrations measured on core samples from the King site three, seven, and 10 months post-collection versus depth. Error bars represent analytical error of ± 10%.

A strong linear correlation exists between the CH_4 concentrations measured at three and seven months (Figure 4.17; $R^2 = 1.00$). These static concentrations with time suggest that neither production nor consumption of CH_4 occurred in the IsoJars® over the time period of analysis. This correlation also suggests that the concentrations in the IsoJars® reached equilibrium within the initial three month storage period. As previously mentioned, Hendry et al. (2016 (a)) report that CH_4 from geologic materials similar to those studied at the King site reaches equilibrium in IsoJars® in < 10 d. The μ and σ of CH_4 concentrations through each unit measured at three and seven months are summarized in Table 4.4. Given the strong positive correlation between the measurement times, the three month CH_4 concentrations will be the focus of the following discussion and the transport modeling.

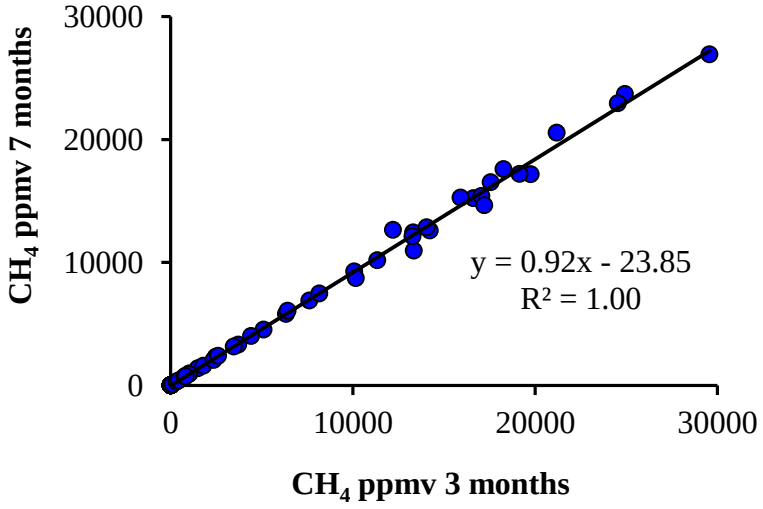

Figure 4.17. Cross-plot of CH_4 measured on the King site samples at three and seven months after collection. The R^2 value of 1.00 indicates a strong correlation, suggesting the CH_4 concentration did not change between measurements.

CH_4 concentrations were below detection limit of the GC (< 5 ppmv) throughout the entire depth of the till and across the till-clay contact to a depth of 89 m BGS. Concentrations increase from 0.2 mg L^{-1} at 89 m BGS through the Snakebite, peaking in the Ardkenneth at 39 mg L^{-1} at 162 m BGS. Concentrations then decrease through the Ardkenneth to 8 mg L^{-1} at 188 m BGS and then increase into the Beechy member, to 49 mg L^{-1} at the base of the borehole (~240 m BGS).

Bernard et al. (1978) estimate that gas loss from exposed core sections during sampling is 0.1 mm/1 min. Considering the cross-sectional areas of the cores collected in this study, that rate equates to ~3.2 x 10^{-6} m^3 min^{-1}. During sampling, cores were exposed for less than 15 min; according to Bernard et al.'s estimation, very little gas would escape over that time frame. It is assumed that significant gas loss did not occur during sampling for this project.

Table 4.4. The μ and σ of CH_4 and C_2H_6 concentrations measured in the IsoJars® at three and seven months after collection. Outliers were not included in the calculations of μ and σ.

		Three months				Seven months			
		CH_4 (mg L^{-1})		C_2H_6 (mg L^{-1})		CH_4 (mg L^{-1})		C_2H_6 (mg L^{-1})	
Unit	n	μ	σ	μ	σ	μ	Σ	μ	σ
Battleford	23	0.01	0.02	0.00	0.02	0.00	0.01	0.00	0.00
Snakebite	20	6	6	0.03	0.02	5	6	0.02	0.02
Ardkenneth	14	27	8	0.05	0.05	25	7	0.03	0.04
Beechy	9	45	13	0.21	0.07	41	12	0.17	0.06

The peak in CH_4 in the Ardkenneth was investigated in a similar manner as Cl^- and δ^2H using Eq. 4.1. Using a D_e for CH_4 of 2.4 x 10^{-10} m^2 s^{-1} (Jacops et al., 2014), a diffusion distance of ~0.9 m was obtained. The CH_4 profile is not high enough resolution over the Ardkenneth-Snakebite contact (3 m or greater) to show this diffusion length. Yet the transition in CH_4 concentrations over the Ardkenneth-Snakebite contact is abrupt, similar to Cl^- and δ^2H, suggesting that diffusion of CH_4 into the Snakebite from the peak in the upper Ardkenneth has not yet occurred. This supports the possibility the timing of the peak is coincident with the filling of the reservoir into Lake Diefenbaker.

The impact of under- or over-estimating θ_v on the dissolved CH_4 concentrations was tested by varying θ_v. Samples from the ~160-170 m BGS depth interval in the upper Ardkenneth were of particular interest due to their high sand content and resulting reduced cohesion. Figure 4.18 demonstrates that a large increase in the θ_v (70%) would be required to reduce the dissolved concentrations to values consistent with data measured above and below this interval. Such an increase is unlikely, and the fact that the peak in CH_4 corresponds to peaks in the Cl^-, Br^-, δ^2H and $\delta^{18}O$ profiles across the same depth interval further confirms that the trend in the CH_4 data

across the Ardkenneth is not an artifact of sample collection, the result of analytical error, or due to an erroneous θ_v used in the calculation of dissolved gas concentration. As noted above, this interval contains the highest sand content (Figure 4.4) and the increase in concentrations could be indicative of a zone of increased *K* allowing lateral migration of the solutes from an external source.

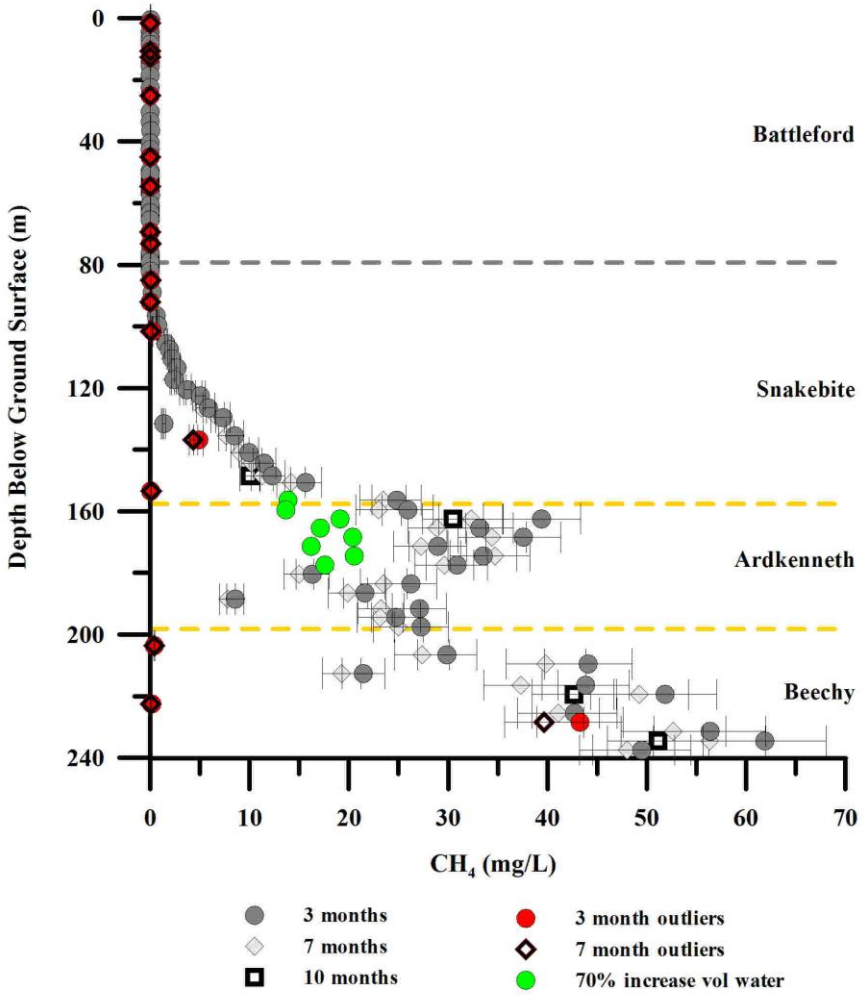

Figure 4.18. The CH_4 versus depth from the 2013 King site core with samples in green showing that a 70% increase in the θ_v calculated in the cores would be necessary for CH_4 concentrations through the upper Ardkenneth to follow the local trend of the surrounding samples.

Given the similarity of the shapes of the CH_4 and Cl^- profiles, the relationship between the two species was investigated further. Figure 4.19 is a cross-plot of CH_4 versus Cl^- from the 2013 King site core; the plot shows that these data are correlated ($R^2 = 0.59$). This correlation

suggests that CH_4 exhibits conservative behaviour in the profile, similar to the conservative species Cl^-, Br^- and the isotopes of pore water. If the data above the till-clay contact (measured CH_4 values < 5 ppmv) and the data points within the high *K* zone in the Upper Ardkenneth (~156-186 m BGS) are excluded, the CH_4 profile from the 2013 King site sediments displays a near-linear increase in concentration with depth (Figure 4.20 (a)). If the corresponding data points are also excluded from the Cl^- profile, the CH_4 data actually have a stronger linear correlation with depth than the Cl^- data (R^2 CH_4 = 0.86 vs. R^2 Cl^- = 0.79). This supports the inference that CH_4 could be behaving as a conservative tracer at the King site.

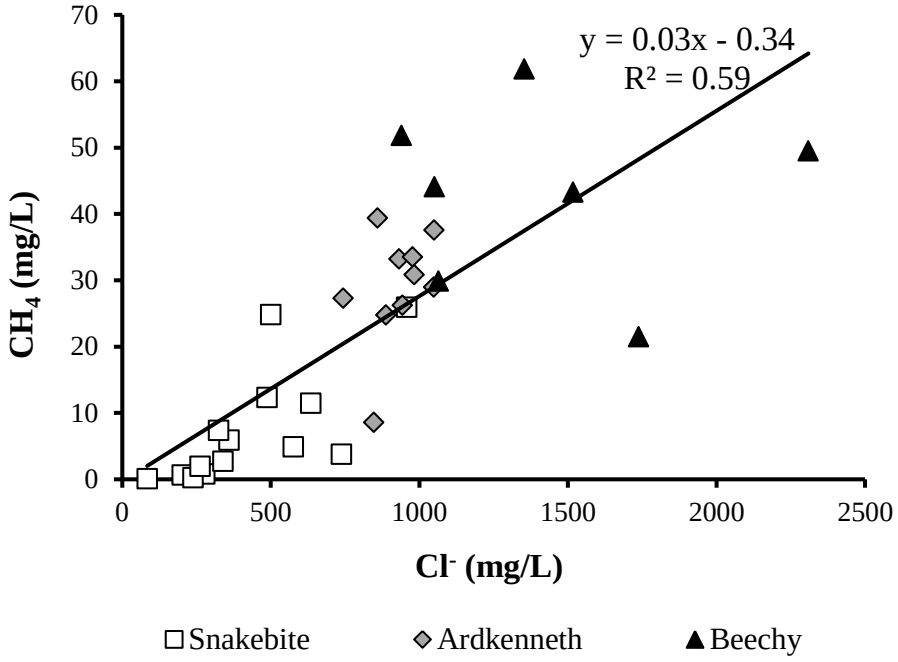

Figure 4.19. Cross-plot of CH_4 and Cl^- concentrations from the King site 2013 data set. The data are plotted according to geologic unit. The linear regression demonstrates the correlation between the two species.

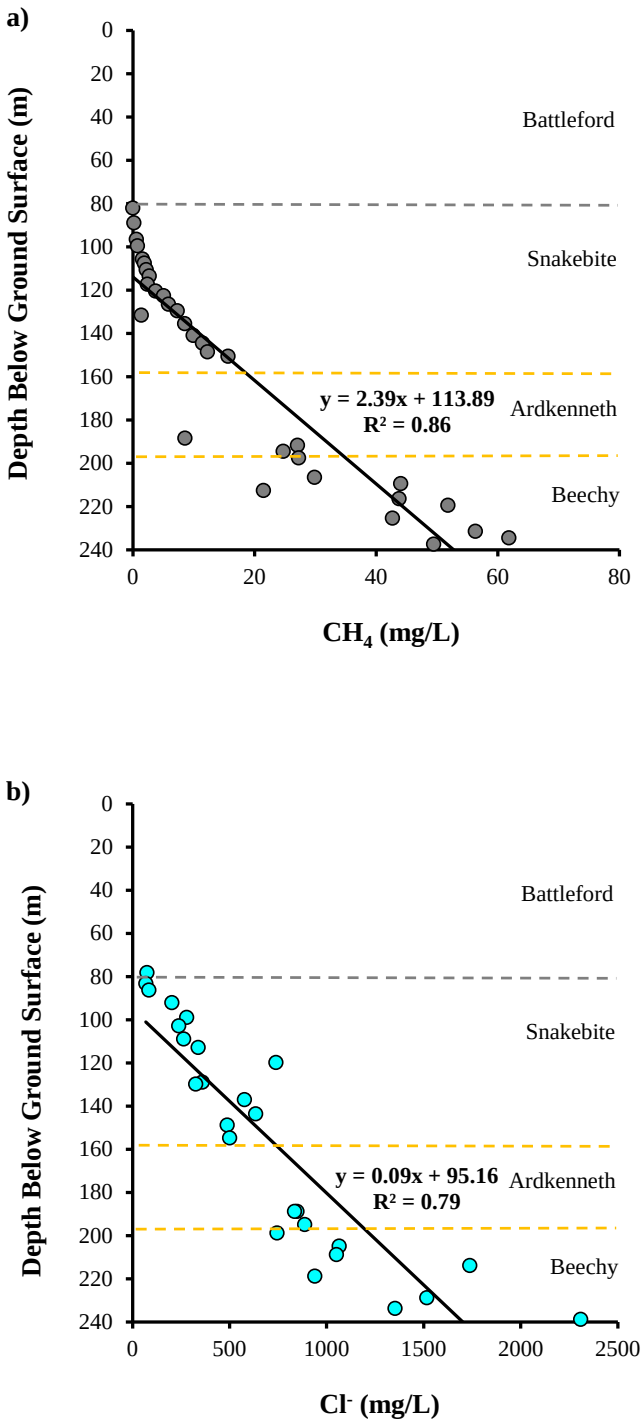

Figure 4.20. Concentrations of (a) CH_4 and (b) Cl^- with depth in the pore waters of the 2013 King site core. Data points above the till-clay contact and in the upper Ardkenneth (156-186 m BGS) were excluded to demonstrate the linear increase in concentration with depth. The CH_4 data produce a stronger correlation than the Cl^- (a known conservative solute).

Hendry et al. (2016 (b)) measured Cl^- and CH_4 concentrations with depth in till and Cretaceous sediments collected at four sites ~350 km southeast of the King site. These data are cross-plotted in Figure 4.21 along with the 2013 King site data. The correlation between Cl^- and CH_4 in the Hendry et al. data is much stronger than the King site data shown in Figure 4.19 (R^2 = 0.90). The Cl^--CH_4 relationship in the Hendry et al. (2016 (b)) data is consistent with that from the King site, but covers a greater range in concentrations and further supports the overall conservative nature of the CH_4 in the shales. The similarity in this relationship at both sites separated by ~350 km suggests that transport of CH_4 is consistent across the region. The inset plot in Figure 4.21 includes only the Snakebite Cl^--CH_4 data from the King site (86-154 m BGS), demonstrating a lack of correlation. This brings into question the conservative behaviour of CH_4 in that unit, which will be explored further on in the transport modeling.

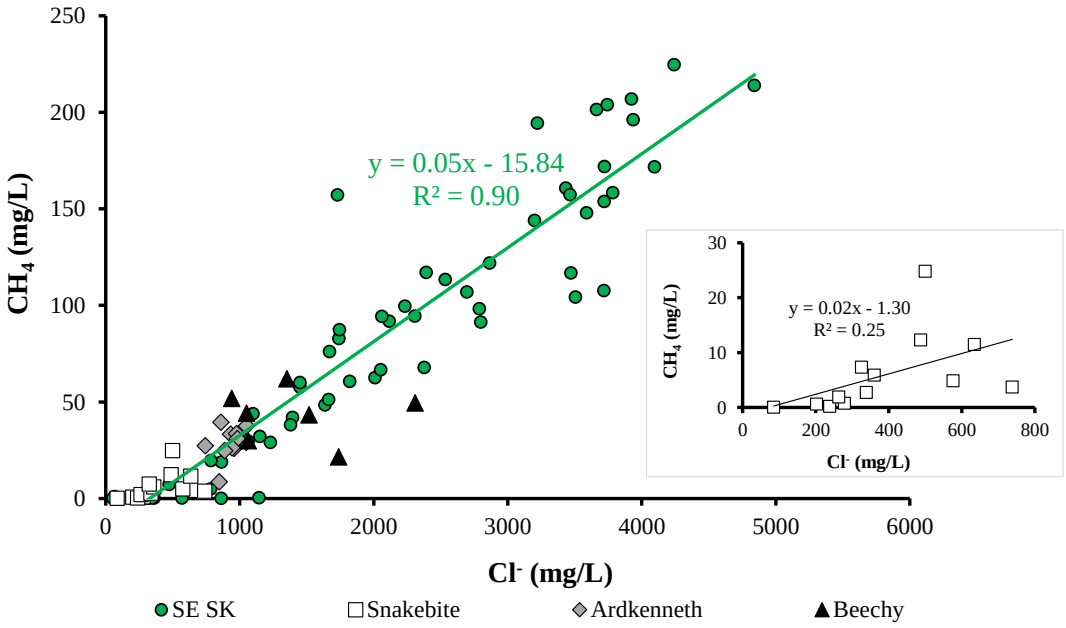

Figure 4.21. The Cl^- versus CH_4 concentrations from Figure 4.19 of the 2013 King site core and data from four sites in southeastern Saskatchewan (SE SK; Hendry et al., 2016 (b)). Those samples are an older Quaternary till and Cretaceous-aged shales. The linear regression line applies to the data from Hendry et al. (2016 (b)) and presents a strong correlation, suggesting CH_4 behaves conservatively in those sediments. The inset plot shows only the Snakebite data from the King site (86-154 m BGS) and the lack of correlation in that unit.

To investigate whether a relationship exists between the δ^2H and the CH_4 concentrations of the King site pore waters, the two parameters were cross-plotted (Figure 4.22). Only the 2013 vapour and squeezed data were used; at depths where measurements were made by both methods, the averages of the two measurements were used. The data in the peak in the Ardkenneth in both data sets (160-183 m BGS) was excluded from this plot. The data exhibit a positive linear correlation, with a moderate R^2 value, comparable to that of the Cl^--CH_4 data, suggesting the CH_4 transports in a similar conservative manner as δ^2H.

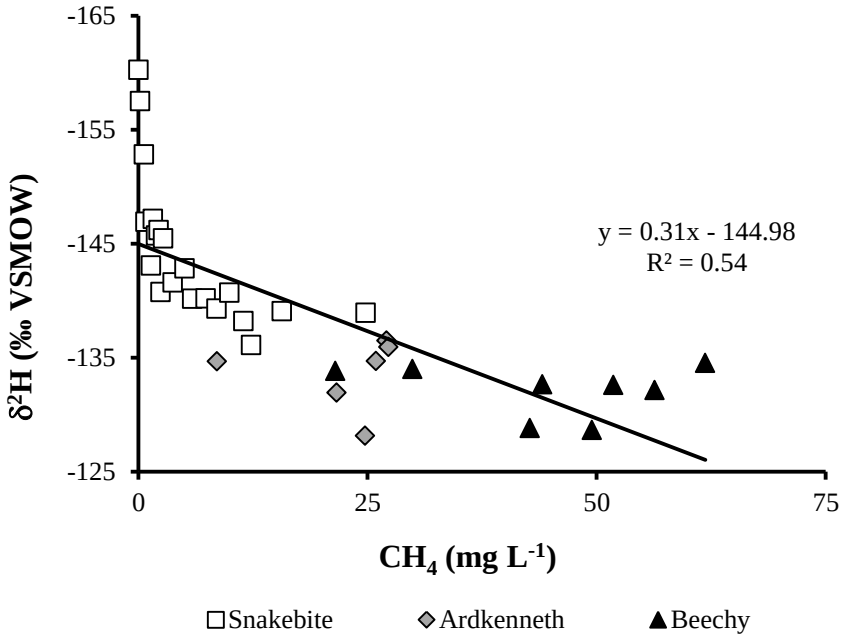

Figure 4.22. The δ^2H versus the CH_4 of the King site pore waters. The δ^2H data includes only the 2013 vapour equilibration and squeezed data, and neither the δ^2H nor the CH_4 data sets include data points over the interval 160-183 m BGS.

The results of the investigation into whether desorption or production of CH_4 occurred in the IsoJars® over time are presented in Figure 4.23 (a–d). All of the measurements made on the three till samples (54, 63, and 79 m BGS) were BDL throughout the experiment, and as such, the till results cannot be discussed. Data for the bedrock samples were converted to mg L^{-1}. Figure 4.23 (a) includes concentration measurements at three, seven, and 10 months post-collection, and 24 hours after the 1st flush. The measurements were within the 10% analytical error of the GC.

After the first flush with N_2, CH_4 concentrations decreased considerably. Figure 4.23 (b) shows that the CH_4 concentrations after the 1st flush remained below 1 mg L^{-1} and approached equilibrium 30 d after the 1st flush, never approaching similar concentrations as were present prior to the 1st flush. Figures 4.23 (c) and (d) show similar trends of concentrations increasing up to maximums of 0.06 mg L^{-1} and 0.04 mg L^{-1} in the IsoJars® after the 2nd and 3rd flushings, respectively. After the 2nd flush, concentrations did not reach the maximum concentrations measured after the 1st flush in a 40 d time period. After the 3rd flush, concentrations did not recover to the same concentrations as measured in the IsoJars® after the 2nd flush. These data indicate that only ~1% of the CH_4 initially measured in the IsoJars® at three months after collection was measured 30 d after the 1st flush. The three-month measurements therefore represent the majority of the available CH_4 in the sediments. From these data it can be concluded that no measureable production or desorption of CH_4 occurred over the time frames measured. These data are consistent with experiments conducted on similar sediments by Hendry et al. (2016 (b)). The results of the flushing experiment are in keeping with reports on the CH_4 sorption capacity of shales with low TOC (Chalmers and Bustin, 2008). That study determined a significant positive relationship between TOC and sorption capacity, and concluded that shales with TOC < 2 wt% have extremely low sorption capacity. All samples analyzed for TOC from the 2013 King site core contain < 2% TOC, therefore sorption should not be a source of CH_4, supported by the data presented in Figures 4.23 (a–d).

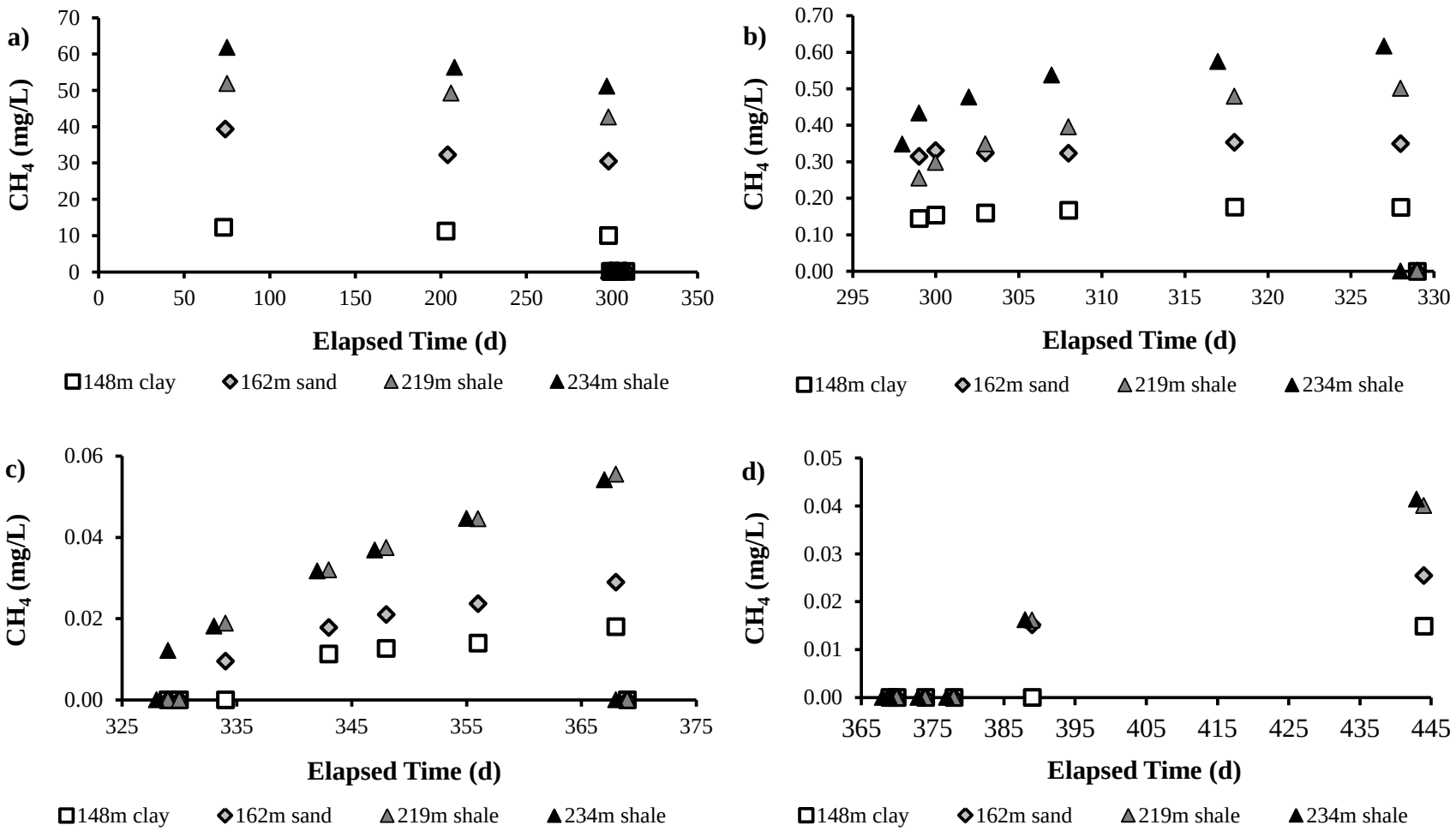

Figure 4.23. Concentrations of dissolved CH_4 from bedrock core samples from the 2013 King site core in IsoJars® with time: (a) after three, seven, and 10 months post-collection and one d after the 1st flush; (b) one to 30 d after the 1st flush and one d after the 2nd flush; (c) one to 40 d after the 2nd flush and one d after the 3rd flush; (d) one to 76 d after the 3rd flush with N_2.

The concentration-depth profiles of C_2H_6 and C_3H_8 from the King site cores are presented in Figure 4.24 ((a) and (b)). The maximum concentrations were 0.25 mg L^{-1} and 0.09 mg L^{-1}, for C_2H_6 and C_3H_8, respectively. The concentrations of both of these compounds are much lower than the CH_4 (maximum 61.85 mg L^{-1}).

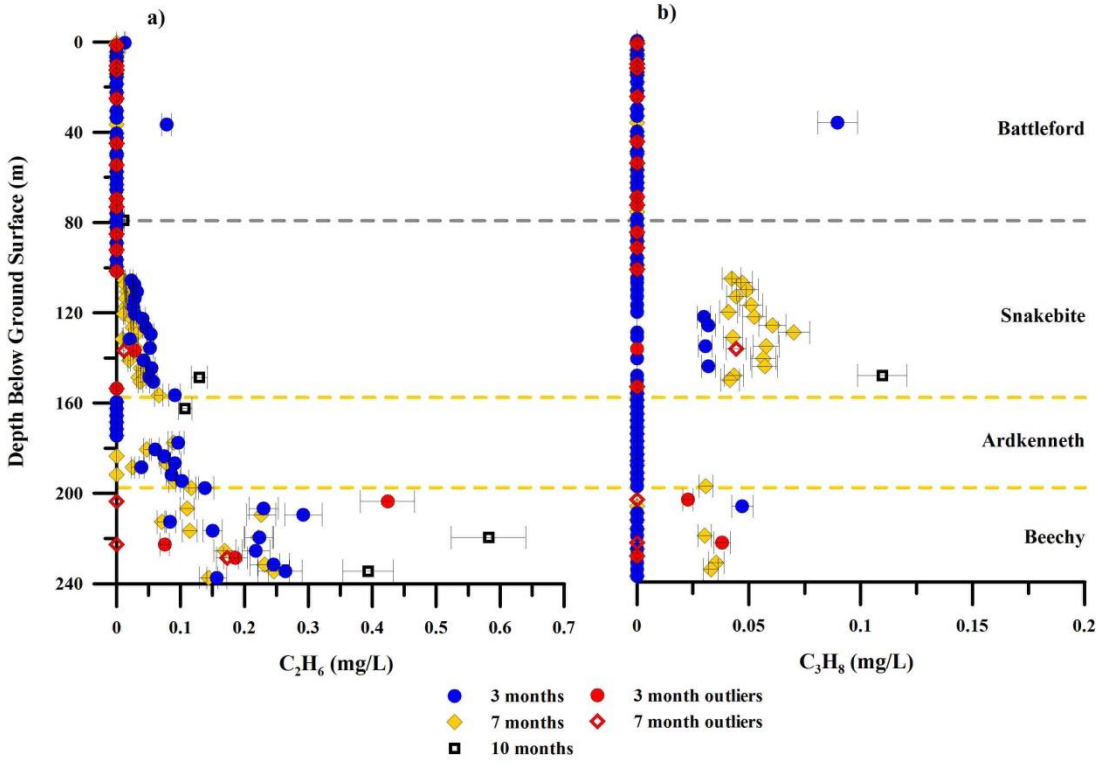

Figure 4.24. (a) C_2H_6 and (b) C_3H_8 concentrations versus depth measured at three, seven, and 10 months after the core samples were collected at the King site in 2013. Error bars are the ± 10% error of the GC. The C_2H_6 profile replicates that of CH_4, but the C_3H_8 profile shows a sporadic increase in concentrations over time.

The C_2H_6 profile mimics the shape of the CH_4 profile, increasing below the till-clay interface and reaching maximum concentrations at the base of exploration. The μ C_2H_6 in the Snakebite is 0.02 ± 0.02 mg L^{-1} (n = 20). In the Ardkenneth, the μ is 0.03 ± 0.04 mg L^{-1} (n = 14) and the Beechy has a μ of 0.17 ± 0.06 mg L^{-1} (n = 9). Similar to the CH_4 data in Figure 4.17, the three and seven month concentrations of C_2H_6 have a strong R^2 value (0.92; Figure 4.25). This correlation indicates that the concentrations of C_2H_6 in the headspace of the IsoJars® did not

change in the time frame between measurements, and that the concentrations reached equilibration during the initial three month storage period.

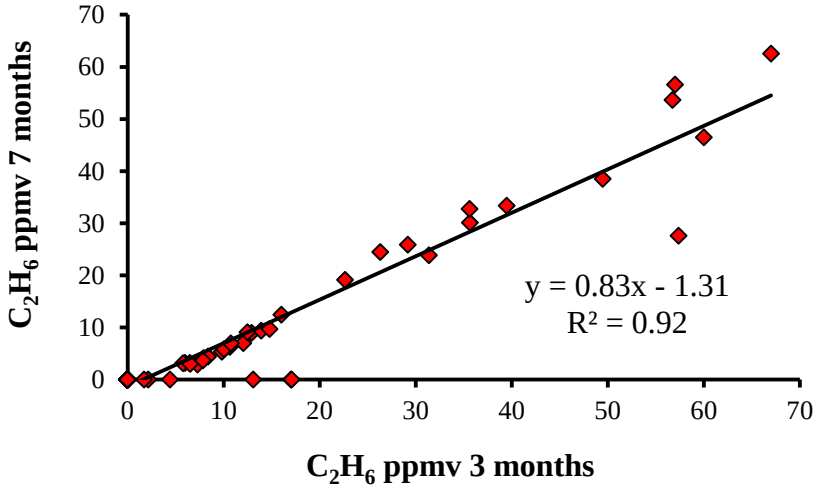

Figure 4.25. Cross-plot of C_2H_6 concentrations measured on the 2013 King site core samples at three and seven months after collection. The strong correlation indicates concentrations did not change over the time frame between measurements.

Only seven samples yielded C_3H_8 concentrations > 5 ppmv at the initial three month measurement, while 20 samples yielded C_3H_8 concentrations > 5 ppmv at the seven month measurement. Given that the concentrations of C_3H_8 increased over that time, it is likely that equilibrium concentrations were not achieved for C_3H_8 during the test period. In the seven month data set, the samples between 105-150 m BGS have a μ C_3H_8 of 0.05 ± 0.01 mg L^{-1} (n = 15) while four samples (197, 219, 231, and 234 m BGS) have a μ C_3H_8 of 0.03 ± 0.002 mg L^{-1}. Leythaeuser et al. (1982) determined the D_e of C_3H_8 in shales (5.55 x 10^{-11} m^2 s^{-1}) is lower than the D_e of C_2H_6 (1.11 x 10^{-10} m^2 s^{-1}) and D_e of CH_4 (2.12 x 10^{-10} m^2 s^{-1}). Processes that impede mobility of a compound such as *K* and tortuosity exert greater control on molecules of greater chain length (Leythaeuser et al., 1982). The lower D_e and longer chain length of C_3H_8 than C_2H_6 and CH_4 is suggested to be the reason for the greater concentrations of C_3H_8 at seven months than at three months.

The extremely low concentrations of C_2H_6 and C_3H_8 (< 0.25 mg L^{-1}), and the comparatively high concentrations of CH_4 (maximum 61.85 mg L^{-1}) give the King site gases a trait similar to bacterial gases. Many studies report that microbial gases do not contain significant concentrations of higher-chain hydrocarbons such as ethane, propane, butane or

hexane (Schoell, 1980; Whiticar et al., 1986; Taylor et al., 2000). Thermogenic "dry" gases contain low concentrations of C_{2+} and high CH_4 (Schoell, 1983), thus this characteristic is not definitive of bacterially-generated gases. Schoell (1983) proposed that natural gases with < 2% C_{2+} hydrocarbons classify as bacterial. The gases measured from the King site sediments contained < 1% of C_{2+} components. As such, they fit within Schoell's definition of bacterial gases.

In the vicinity of the King site, concentrations of C_2H_6 between 140–240 ppmv were measured in water wells completed in the Judith River aquifer (Taylor et al., 2000). This Cretaceous aquifer is located ~45 m below the base of the 2013 King site borehole (Arden Marsh, Saskatchewan Geological Survey, personal communication). Taylor et al. (2000) purported that the C_2H_6 in the Judith River aquifer was the result of in-situ bacterial production based on ^{13}C-depleted isotope values and conditions feasible for such bacterial activity in the aquifer (i.e. low temperatures, available organic matter, anoxic conditions). It is consistent that gases in the shallower geologic units at the King site which directly overlie the Judith River aquifer should also contain gases of bacterial origin.

4.6 Isotopes of dissolved organic gases

In addition to the gas composition data, the gas isotope data also suggest a bacterial origin of the natural gases measured in the King site sediments. Foremost, the low values of the $\delta^{13}C_{CH4}$, $\delta^{2}H_{CH4}$, and $\delta^{13}C_{C2H6}$ are characteristic of bacterial gases. Furthermore, the King site gas composition and isotope data fall into categories defined as bacterial based on a number of relationships reported in the literature. These relationships include, but are not limited to, the $\delta^{13}C_{CH4}$ versus: $\delta^{2}H_{CH4}$, $\delta^{13}C_{C2H6}$, and C_2H_6/CH_4. These relationships and their applications for genetic categorization of natural gases are discussed below.

The profiles of gas isotopes versus depth measured on the 2013 King site core are presented in Figure 4.26 (a–c). Because gas compositions were not measured in the same IsoJars® as the isotope analysis (vertically separated by 0.1 m), concentration data from the adjacent IsoJar® samples were assumed applicable to the gas isotope samples. However, the impact of O_2 ingress into the IsoJars® of the samples collected for gas isotope analysis could not be quantified. Twenty-five samples that were BDL of the GC for CH_4, C_2H_6, and C_3H_8 (< 5 ppmv) were not submitted for gas isotope analysis. Of the 57 samples that were submitted, the

concentrations in the following number of IsoJars® were BDL for the respective isotopic analyses (^{13}C = 0.05 mg L^{-1}; ^{2}H = 0.20 mg L^{-1}): 20 for $\delta^{13}C_{CH4}$, 42 for $\delta^{13}C_{C2H6}$, 55 for $\delta^{13}C_{C3H8}$ and 25 for $\delta^{2}H_{CH4}$. The inability to yield analytical results was attributed to insufficient gas concentrations in the IsoJars® for analysis. Given that ~20% of the IsoJars® measured for gas concentrations demonstrated ingress of O_2, it is likely that some of the gas isotope IsoJars® also experienced leakage during sample collection, transport, or storage.

A few isotope values in the profiles presented in Figure 4.26 are questionable because they deviate noticeably from the local trends of the surrounding samples. These data points include 107, 197, 206, and 237 m BGS from the $\delta^{13}C_{CH4}$ profile, 105 and 197 m BGS from the $\delta^{2}H_{CH4}$ profile, and 191 m BGS from the $\delta^{13}C_{C2H6}$ profile. It is reported that oxidation of CH_4 causes the residual CH_4 to become enriched in ^{13}C (Coleman et al., 1981). If the outliers were consistently enriched between all three profiles, it could be concluded that the samples experienced oxidation. However, all the samples do not correlate between the profiles, and the $\delta^{13}C_{C2H6}$ outlier is depleted with respect to ^{13}C rather than enriched. One of the outliers does correlate between the $\delta^{13}C_{CH4}$ and $\delta^{2}H_{CH4}$ profiles (197 m BGS), and that IsoJar® sample did not yield results for $\delta^{13}C_{C2H6}$. It was therefore concluded that that sample was contaminated with O_2 and that data point does not appear in further figures or discussion. Because the other five samples do not correlate as outliers between the gas isotope profiles, they cannot be removed from the respective data sets and were included in statistics calculations and figures.

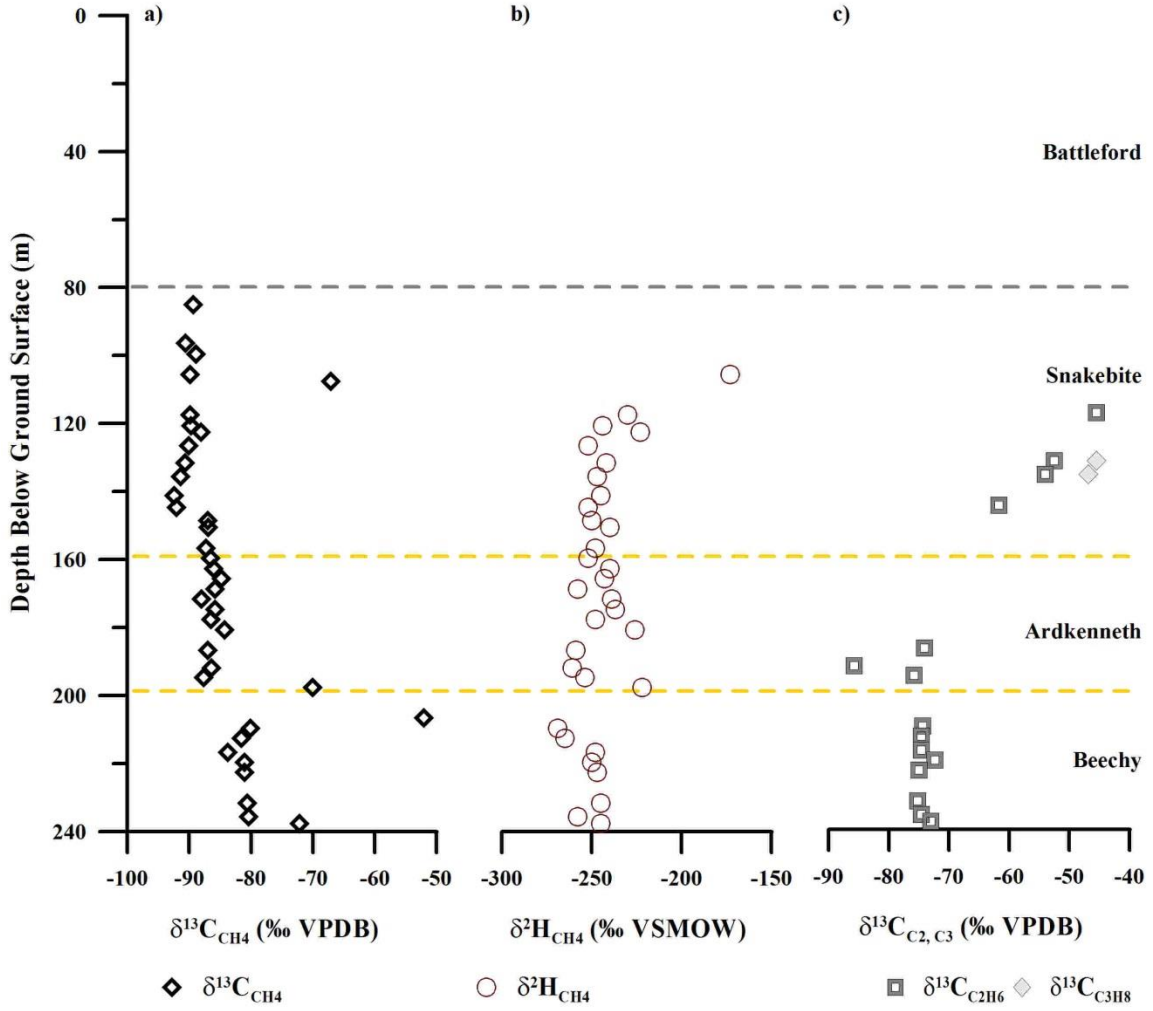

Figure 4.26. Isotopes of dissolved gases versus depth from the 2013 King site core: (a) $\delta^{13}C_{CH4}$, (b) $\delta^{2}H_{CH4}$, and (c) $\delta^{13}C_{C2H6}$ and $\delta^{13}C_{C3H8}$.

The $\delta^{13}C_{CH4}$ in Figure 4.26 (a) become increasingly enriched in ^{13}C with increasing depth. The μ $\delta^{13}C_{CH4}$ in the Snakebite clay is –88.2‰ (± 5.9‰, n = 16). In the Ardkenneth, $\delta^{13}C_{CH4}$ has a μ of –86.3‰ (± 1.1‰, n = 11), and in the Beechy member, the $\delta^{13}C_{CH4}$ is further ^{13}C-enriched, with a μ of –77.0‰ (± 9.9‰, n = 9). $\delta^{13}C_{CH4}$ values < –60‰ are characteristic of gases of bacterial origin (Schoell, 1980; Whiticar, 1999). As such, all $\delta^{13}C_{CH4}$ of the King site CH_4 can be defined as bacterial.

Taylor et al. (2000) measured $\delta^{13}C_{CH4}$ between –76.9 and –80.9‰ VPDB in gases collected from wells completed in the underlying Judith River aquifer near Birsay, SK and

classified those gases as bacteriogenic. The $\delta^{13}C_{CH4}$ was measured on dissolved gases from water wells in Ordovician bedrock in southern Ontario, which ranged from –70‰ to –89‰ (Aravena and Wassenaar, 1993). That study concluded that those gases were produced by bacterial activity. The range of $\delta^{13}C_{CH4}$ of the King site samples is consistent with other reported values of $\delta^{13}C_{CH4}$ of bacterial gas.

The overall trend of enriching ^{13}C in CH_4 with depth in the King site samples in Figure 4.26 (a) could be the result of diffusive fractionation resulting from different D_e of the heavier and the lighter isotopes. ^{12}C has a higher D*e* and therefore travels faster, enriching the gas in ^{12}C as it diffuses (Schloemer and Krooss, 2004). The trend of depletion of ^{13}C in CH_4 in diffused gases is reported in diffusion experiments (Prinzhofer and Pernaton, 1997; Schloemer and Krooss, 2004). It is noted in the literature that it would be unlikely that diffusion of a thermogenic gas could alter its isotopic signature so significantly that it could be confused with bacterial gas (Xia and Tang, 2012). Considering the effect of diffusion on $\delta^{13}C_{CH4,}$ it could be that the $\delta^{13}C_{CH4}$ values in the Beechy member are more representative of the source CH_4 values than the values measured from the Snakebite samples. Hendry et al. (2016) simulated transport of $^{13}C_{CH4}$ through correlating Cretaceous geology in southeastern Saskatchewan and concluded that the $\delta^{13}C_{CH4}$-depth profile at that site was the result of diffusive fractionation. The King site $\delta^{13}C_{CH4}$ data shows the same trend of CH_4 enriching in ^{13}C with depth as the Hendry et al. (2016) data, therefore it is reasonable to conclude that the King site $\delta^{13}C_{CH4}$-depth profile was developed by diffusive fractionation.

Interestingly, neither the $\delta^{13}C_{CH4}$ nor the $\delta^{2}H_{CH4}$ between depths ~156–183 m BGS deviate from the trend in the profile as the CH_4, Cl^-, Br^- concentrations and δ^2H values do. This suggests that the CH_4 within that interval is consistent in origin with the CH_4 in the surrounding units.

In an attempt to investigate the relationship between $\delta^{13}C_{CH4}$ and depth, a linear regression was applied to the data in Figure 4.26 (a) (shown in Figure 4.27 (a)). The relationship is not linear in that case. Three data points were removed (107, 206, and 237 m BGS) due to their deviation from the local trends in the profile and a linear regression was applied (Figure 4.27 (b)). That version of the $\delta^{13}C_{CH4}$ profile has a strong positive linear correlation with depth ($R^2 = 0.72$), adding support to the argument that CH_4 exhibits conservative behavior in these

sediments and transports via diffusion. There was no overwhelming evidence that provided reason to remove the three data points from the $\delta^{13}C_{CH4}$ data set (107, 206, and 237m BGS), but the strong correlation of $\delta^{13}C_{CH4}$ with depth excluding those data points warrants further investigation.

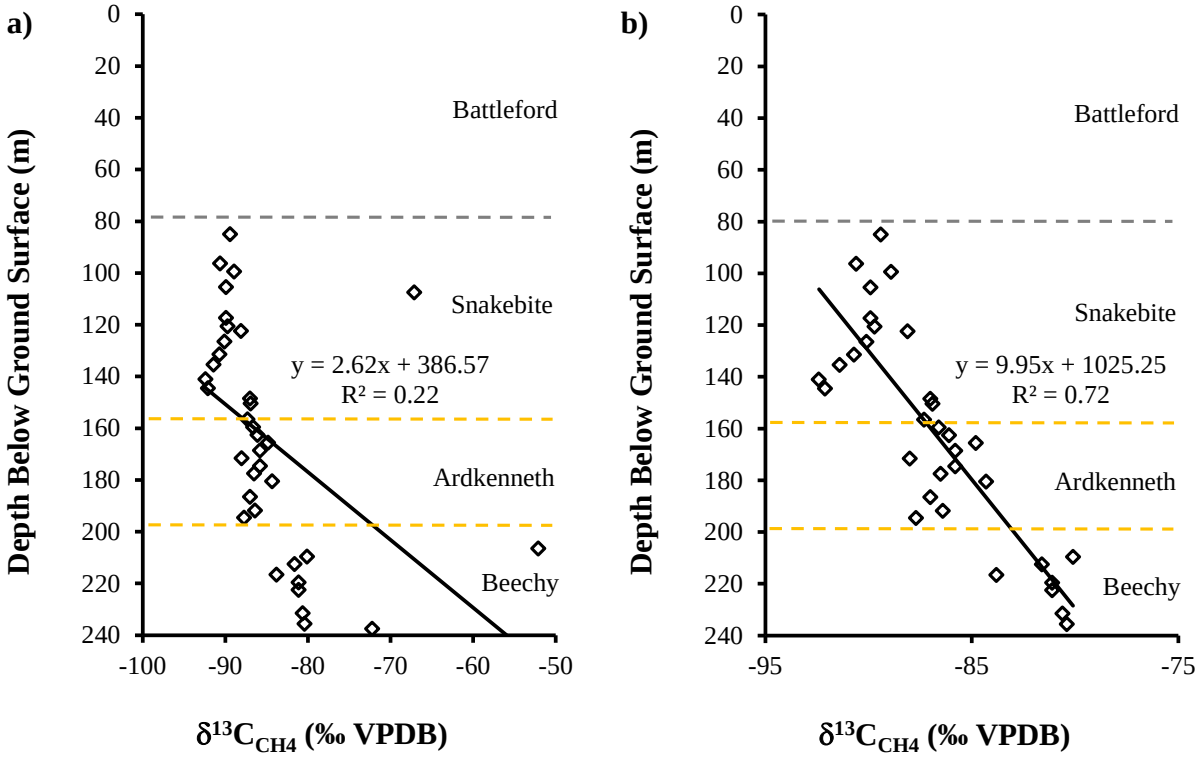

Figure 4.27. The $\delta^{13}C_{CH4}$-depth profile of the King site gases with (a) all data points, and (b) with three data points removed (107, 206, and 237 m BGS). A stronger correlation is obvious in (b) with the questionable data points removed.

Abrams (1996) used plots of $\delta^{13}C_{CH4}$ versus CH_4 concentrations to detect processes such as mixing, microbial activity, and define groups of gases. That study observed negative correlations between the two parameters. The King site $\delta^{13}C_{CH4}$ and CH_4 were plotted with all data points included (Figure 4.28 (a)). While this plot highlights distinct compartmentalization of the gases between geologic units at the King site, no relationship was present. Removing three of the questionable data points (107, 206, and 237 m BGS) revealed that contrary to the Abrams (1996) study, the $\delta^{13}C_{CH4}$-CH_4 of the gas from the King site sediments has a strong positive correlation; the lowest concentration samples had the lightest isotopic values and vice

versa (Figure 4.28 (b)). Whether this is the product of diffusive fractionation is interesting and worthy of further investigation, considering removal of the three questionable data points.

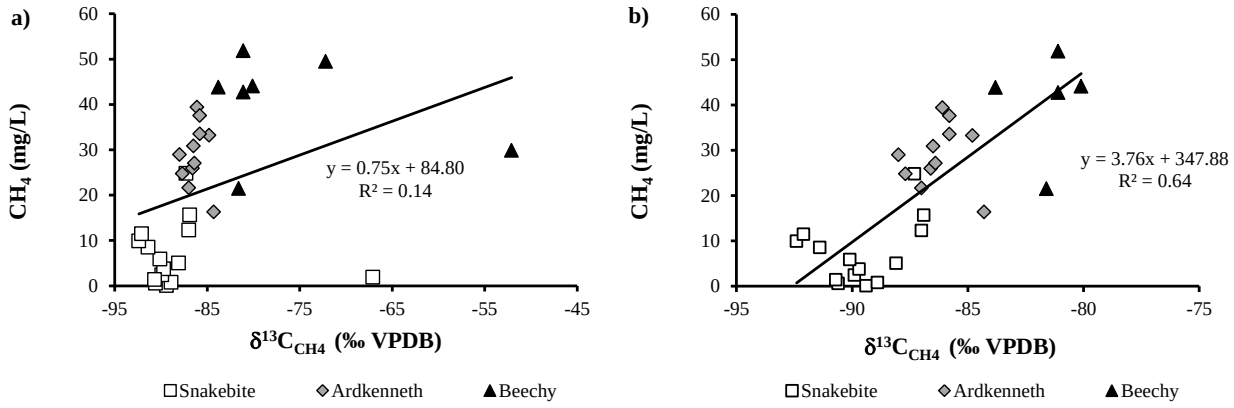

Figure 4.28. CH_4 concentrations versus the $\delta^{13}C_{CH4}$ of the gases measured from the King site sediments with (a) all data points, and (b) three data points removed (107, 206, and 237 m BGS). The parameters show a positive linear correlation in (b).

The δ^2H_{CH4} values in Figure 4.26 (b) deplete in ^2H with increasing depth. The $\mu\ \delta^2H_{CH4}$ in the Snakebite is –237‰ (± 22‰, n = 12). The $\mu\ \delta^2H_{CH4}$ in the Ardkenneth is lighter, –247‰ ± 11‰ (n = 11), and the lightest δ^2H_{CH4} values are from the Beechy, which have a μ of –253‰ (± 9‰, n = 8). The low δ^2H_{CH4} values of the King site samples support the observation that this CH_4 is bacterial in origin because CH_4 with δ^2H values < –150‰ are classified as bacterial (Schoell, 1980).

Unlike the $\delta^{13}C_{CH4}$ of the King site gases; the δ^2H_{CH4} values do not demonstrate linearity with depth (Figure 4.29). With all the data points included (Figure 4.29 (a)), the data yield a greater R^2 (0.25) than with the one questionable data point (105 m BGS) removed (R^2 = 0.19; Figure 4.29 (b)). Perhaps this is reflective of the greater scatter in the δ^2H_{CH4} data than in the $\delta^{13}C_{CH4}$; the σ of δ^2H_{CH4} in the Snakebite and Ardkenneth is 22 and 11‰, respectively, while the σ is < 6‰ in the $\delta^{13}C_{CH4}$ data. This increased scatter could be a result of the accuracy of the δ^2H_{CH4} measurement, which is ± 5‰ compared to that of ± 0.5‰ for $\delta^{13}C_{CH4}$.

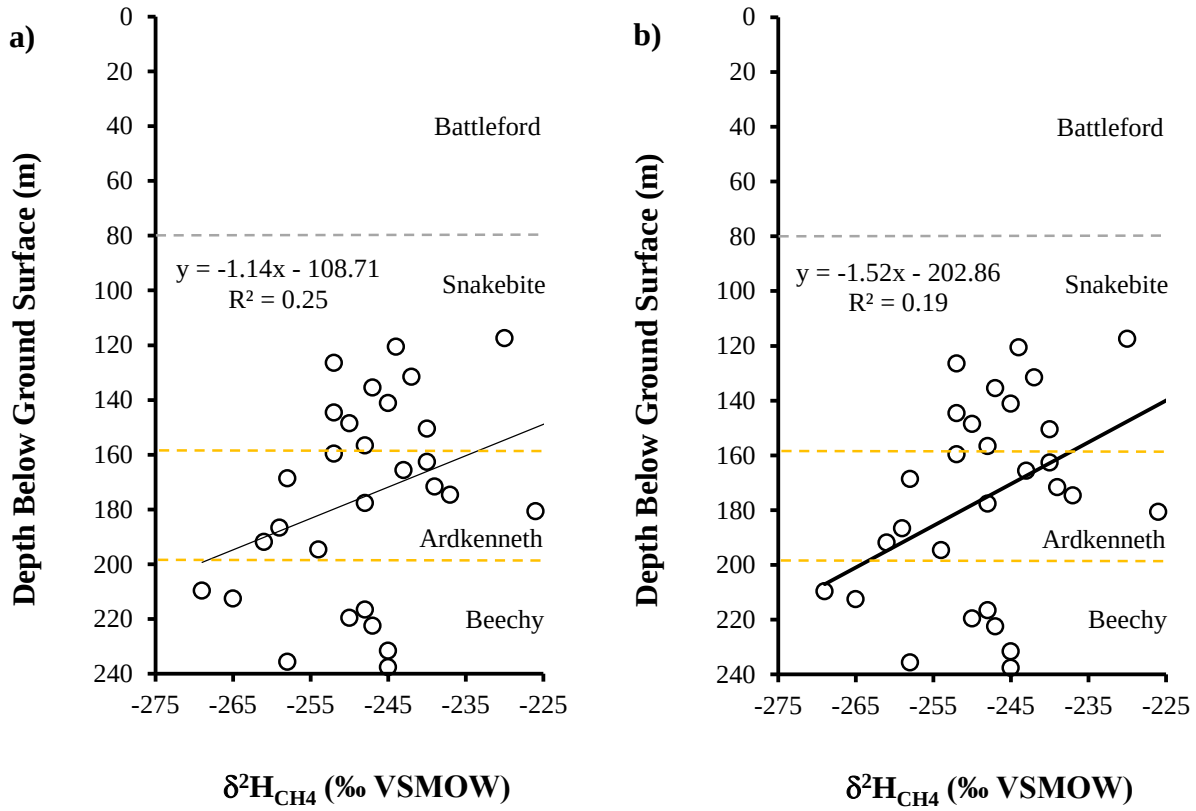

Figure 4.29. The δ^2H_{CH4}-depth profile of the King site gases with (a) all data points, and (b) one data point removed (105 m BGS).

One relationship used to characterize the origin of a gas is that between $\delta^{13}C_{CH4}$ and δ^2H_{CH4} by which gases of specific origins plot within distinct regions in these diagrams (Figure 4.30; Schoell, 1983; Whiticar et al., 1986; Whiticar, 1999). On this plot, the King site gases fall within the field characteristic of gases of bacterial origin. The migration of δ^2H_{CH4} is reportedly more complicated than that of $\delta^{13}C_{CH4}$, because the initially diffused CH_4 is enriched in ^2H (Prinzhofer and Pernaton, 1997). This is the trend demonstrated by the δ^2H_{CH4} profile from the King site (Figure 4.26 (b)).

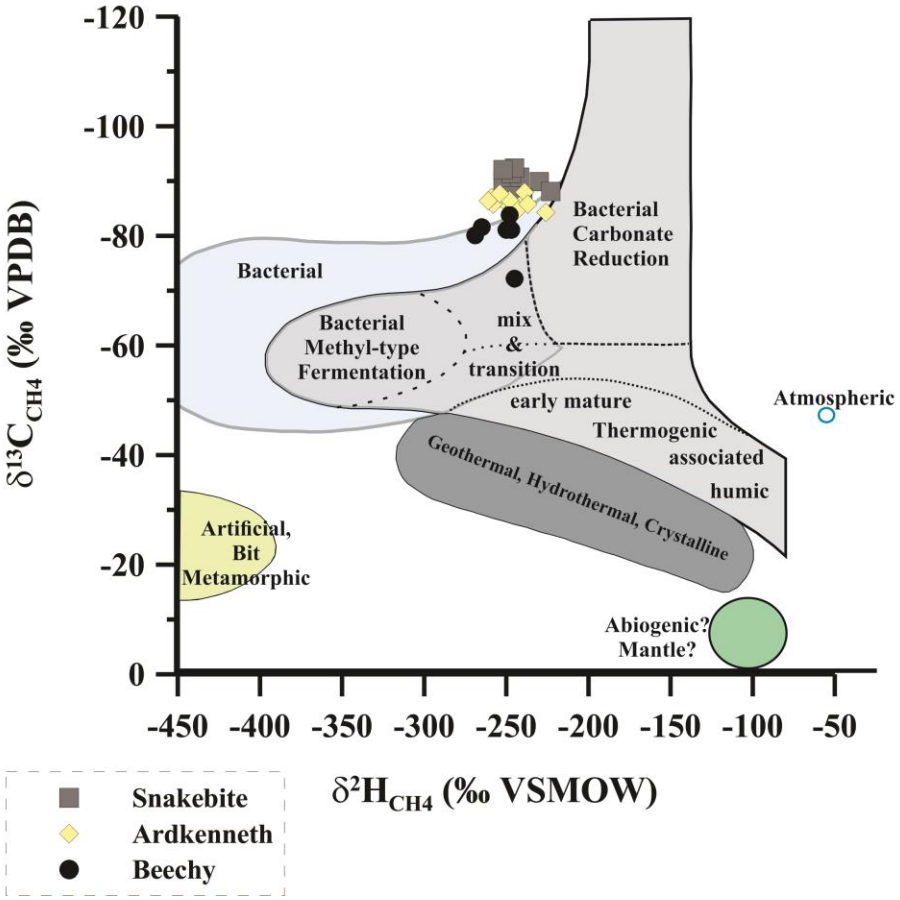

Figure 4.30. $\delta^{13}C_{CH4}$ versus $\delta^{2}H_{CH4}$ (after Whiticar, 1999). The data from the 2013 King site core plot nearest the regions characteristic of gases of bacterial origin.

The $\delta^{13}C_{C2H6}$ values of samples in the Snakebite deplete in ^{13}C with increasing depth, and have a μ of –53.4‰ (± 6.6‰, n = 4; Figure 4.26 (c)). The C_2H_6 in the Ardkenneth and Beechy units is depleted in ^{13}C in comparison to that in the Snakebite. Values from the Ardkenneth have a μ of –78.6‰ (± 6.3‰, n = 3), and values are relatively constant through the Beechy member with a μ of –74.2‰ (± 1.0‰, n = 8). Aside from one sample in the Ardkenneth (191 m BGS $\delta^{13}C_{C2H6}$ = –85.8‰), the other two Ardkenneth samples have $\delta^{13}C_{C2H6}$ values consistent with those in the Beechy. The fractionation in $\delta^{13}C$ with diffusion also effects $\delta^{13}C_{C2H6}$, however, diffusive isotope effects are greater for CH_4 than for C_2H_6 because of the greater D_e of CH_4 (Schloemer and Krooss, 2004). This could be the reason the $\delta^{13}C_{C2H6}$ values do not obviously demonstrate diffusive fractionation effects between the Ardkenneth and Beechy units. The range of $\delta^{13}C_{C2H6}$ values in the King site data agree with the range of –68.1 to –73.9‰ measured by

Taylor et al. (2000) in the Judith River aquifer near Birsay, SK. The C_2H_6 from the Judith River was concluded to be of bacterial origin in that study. As the King site C_2H_6 is isotopically similar to the Judith River gas measured by Taylor et al. (2000), it is concluded that the $\delta^{13}C_{C2H6}$ values of the King site gases further support the bacterial origin. Figure 4.31 shows that the $\delta^{13}C_{C2H6}$ data potentially have a linear relationship with depth, and with the one outlying data point removed (191 m BGS; Figure 4.31 (b)), linear correlation with depth is stronger (R^2 = 0.84).

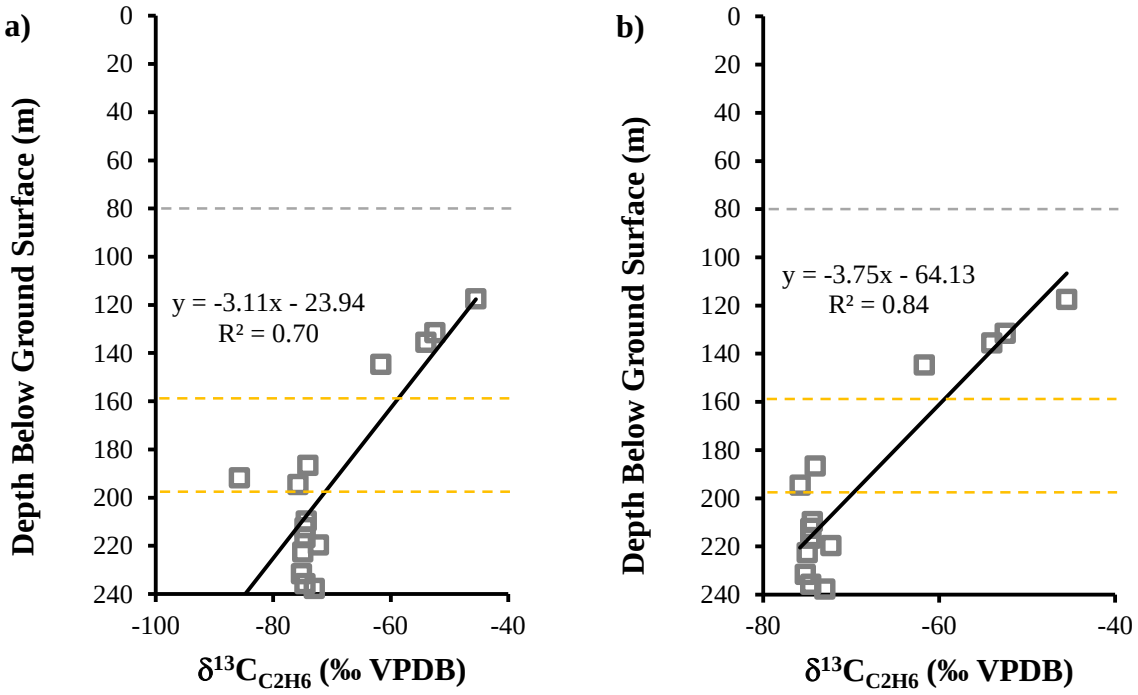

Figure 4.31. The $\delta^{13}C_{C2H6}$-depth profile of the King site gases with (a) all data points, and (b) one data point removed (191 m BGS).

The $\delta^{13}C_{C2H6}$ values of the King site gases were plotted against the C_2H_6 concentrations (Figure 4.32 (a) and (b)). Including all data points (Figure 4.32 (a)), the parameters do not have a strong correlation. By removing the one questionable data point (191 m BGS), the correlation marginally improves. While these plots exhibit compartmentalization of the gas between geologic units similar to the $\delta^{13}C_{CH4}$-CH_4 data in Figure 4.28, the $\delta^{13}C_{C2H6}$-C_2H_6 plots show the opposite trend to that of the $\delta^{13}C_{CH4}$-CH_4 data. In the case of C_2H_6, the isotopic value becomes heavier with lower concentrations. As with previous data, it is not certain if removal of the

questionable data point is justifiable, and determining the precise reason for the outstanding data points would be appropriate before in-depth interpretation of these isotope-concentration relationships.

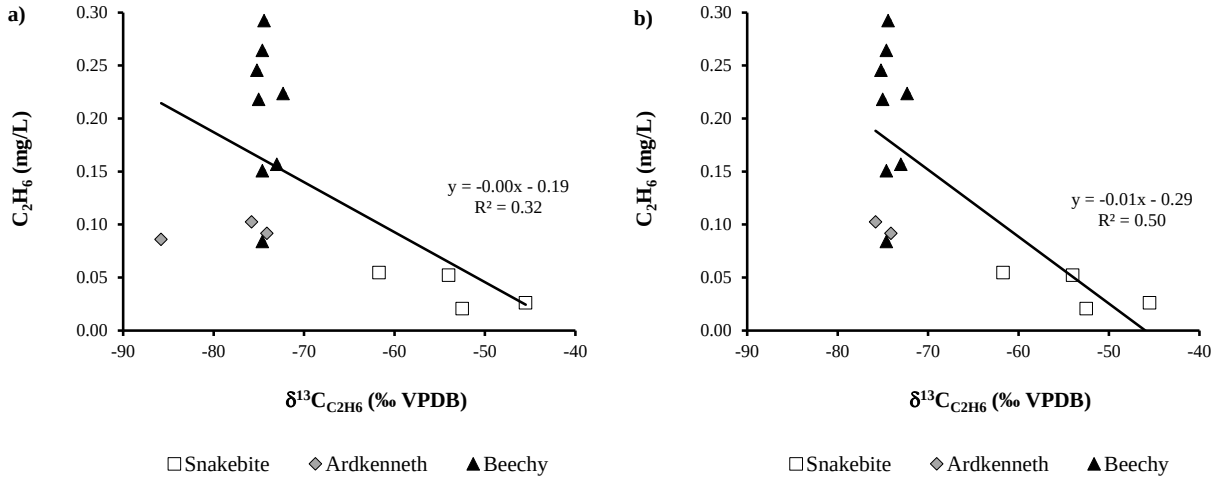

Figure 4.32. C_2H_6 concentrations versus the $\delta^{13}C_{C2H6}$ of the gases measured from the King site sediments with (a) all data points, and (b) one data point removed (191 m BGS). The parameters show a negative linear correlation in (b).

Schoell (1983) showed that when the $\delta^{13}C_{CH4}$ and $\delta^{13}C_{C2H6}$ of a gas are co-genetic, the C_2H_6 is typically enriched in ^{13}C over the CH_4 by 5-10‰. That study used plots of $\delta^{13}C_{CH4}$ versus $\delta^{13}C_{C2H6}$ to also identify processes that affect the isotopic composition of gases; trends enriching ^{13}C in both gases include maturation, migration, and mixing. When the data from the King site is plotted in this manner, it is obvious that the CH_4 is enriched in ^{13}C in the older sediments (Figure 4.33). The relationship between $\delta^{13}C_{CH4}$-$\delta^{13}C_{C2H6}$ suggests the gas from the King site sediments is co-genetic, because the C_2H_6 is enriched in ^{13}C over the corresponding CH_4 by (on average) 8‰ and 6‰, in the Ardkenneth and Beechy units, respectively. The C_2H_6 from the Snakebite gases are, however, enriched in ^{13}C on average by 38‰. The difference in $\delta^{13}C_{CH4}$-$\delta^{13}C_{C2H6}$ in the Snakebite versus in the other two units could reflect the immaturity of the gas in that younger geologic unit. The isotopic separation between CH_4 and C_2H_6 decreases as gases mature; an "isotopically mature" gas would have the same isotopic composition as its source (Schoell, 1983).

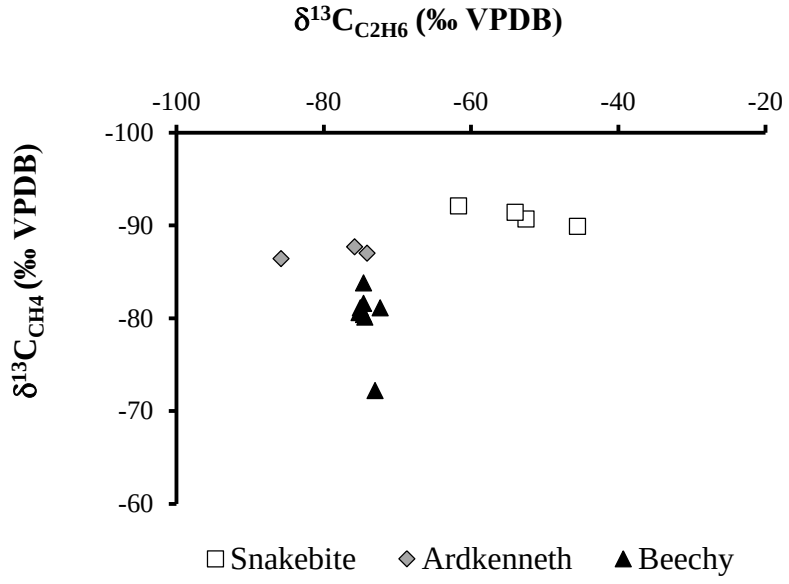

Figure 4.33. $\delta^{13}C_{CH4}$ versus $\delta^{13}C_{C2H6}$ of the 2013 King site core (after Schoell, 1983). The plot demonstrates that the partitioning between $\delta^{13}C_{CH4}$ and $\delta^{13}C_{C2H6}$ decreases with increasing age and depth of the sediments, perhaps indicating increasing maturity.

Propane of thermogenic origin is reported to have $\delta^{13}C$ values ranging between –22 to –45‰, depending on the extent of biodegradation the gas has experienced (Berner and Faber, 1987; Ricchiuto and Schoell, 1987; Rowe and Muehlenbachs, 1999; Zou et al., 2007). Hinrichs et al. (2006) measured $\delta^{13}C_{C3H8}$ values of bacterial propane from marine sediments and reported values ranging between –10 and –30‰. The $\delta^{13}C_{C3H8}$ of the two samples from the Snakebite sediments at the King site are –45.5 and –46.8‰, which fall within the thermogenic range. Although inconsistent with the conclusions based on the $\delta^{13}C_{CH4}$, $\delta^{13}C_{C2H6}$, $\delta^{2}H_{CH4}$, the gas compositional data, and the relationships between those parameters, the paucity of $\delta^{13}C_{C3H8}$ data points suggests it more reasonable to base conclusions on those several lines of evidence which are in agreement of a bacterial origin for the gases in the King site sediments.

Prinzhofer and Pernaton (1997) use a plot of the ratio of C_2H_6/CH_4 versus $\delta^{13}C_{CH4}$ to determine if a gas is a mixture of thermogenic and bacterial gas; mixed gases fall in a straight line on such a plot. Plotting the 2013 King site on this type of plot (Figure 4.34) indicates that these data exhibit scatter and do not follow a linear trend. The lack of a relationship between

these parameters suggests that the gases from the King site sediments are not a mix between bacterial and thermogenic gases.

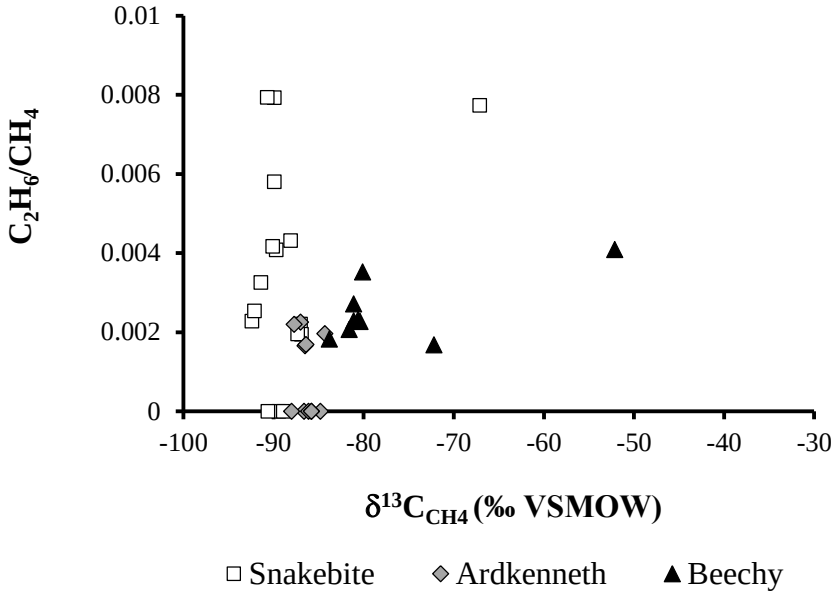

Figure 4.34. The C_2H_6/CH_4 ratio versus the $\delta^{13}C_{CH4}$ of the King site 2013 core (after Prinzhofer and Pernaton, 1997). The plot is not consistent with trends typically observed by thermogenic and bacterial mixed gases.

4.7 Solute transport modeling

The finite element model Hydrus–1D 4.16 (Šimůnek et al., 2013) was used to simulate the evolution of the measured δ^2H values and CH_4 concentrations with depth at the King site. This modeling also allowed the Hydrus modeling results to be compared to the simulations of δ^2H transport undertaken by Hendry and Wassenaar (1999) and Hendry et al. (2011) for the same study site. This ensures that the parameters used in the current modeling were appropriate, and that the results of the current model were consistent with these previous interpretations prior to undertaking modeling of the CH_4 profile.

4.7.1 Model parameters

For the modeling scenarios, it was assumed that groundwater flow was at steady state and solute transport was dominated by vertical transport (Shaw and Hendry, 1998; Hendry and Wassenaar, 1999). The timescales considered in the simulations are significantly greater than

the length of time required for the sediments to dissipate the transient hydraulic pressures induced by glaciations (up to 2.7 ka), as demonstrated by Shaw and Hendry (1998). Given the δ^2H and CH_4 profiles in the Cretaceous clay prior to till deposition and the source of the CH_4 at depth below the clay are uncertain, the resulting simulations can only be considered conceptual.

Hydrus–1D (Šimůnek et al., 2013) applies Eq. 2.5 in the modeling of solute transport. For the CH_4 simulations, Eq. 2.6 was applied, to include a first-order consumption reaction. This term was not required for the δ^2H modeling because it is a conservative (non-reactive) tracer. As diffusion was determined to be the dominant mechanism of solute transport, *v* was considered negligible and the $v\frac{\partial C}{\partial x}$ term in Eq. 2.5 was set equal to zero in many simulations (Hendry and Wassenaar, 1999). To determine the sensitivity of the model to *v*, some simulations included the *v* term.

In keeping with the model of Hendry and Wassenaar (1999), a constant D_e of 1.7 x 10^{-10} m^2 $s^{-1}$was used for δ^2H for all geologic units with the calculated average n_T of 0.29 and 0.34 assigned in the Battleford and Snakebite, respectively. The Ardkenneth and Beechy members were considered as one unit for the modeling and the average n_T through those two units were used (0.36; given the consistency of measured physical properties between the units, as presented in Table 4.1). These units will be referred to as the Lower Shale. In the case of CH_4, a constant D_e value of 2.4 x 10^{-10} m^2 s^{-1}, measured by Jacops et al. (21 °C; 2013), was used in the simulations with the same porosities as applied in the δ^2H models. It was assumed that the effective porosity (n_e) and n_T are equivalent for both components. This assumption is consistent with Hendry and Wassenaar (1999) for δ^2H. The lack of charge on CH_4 molecules precludes ion exclusion effects, suggesting that the molecules have access to n_T (Iversen and Jørgensen, 1993; Jacops et al., 2013). Hendry et al. (2009) investigated the relationship between *n* and D_e proposed by Boudreau (1996) and determined that as *n* increased, D_e decreased. The effects of this relationship on the following simulations was not examined as part of this study, but may be considered in future work. A summary of the physical properties used in Hydrus 1-D are presented in Table 4.5.

To determine the best fit between the models and the measured data, the error between the measured and predicted δ^2H values at each depth was calculated (measured value – predicted value). The errors were squared and then added to compile the sum of the squares of the error

(SSE). The model producing the lowest SSE was considered to yield the best fit (Patriarche et al., 2004; Horton and Leonard, 2005). Given the multitude of δ^2H data available for the King site, the predicted value at each depth was compared to the average of all of the measured values at a corresponding depth. The values of δ^2H and concentrations of CH_4 in the peak in the Ardkenneth (157-189 m BGS) were not included in the calculation of SSE.

Table 4.5. Description of parameters used in the Hydrus-1D simulations.

Unit	K ($m\ s^{-1}$)	ρ_b ($kg\ m^{-3}$)	$n_T = \theta_v$	Depth (m)	$D_e\ \delta^2H$ ($m^2\ s^{-1}$)	$D_e\ CH_4$ ($m^2\ s^{-1}$)
Battleford	2.7×10^{-11}	2160	0.29	0-80	1.7×10^{-10}	2.4×10^{-10}
Snakebite	2.5×10^{-12}	2100	0.34	80-159	1.7×10^{-10}	2.4×10^{-10}
Lower Shale	2.5×10^{-12}	2010	0.36	159-240	1.7×10^{-10}	2.4×10^{-10}

4.7.2 δ^2H conceptual model

Groundwater movement in the oxidized till is controlled by the presence of fractures and is seasonally dynamic (Hendry and Wassenaar, 1999; Hendry and Woodbury, 2007; Hendry and Wassenaar, 2009). In contrast, groundwater movement in the underlying unoxidized till is vertically downward with *v* between 0.5-0.8 m/10 ka (Shaw and Hendry, 1998). The dark grey till (unoxidized) at the study site was first observed at 5 m BGS. As such, the top of the unoxidized till at 5 m BGS was assumed to be the upper boundary condition for the δ^2H modeling and the concentration was constant at this boundary. This depth was consistent with other observations across the King site which varied between 3.9 and 4.9 m BGS based on distinct colour transitions and visibility of fractures in oxidized till core samples (Shaw and Hendry, 1998; Hendry and Wassenaar, 2009; Stumpp and Hendry, 2012). Since groundwater movement in the oxidized till is dynamic, δ^2H values collected above 5 m BGS, in both the present data set and in data previously collected at the site, were used to define the upper boundary condition but were not modeled, however. The model domain was extended from the base of the oxidized till zone to the base of the Beechy member. The δ^2H values increase linearly through the Beechy to the base of exploration, and the lower boundary was set as a constant concentration boundary.

The transport of δ^2H was simulated in two phases using two different domains as conceptualized in Figure 4.35. Phase I investigated the time required to generate the δ^2H profile across the till-clay interface with the domain extending from the top of the unoxidized Battleford till to the base of the Beechy. The development of the curvature of the profile in the upper till during the Holocene (Hendry and Wassenaar, 1999) was simulated in Phase II with the domain extending from the top of the oxidized till to the base of the Battleford.

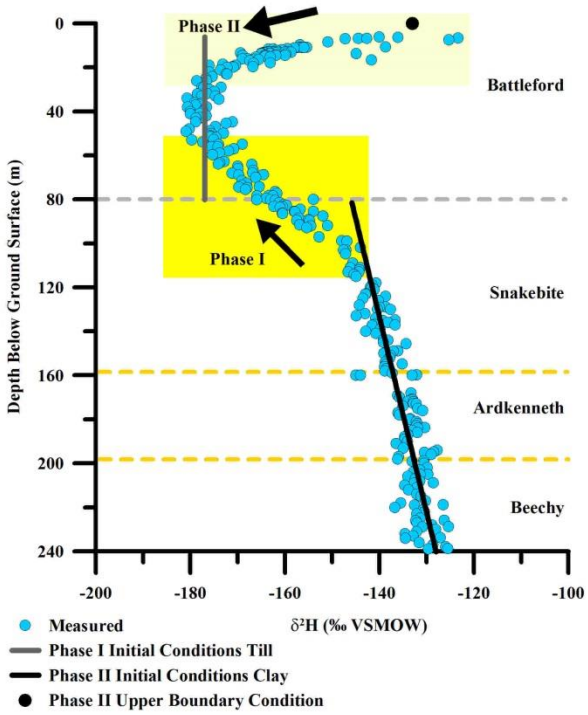

Figure 4.35. Conceptualization of the two phases of δ^2H transport modeling at the King site. Phase I simulated the time required to develop the curvature of the profile across the till-clay interface since deposition of the till. Phase II simulated the time required to develop the curvature from δ^2H values of modern day precipitation to the ^2H-depleted values attributed to glacial waters. The yellow boxes highlight the focal points of the modeling in Phase I and Phase II.

The initial δ^2H in the till (throughout deposition) and the Cretaceous sediments (prior to till deposition) are not known. In Phase I, an initial value of –177‰ was assigned through the entire thickness of the till (0-80 m BGS). This is the μ value of δ^2H measured in the 2013 core between 20-50 m BGS, an interval over which the isotopic values are relatively constant with depth. This value is consistent with –178‰ used by Hendry and Wassenaar (1999) and Hendry

et al. (2011). The corresponding μ $\delta^{18}O$ value over this depth interval in the King site data (–23‰) is typical of glacial waters (Remenda et al., 1994). The $\delta^{2}H$ of the glacial water was assumed to be constant over the timing of till deposition based on the homogeneity of the physical properties of the sediments (Shaw and Hendry, 1998; Hendry and Wassenaar, 1999).

The initial $\delta^{2}H$ profile across the Snakebite and Lower Shale prior to till deposition was assumed to be near steady state and consequently the initial conditions were represented by a linear depth profile from the top of the Snakebite to the base of the Beechy. Near steady state depth trends through the Cretaceous have been measured elsewhere. A near-linear $\delta^{2}H$ depth profile (Figure 4.36 (K2)) was measured through Cretaceous geology approximately 350 km southeast of the King site, near Esterhazy, SK (Hendry et al., 2013). Cretaceous formations including the Bearpaw through Milk River equivalent in age to those at the King site underlie southeastern Saskatchewan (Saskatchewan Ministry of Economy, 2014). As demonstrated in Figure 4.36 (K2), the $\delta^{2}H$ values increase linearly with depth through the Cretaceous sediments in the Esterhazy data. A model of the corresponding $\delta^{18}O$ profile at the Esterhazy site suggests that diffusion between two end members (meteoric surface waters and basinal brines) evolved into a near-linear profile over geologic time (Hendry et al., 2013). Assuming a linear profile existed in the Snakebite and Lower Shale at the King site prior to till deposition seems reasonable based on the Esterhazy data set.

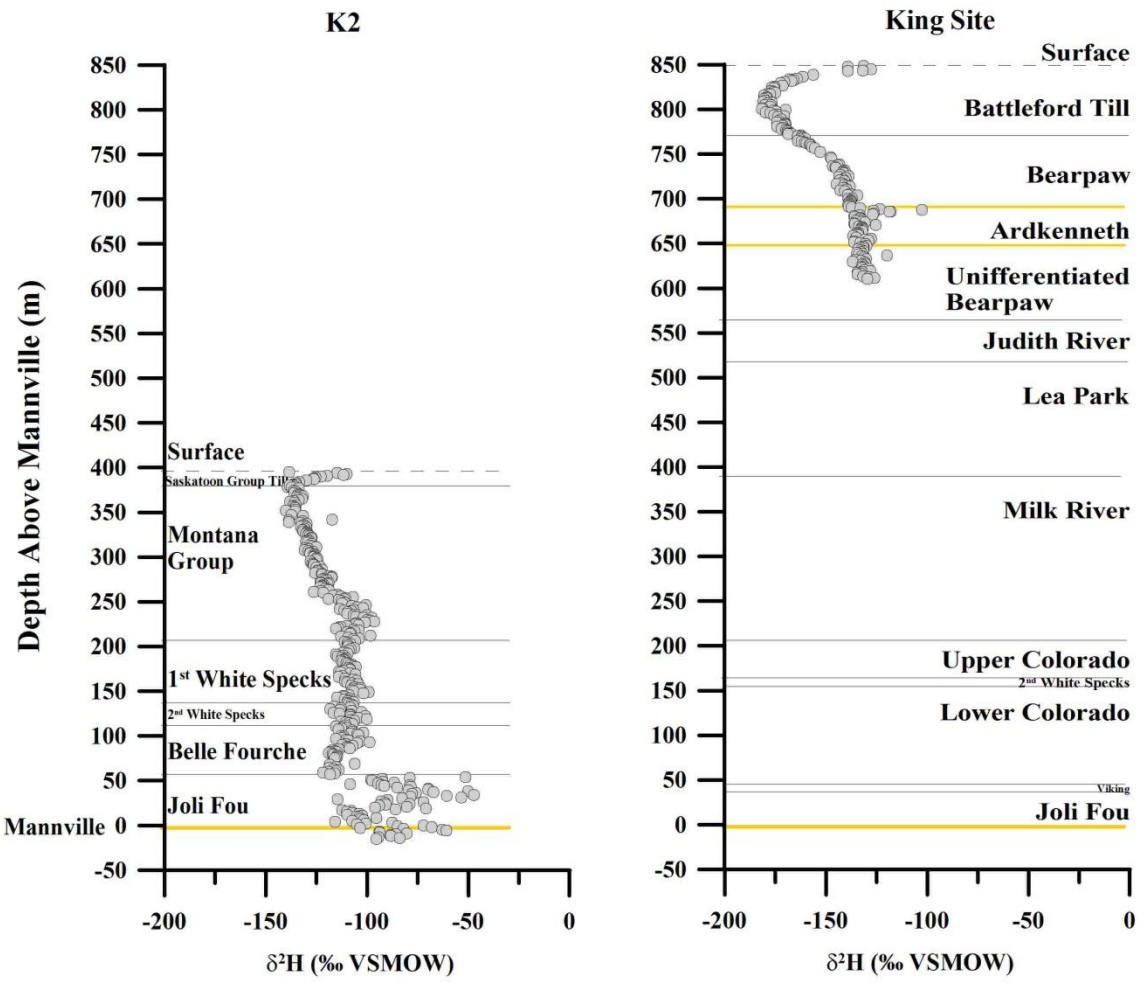

Figure 4.36. δ^2H profiles from a site near Esterhazy, SK (K2; Hendry et al., 2013) and the 2013 King site data. The profiles are shown with the Cretaceous Mannville aquifer as datum and pass through correlating Cretaceous geology. At the K2 site, the Montana Group sediments include the Bearpaw, Judith River, Lea Park and Milk River (Saskatchewan Ministry of the Economy, 2014).

The lower boundary at the base of exploration at the King site (240 m BGS) was assumed to be –128‰. This is the μ δ^2H at the bottom of the 2013 profile (236-239 m BGS). Linear extrapolation upwards from –128‰ at 240 m BGS to the top of the Snakebite (80 m BGS) suggested that the δ^2H of the pore water at the till-clay contact was approximately –145‰. Simulations performed using a δ^2H value at the till-clay contact between –143 and –150‰ (data not presented) showed that a δ^2H value of –146‰ produced the lowest SSE values. This value

differed from that of Hendry and Wassenaar (1999) and Hendry et al. (2011) because the current study showed higher resolution values over a greater thickness of bedrock. Hendry and Wassenaar (1999) defined the top of the Ardkenneth aquifer as their lower boundary with a fixed value of –144‰ based on δ^2H values of three water well samples from the Ardkenneth near the King site, and two pore water samples from cores in the Snakebite (deeper than 105 m BGS). Hendry et al. (2011) observed that using a value of –142‰ for the lower boundary improved modeling results. Phase I was simulated over a range of time frames (27-43 ka BP) as in Hendry and Wassenaar (1999) and Hendry et al. (2011).

Phase II simulated the evolution of the δ^2H profile through the upper portion of the till using the results from the 20 and 30 ka simulations derived in Phase I. In Phase II, a fixed δ^2H value representative of modern precipitation was applied to the upper boundary at 5 m BGS using a constant initial δ^2H condition with depth as described previously. Simulations performed using a range of upper boundary condition values (–130 to –136‰) (data not presented) yielded the lowest SSE using a value of –133‰. This value is consistent with those used by Hendry and Wassenaar (1999) and Hendry et al. (2011) who used δ^2H values of –136 and –130‰, respectively. The lower boundary condition in Phase II simulations remained the same as in Phase I. Simulations were executed over time frames between 7-13 ka, in keeping with previous modeling exercises (Hendry and Wassenaar, 1999; Hendry et al. 2011).

4.7.3 δ^2H simulation results

The simulations producing the lowest SSE were those with zero *v*; Phase I over 20 ka and Phase II over 7 ka (Table 4.6). Given the goodness of fit for the 20 ka results, this timeframe was used to determine the sensitivity of the δ^2H model to *v*. Downward groundwater fluxes of 0.5 and 1.0 m/10 ka were applied in the model. Shaw and Hendry (1998) estimated the downward *v* at the King site to be between 0.5 and 0.8 m/10 ka. Hendry and Wassenaar (1999) obtained the best visual fit of their δ^2H model using a *v* of 1.0 m/10 ka. Hendry et al. (2011) applied 1.0 m/10 ka to their model, but found a better fit was obtained using zero *v*. Figure 4.37 demonstrates that a *v* of 0.5 m/10 ka provides a reasonable fit, and that a *v* of 1.0 m/10 ka does not fit the measured data as well. The SSE of models including *v* are greater than those models with no *v* (Table 4.6).

The models with the five lowest SSE are presented in Figure 4.38 and the values of SSE for these simulations at varying elapsed times and *v* are presented in Table 4.6. The five models presented in Figure 4.38 are simulations with no *v*. The time frames ranged between 20-30 ka for Phase I and 7-11 ka for Phase II. As Figure 4.38 demonstrates, the visual differences in the modeled profiles are slight amongst simulations with the lowest SSE, suggesting a range of acceptable possibilities. The timelines produced in this modeling exercise are in keeping with the transport times of 20-30 ka for the till-clay interface development and 7.5-10 ka for development of the upper portion of the profile by Hendry and Wassenaar (1999) while the best fit obtained by Hendry et al. (2011) for similar data was 20 ka for Phase I and 7-13 ka for Phase II. The Battleford till was reportedly deposited approximately 20 ka BP (Christiansen, 1967) so the results of this current model are in keeping with the reported time frame of till deposition. The interval 7-11 ka for Phase II is comparable to climate records of the Holocene for the south-central parts of Saskatchewan (Sauchyn and Sauchyn, 1991). Re-creations of the last (Wisconsinan) deglaciation suggest the area around the King site was deglaciated approximately 14 ka BP and the entire region ice-free by 10 ka BP (Christiansen, 1979). The results of the above-described simulations of the δ^2H profile are consistent with these time frames.

To further assess if the best-fit modeling outcome supports the inference that the system is diffusion dominated, a Péclet number (*P*) was calculated using (Remenda et al., 1996):

$$P = \frac{v^2 T}{D} \qquad \text{(Eq. 4.2)}$$

For the purpose of this calculation, a *v* of 0.5 m/10 ka and a model duration (*T*) of 27 ka were used, and D = D_e, which was 1.7 x 10^{-10} m^2 s^{-1} (converted to m^2 y^{-1}). A $P <<< 1$ confirms diffusion to be the dominant transport mechanism in the system under investigation (Huysmans and Dassargues, 2004). Using the above definition of *P* (Eq. 4.1), Remenda et al. (1996) determined that parameters producing a $P > 0.1$ would not provide a satisfactory fit between their measured and modeled data. The calculated *P* using the parameters from the aforementioned simulations in this study was 0.01, which is much less than the reported acceptable values of 1 and 0.1. Therefore, the δ^2H profiles in the current study are consistent with diffusion-dominated transport.

Table 4.6. The effects of time and *v* on the SSE of the simulations performed for the δ^2H profile at the King site.

Phase I (ka BP)	**Phase II (ka BP)**	***v* ($m\ d^{-1}$)**	**SSE**
20	7	0	571
30	7	0	573
20	9	0	620
30	9	0	623
20	11	0	716
30	11	0	728
20	13	0	841
30	13	0	870
20	7	0.5 m/10 ka	1023
20	9	0.5 m/10 ka	1162
20	11	0.5 m/10 ka	1370
20	13	0.5 m/10 ka	1607
20	7	1.0 m/10 ka	1748
20	9	1.0 m/10 ka	2046
20	11	1.0 m/10 ka	2425
20	13	1.0 m/10 ka	2842

The model-derived time frames for development of the δ^2H profile at the King site are consistent with previous modeling studies (Hendry and Wassenaar, 1999; Hendry et al., 2011). Slight differences are attributed to the higher resolution and increased depth of the 2013 profile and slightly modified boundary conditions or independently measured physical parameters. However, the good agreement between the simulations from this study and the field data conclude that diffusion is the dominant mode of solute transport at the King site. Based on the goodness of fit, it was concluded that the input parameters used in Hydrus were appropriate and applicable to modeling the CH_4 concentration-depth profile.

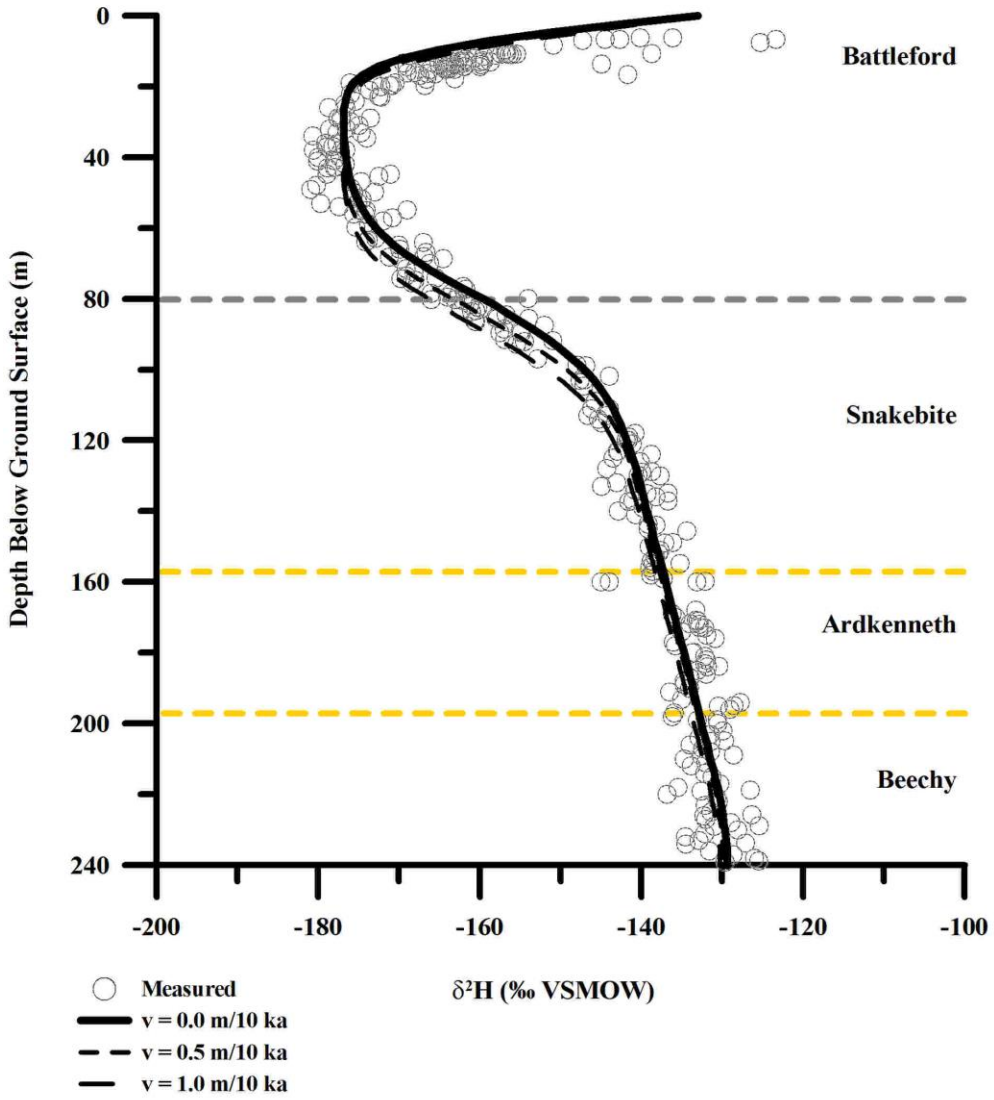

Figure 4.37. Measured and simulated δ^2H results for the 2013 King site core. The simulations display the effects of varying *v* on the model. Best fit was attained with zero *v* over 20 ka for Phase I and 7 ka for Phase II. This time frame is shown here with a range of *v* applied to the simulations.

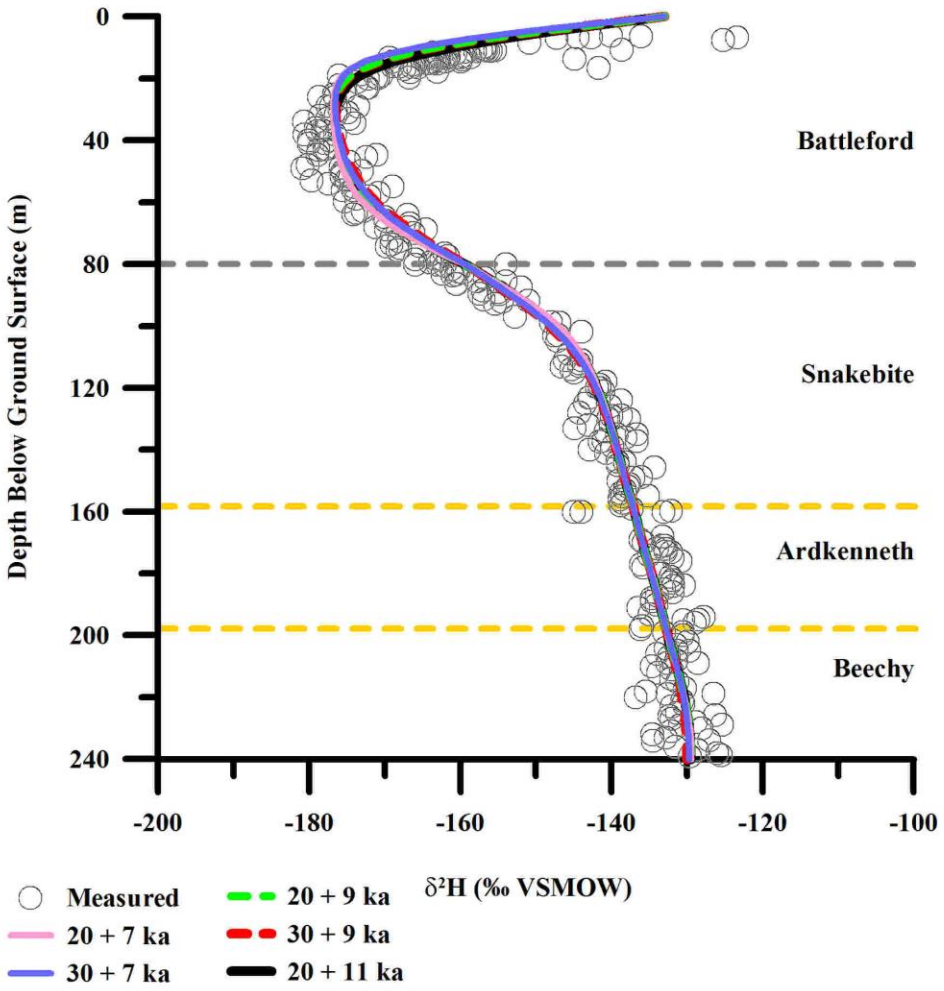

Figure 4.38. Measured and simulated δ^2H results for the 2013 King site core samples. Simulated results are those that yielded the five lowest SSE values in Table 4.6. Zero *v* was applied in these simulations.

4.7.4 Conceptual model of CH_4 fate and transport

Models of CH_4 in shallow sea sediments (< 2-3 m) suggest that CH_4 concentrations increase linearly with depth when no geochemical processes affect its transport. A concave-upward concentration-depth profile will result if there is CH_4 consumption as it diffuses upwards from a source (Claypool and Kaplan, 1974; Barnes and Goldberg, 1976; Martens and Berner, 1977; Bernard et al., 1978; Bernard, 1979; Martens, 1982; Reeburgh, 1982). In this case, the consumption of CH_4 can be described by a first-order reaction (Libes, 2009).

The 80 m of the CH_4 profile in the Snakebite at the King site is concave-upward in shape, suggesting an apparent consumption in CH_4. The King site CH_4 and Cl^- depth profiles exhibit similar trends over most depths, but the profiles diverge in the upper Snakebite (from ~80-130 m BGS). While the Cl^- profile approaches near zero concentration at the top of the Snakebite, the depth of zero-CH_4 concentration occurred ~10 m into the clay profile (~90 m BGS; Figure 4.20 (a)). This difference between the Cl^- and CH_4 profiles suggests that some process affects the distribution of CH_4 over a thickness of the Snakebite that does not affect the distribution of Cl^-. This process could be attributed to the removal of dissolved CH_4 by biological or geochemical consumption.

Accumulations of biogenic gas have been reported in laterally-extensive Cretaceous-aged geologic formations in Alberta and Saskatchewan (Andrews et al., 1991; Ridgley, 1998). Andrews et al. (1991) reported CH_4 concentrations between 115 and 400 mg L^{-1} in groundwater from the Cretaceous Milk River Formation in southeastern Alberta and southwestern Saskatchewan. The Milk River Formation is an aquifer which lies ~219 m below the base of the 2013 King site borehole (~460 m BGS; Arden Marsh, Saskatchewan Geological Survey, personal communication). The reservoir of natural gas in the Milk River was assumed to be the source of CH_4 diffusing upwards into the King site sediments.

The absence of CH_4 in the till precludes its use for estimating the timing of deposition of the Battleford till, as was done using the δ^2H profile. The focus of the CH_4 modeling rather was to investigate the development of the curvature of the CH_4 profile in the upper Snakebite (Figure 4.39). Two approaches were pursued for this investigation; the domain in the first (Approach I) included the Battleford till from surface to 80 m BGS, 80 m of Snakebite clay, and the grouping of the Ardkenneth and Beechy members as the Lower Shale. For comparison to the δ^2H model and to observe whether or not CH_4 transport could have been impacted by the timing of the Battleford till deposition, this approach was executed over similar timeframes (20-50 ka). Saskatchewan experienced numerous glaciations, dating back to the Early Pleistocene (~ 0.78 Ma; Barendregt et al., 2012). To test the impact earlier glaciations may have had on CH_4 transport in the Upper Snakebite, the second modeling approach (Approach II) excluded the Battleford till in the domain, and situated the top of the Snakebite as the upper boundary condition. These simulations were carried out over a longer timeframe (1 Ma). The geologic

units from the base of the Beechy to the top of the Milk River (Figure 4.40) were included as part of the Lower Shale in both approaches and were assumed to have the same physical properties as the Ardkenneth and Beechy.

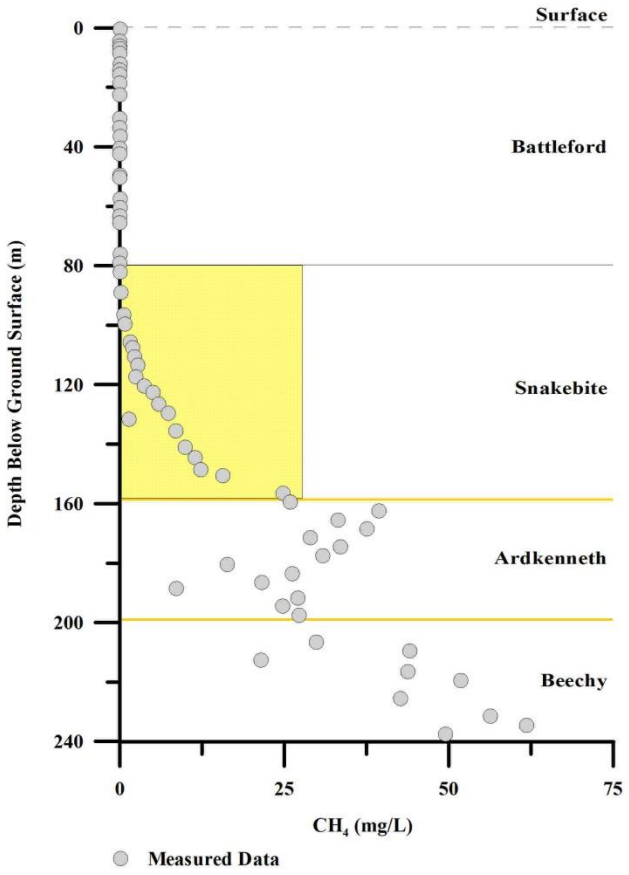

Figure 4.39. CH_4 concentrations versus depth at the King site. The yellow highlighted box indicates the focus of the CH_4 transport modeling using Approach I and II.

The two modeling approaches included assumed initial conditions for CH_4, because defining the initial concentrations was not possible. For Approach I, the CH_4 upper boundary was assigned a constant concentration of zero, and initial conditions remained at 0 mg L^{-1} within the Battleford till. The linear relationship between the measured CH_4 and δ^2H data in Figure 4.22 was used to estimate the initial steady state conditions of CH_4 from the top of the Snakebite to the top of the Milk River prior to till deposition (Figure 4.40 (a)) as being consistent with the initial conditions used for δ^2H. Using δ^2H values of –145‰ at 80 m BGS and –128‰ at 240 m BGS, the regression relationship between CH_4 and δ^2H (Figure 4.22) produced CH_4

concentrations of ~0 mg L^{-1} at 80 m BGS and ~55 mg L^{-1} at 240 m BGS. Extrapolation to the top of the Milk River produced a CH_4 concentration of ~130 mg L^{-1}. This concentration is consistent with reported concentrations of CH_4 in that unit in southwestern Saskatchewan. As such, the lower boundary condition was assigned a constant CH_4 concentration of 130 mg L^{-1}.

In Approach II, the initial conditions through the entire Snakebite were set at a constant value (Figure 4.40 (b)). This was an assumption considered for modeling purposes, while theoretically the concentrations would change with depth according to the solubility of CH_4 as a function of in-situ temperature and pressure conditions. Methane saturation in shallow sea waters (< 2 m) is between 15-30 mg L^{-1} (Martens and Berner, 1977). This concentration would vary with time as the sediments were exposed by erosion and covered by deposition but for the purpose of this exercise, were assumed to be constant through the 80 m thickness of the Snakebite. The constant concentration was varied in trial simulations with different initial concentrations of 5, 10, 15, and 25 mg L^{-1} as the initial condition. From the top of the Ardkenneth (80 m BGS) to the lower boundary (Milk River, 380 m BGS) in Approach II, CH_4 transport was assumed to be at steady state. Concentrations increased linearly from the assigned constant concentration in the Snakebite to the top of the Milk River. The lower boundary concentration was fixed, and was varied in the trial simulations from 75-130 mg L^{-1}. The upper boundary was fixed at a constant concentration of 0 mg L^{-1} assuming that CH_4 would be rapidly oxidized upon exposure to oxygen. The initial conditions for Approach I and selected models for Approach II are depicted in Figure 4.40 (a) and (b), respectively.

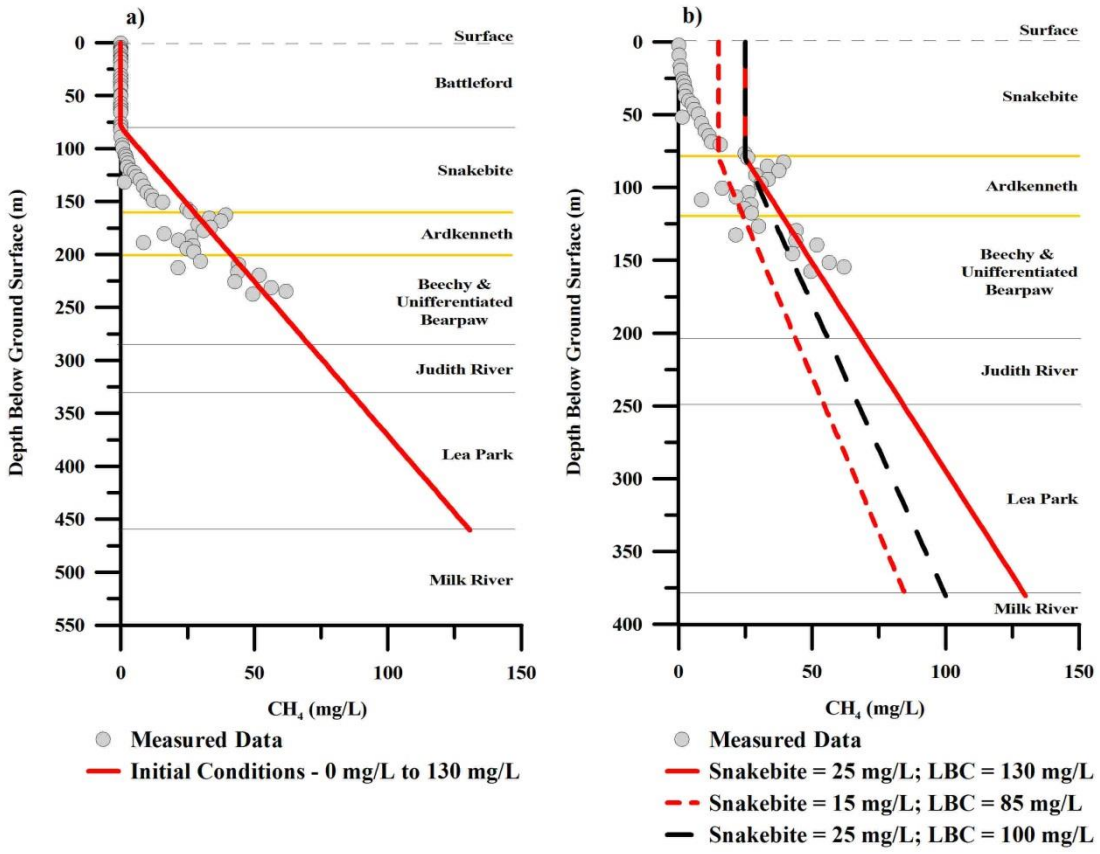

Figure 4.40. CH_4 concentrations versus depth at the King site shown along with the initial conditions that were applied in the two transport modeling approaches. The y-axes are different scales as a result of exclusion of the Battleford till in the domain of Approach II.

Both approaches incorporated a first-order reaction in various thicknesses of layers of the Snakebite. First order reaction constants for the consumption of CH_4 (k_1) reported in the literature range between 8.8×10^{-2} and 1.6×10^{-5} d^{-1} (Martens and Berner, 1977; Bernard, 1979, Martens, 1982; Reeburgh, 1982). The value of k_1 was systematically adjusted throughout the modeling process to improve the fit of the models to the measured data. The thickness of the reaction layer within the Snakebite was varied from 2 to 80 m. It was assumed that CH_4 concentrations were below the solubility limit and degassing was not considered to contribute to CH_4 transport.

The methanotrophs responsible for consumption of CH_4 could have been deposited during one of the glaciation/deglaciations that occurred in southwestern Saskatchewan. Communities of methanotrophs reportedly exist at the forefields of receding glaciers (Bárcena et

al., 2010, 2011). A disturbed zone, ~2 m-thick, was observed at the till-clay interface at the King site; bacteria were present in this zone and this was attributed to exposure and mixing of these sediments during the last glacial period, ~30 ka BP (Lawrence et al., 2000). Alternatively, methanotrophic bacteria may have been present during deposition of the Snakebite in the Late Cretaceous. Birgel et al. (2006) found evidence of both anaerobic and aerobic methane oxidizing bacteria in limestones of Late Cretaceous CH_4 seeps within the Pierre shale in Colorado. It stands to reason then that the bacteria responsible for consumption of CH_4 have multiple possible origins. Detailed investigation into microbial activity within the Snakebite clay and its origins is beyond the scope of this study, but could be considered for future work.

4.7.5 CH_4 simulation results

The results of simulations following Approach I are presented in Figure 4.41 (a-d) and the SSE are summarized in Table 4.7. Over the time frames 20-50 ka, reaction layers of 20, 40, and 80 m thick were determined to be insufficient to cause the curvature of the observed CH_4 profile in the Snakebite (Figures 4.41 (a), (b), and (d)). With a reaction layer thickness of 60 m, the model showed a visually improved match to the measured data. A reaction layer thickness of 70 m was attempted and while it yielded better fits to the measured data than 20 and 40 m (Figure 4.42), the SSE were not lower than some of the simulations using 60 or 80 m reaction layer thicknesses.

As the thickness of the reaction layer increased, the value of k_1 that provided the closest fit of the models to the measured data required adjustment. The simulations with 20 and 40 m-thick reaction layers with the lowest SSE had a k_1 of 6.9×10^{-3} d^{-1} (however, visually these simulations did not provide a satisfactory fit to the measured data). The simulation with a 60 m-thick reaction layer with the lowest SSE had a k_1 of 2.5×10^{-7} d^{-1} and that of the simulations with the 70 and 80 m-thick reaction layers was 1.0×10^{-7} d^{-1}. As the reaction layer thickness increased, the k_1 value decreased. While the k_1 values applied in these modeling exercises are lower than those reported in the literature, it should be noted that the sediments in which those k_1 values were measured were shallow marine sediments, and not deeper and older geologic units as were modeled in this study.

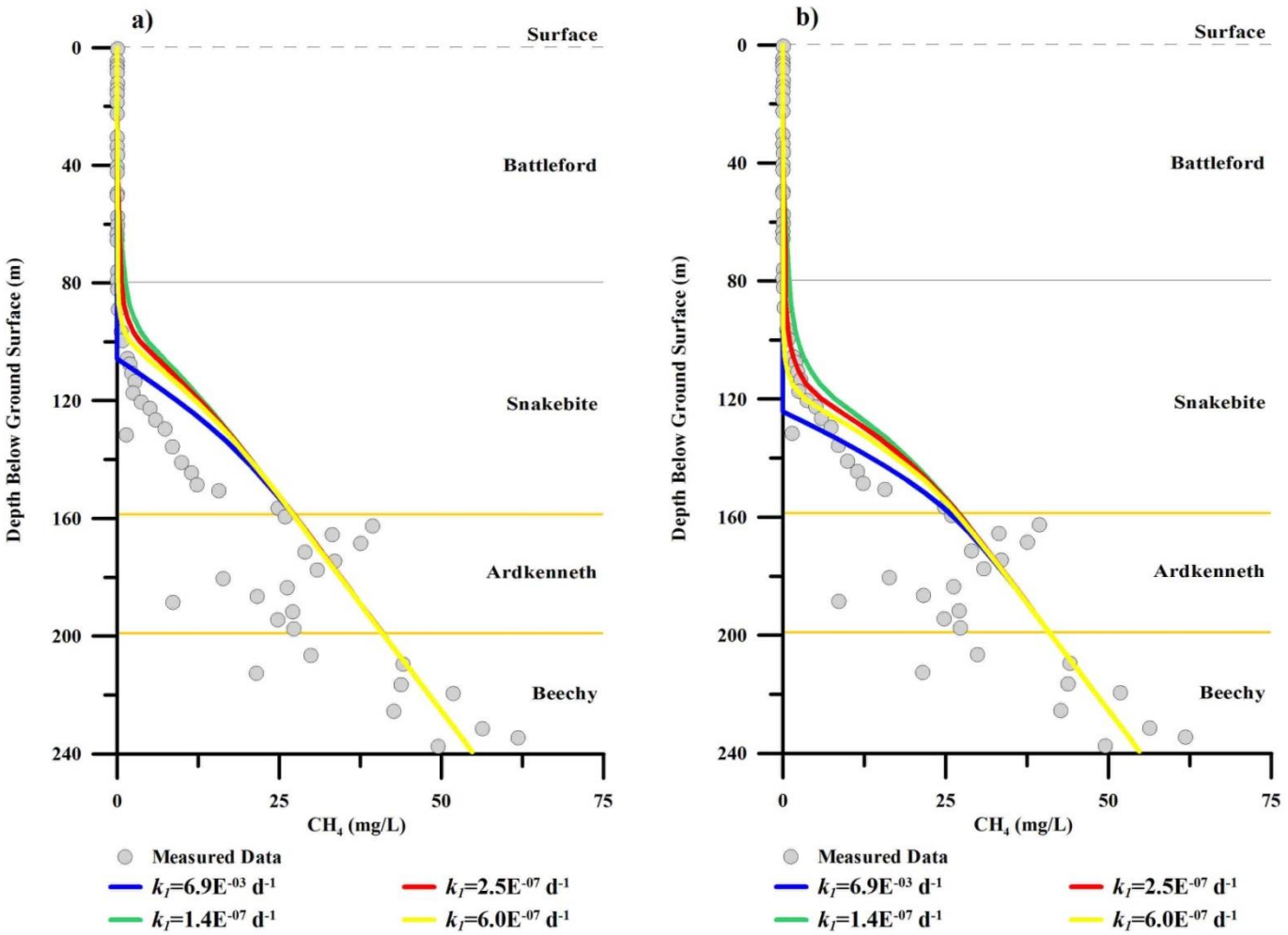

Figure 4.41. Simulations of CH_4 transport with reaction layers (a) 20 m thick and (b) 40 m thick. All simulations shown were executed over 30 ka. The legends depict some of the different k_1 values that were applied in the simulations.

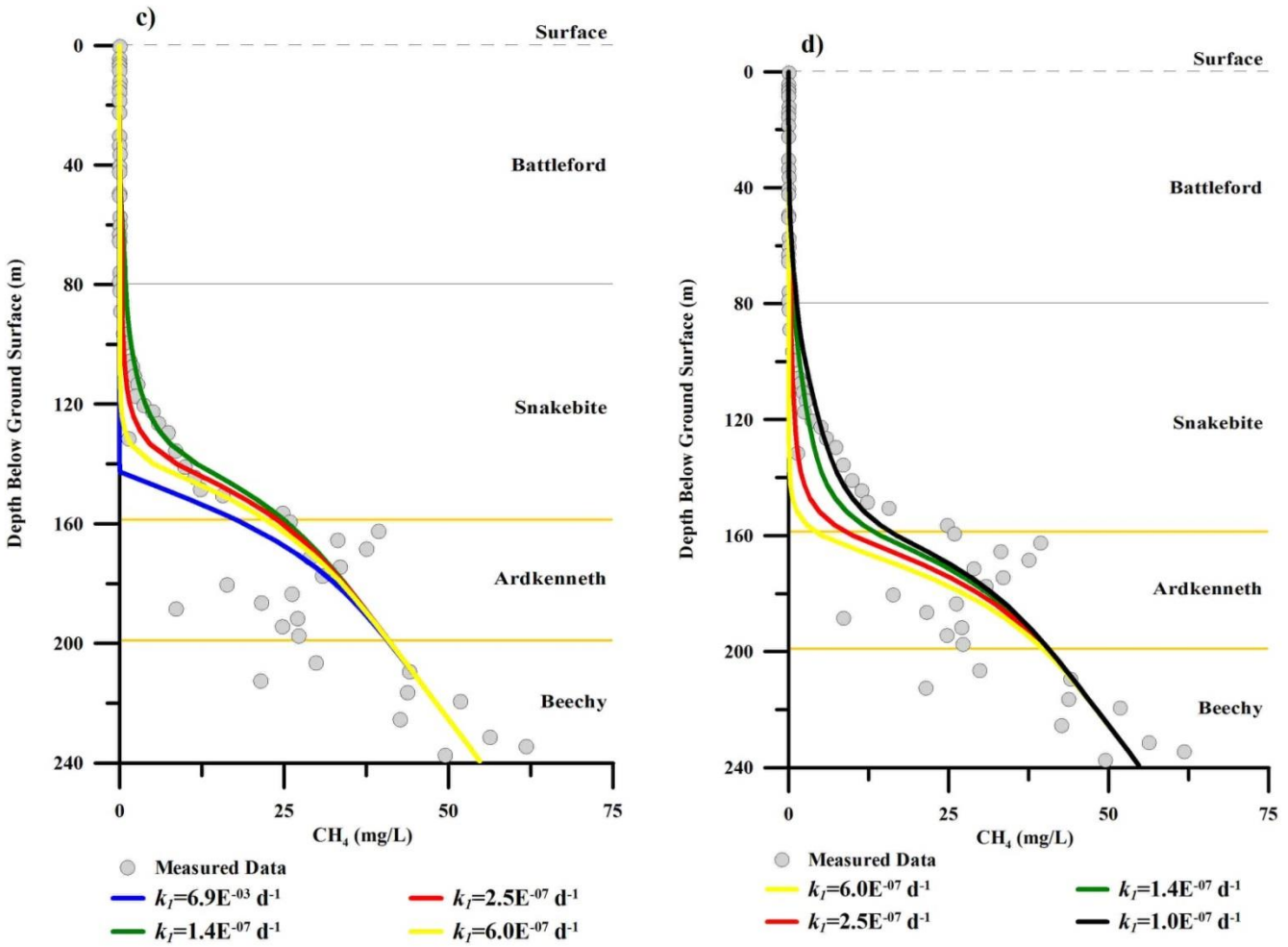

Figure 4.41. Simulations of CH_4 transport with reaction layers (c) 60 m thick and (d) 80 m thick. All simulations shown were executed over 30 ka. The legends depict some of the different k_1 values that were applied in the simulations.

Table 4.7. The calculated SSE between CH_4 transport simulations and measured CH_4 data modeled according to Approach I. These simulations were carried out over 30 ka, with linear initial conditions through the Snakebite from 0 mg L^{-1} at 80 m BGS to 130 mg L^{-1} at the top of the Milk River (460 m BGS). The last SSE presented was calculated from the simulation with two reaction layers (80-115 m and 116-150 m BGS).

Reaction Layer Thickness (m)	k_1 **(d^{-1})**	**SSE**
20	6.9×10^{-3}	3029
	6.0×10^{-7}	3295
	2.5×10^{-7}	3393
	1.4×10^{-7}	3451
40	6.9×10^{-3}	2442
	6.0×10^{-7}	2678
	2.5×10^{-7}	2809
	1.4×10^{-7}	2949
60	6.9×10^{-3}	2534
	6.0×10^{-7}	2286
	2.5×10^{-7}	2260
	1.4×10^{-7}	2332
	1.0×10^{-7}	2433
80	6.0×10^{-7}	2902
	2.5×10^{-7}	2602
	1.4×10^{-7}	2315
	1.0×10^{-7}	2247
70	1.4×10^{-7}	2248
	1.0×10^{-7}	2248
35 34	2.0×10^{-7} 1.0×10^{-7}	2222

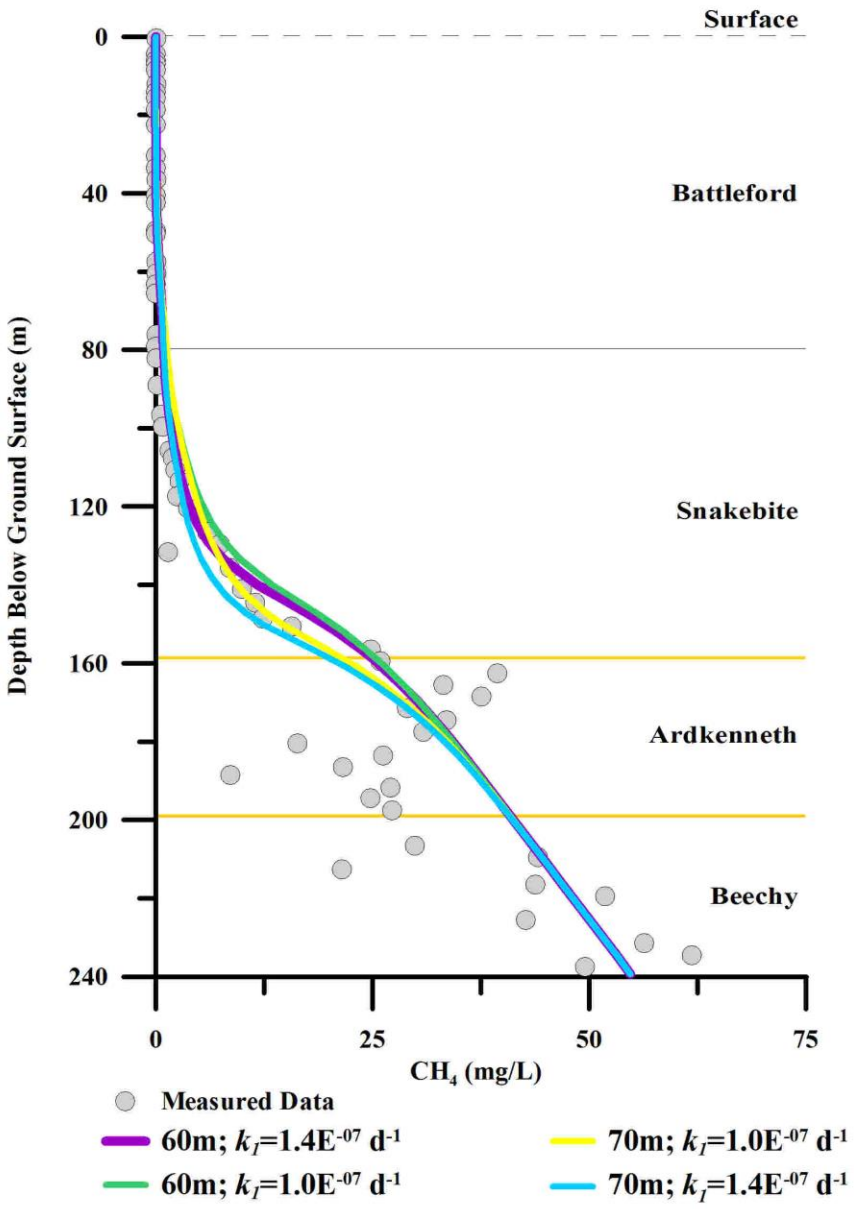

Figure 4.42. Comparison of simulated CH_4 transport with reaction layers 60 and 70 m thick in the Snakebite clay, executed over 30 ka. The legend distinguishes the different values of k_1 applied in the simulations.

To further optimize the simulated profile using Approach I, additional simulations were attempted by incorporating two reaction layers in the Snakebite. The CH_4 profile through the Snakebite shows a change in slope at ~115 m BGS (Figure 4.43). For modeling purposes, it was considered that possibly an influx of glacial water impacted the rate of reaction in the upper

portion of the Snakebite. An influx of oxygen-rich fresh water to a system previously lacking, or low in, oxygen can introduce different bacteria (or simply introduce bacteria) (Birgel et al., 2006). Several types of bacteria are known to use CH_4 for energy, and do so at different rates (Hanson and Hanson, 1996). Perhaps it was the case at the King site that glaciation introduced a new/different set of bacteria to the upper Snakebite.

Using the same domain and timeframes as Approach I, two separate reaction layers were modeled: 80-115 m BGS and 116-150 m BGS. These simulations produced visually satisfactory fits with $k_1 = 2.0 \times 10^{-7}$ d^{-1} in the 80-115 m layer, and $k_1 = 1.0 \times 10^{-7}$ d^{-1} in the 116-150 m layer, over 30 ka (Figure 4.44 (a)). As Figure 4.44 (b) suggests, this model provides a better visual fit over portions of the profile where the other models do not follow the measured data as closely. The SSE of this simulation was also lower than any of the single-reaction layer models.

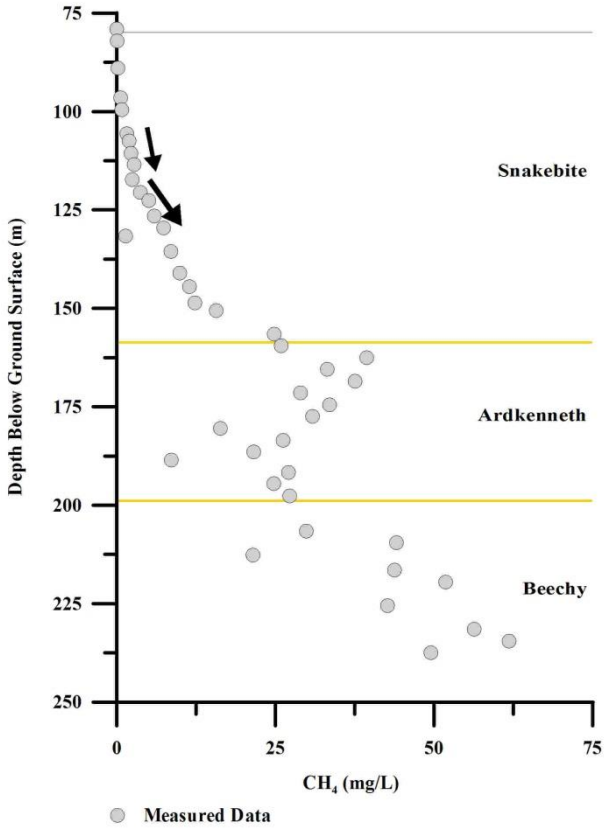

Figure 4.43. The measured CH_4 data with depth from the King site. The arrows indicate the location of a change in slope in the profile at ~115 m BGS. This change in slope was considered to have influenced the transport of CH_4 by causing different consumption rates between the two layers (80-115 m BGS and 116-160 m BGS).

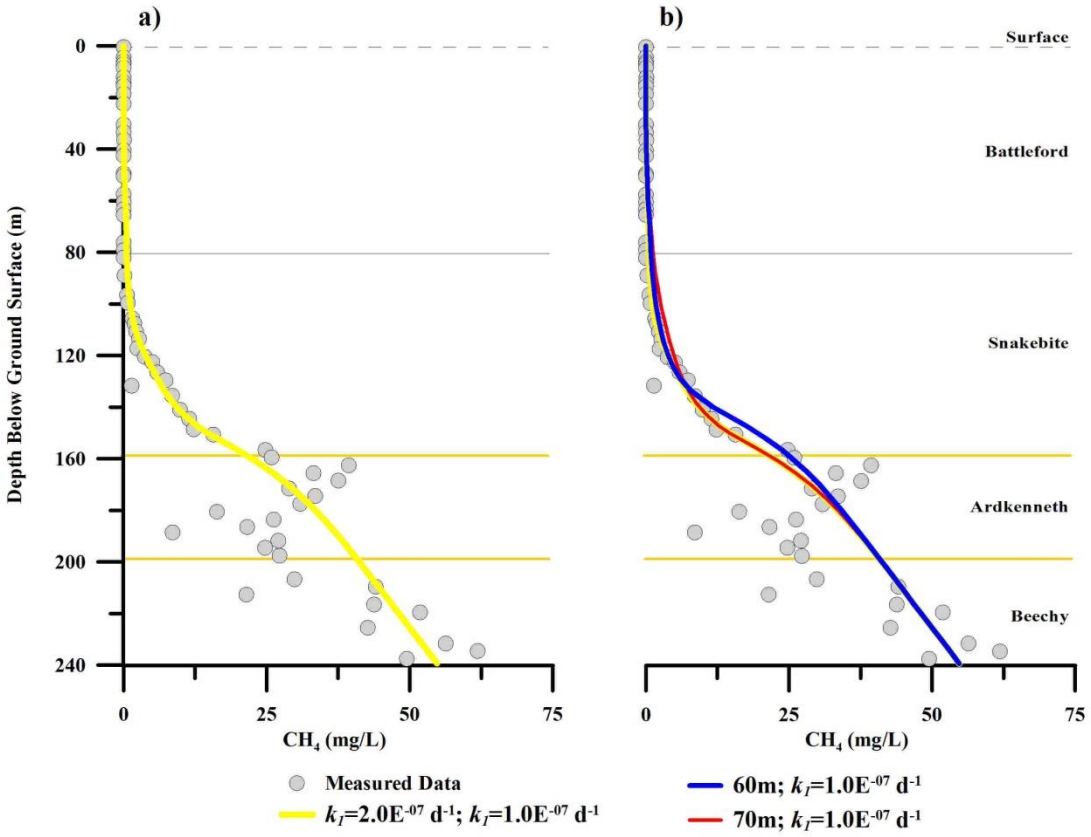

Figure 4.44. Simulations of CH_4 transport with (a) two reaction layers: 80-115 m, k_1 = 2.0 x 10^{-7} d^{-1} and 116-150 m, k_1 = 1.0 x 10^{-7} d^{-1}, and (b) a comparison of the simulation from (a) with two of the simulations that had one reaction layer of 60 and 70 m thicknesses.

The results for Approach II are presented in Figure 4.45 and the SSE are summarized in Table 4.8. Very tight visual fits to the curvature in the upper Snakebite are achieved with the single reaction layer of 30 m thickness over the 1 Ma timeframe with initial conditions of 15 mg L^{-1} through the Snakebite. The modeling scenarios which provided satisfactory visual fits over the Snakebite required lower boundary conditions of between 75-85 mg L^{-1} CH_4, which does not match the measured data through the lower Ardkenneth and Beechy, causing poor SSE. The simulations from Approach I however, also suffered poor matches within the lower portion of the profile. Overall the simulations produced by Approach II have lower SSE and suggest that the consumption of CH_4 took place over a longer timeframe than 30-50 ka, and the reaction layer was ~30 m thick, in the upper Snakebite. The k_1 that offered the best visual fit between the

simulations and measured data was 2.0 x 10^{-7} d^{-1}, which is within the range of k_1 values that were applied in Approach I simulations.

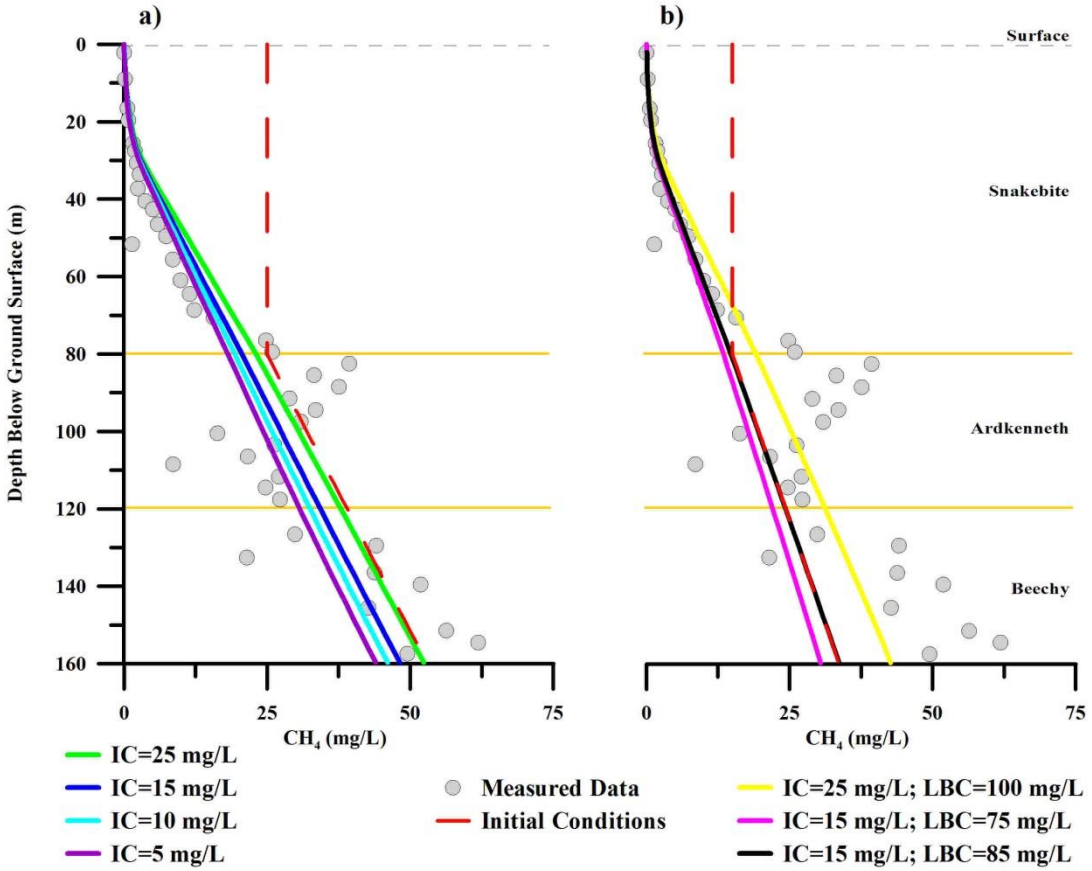

Figure 4.45. Simulations of CH_4 transport according to Approach II. All simulations are shown over 1 Ma with a k_1 = 2.0 x 10^{-7} d^{-1}. The Lower Boundary Condition (LBC) for simulations in (a) was 130 mg L^{-1}, and the Initial Conditions (IC) through the Snakebite were varied at 25, 15, 10 and 5 mg L^{-1} CH_4. The LBC for the simulations in (b) are presented in the legend.

Table 4.8. A summary of the calculated SSE between the CH_4 transport simulations and the measured 2013 King site CH_4 data, modeled according to Approach II. The simulations below were carried out over 1 Ma and the reaction layer was 30 m thick through the top of the Snakebite. The initial conditions in the Snakebite were constant values, varied between simulations, as was the lower boundary condition.

k_1 (d^{-1})	Snakebite Initial Conditions (mg L^{-1})	Lower Boundary Condition (mg L^{-1})	SSE
7.0×10^{-7}	25	130	1678
2.0×10^{-7}	15	130	1757
2.0×10^{-7}	10	130	1731
2.0×10^{-7}	5	130	1824
7.0×10^{-7}	25	100	1965
2.0×10^{-7}	25	100	1972
2.0×10^{-7}	15	85	3519
2.0×10^{-7}	15	75	4461

In summary, modeling of CH_4 transport with a first order reaction shows that reasonable fits to the measured CH_4 data can be obtained by varying the initial conditions and lower boundary conditions. Poorly constrained initial conditions in a modeling scenario increase the uncertainty in the model representing the natural system (Bear and Cheng, 2010). The difficulty in defining the initial CH_4 conditions at the King site therefore poses a challenge in developing a unique modeling solution. This challenge is compounded by the presence of the lateral movement of solutes within the Ardkenneth which cannot be solved with one-dimensional modeling. Therefore, the CH_4 models presented above must be considered non-unique. It is clear that consumption of CH_4 controls its transport in the Snakebite, and that CH_4 is not behaving conservatively in at least the upper 30 m of that geologic unit. Future work should involve a more robust, two-dimensional modeling approach.

CHAPTER 5

CONCLUSIONS

The requirement for baseline gas compositional and isotopic data from shallow groundwater systems cannot be underestimated. Such information is crucial in fugitive gas migration investigations to distinguish natural in-situ gas versus foreign gas migrated from depth. This study provides baseline compositions of natural gases and their isotopes in Cretaceous and Quaternary strata that are laterally extensive across North America. The combination of data used to characterize the gases (bulk composition, $\delta^{13}C_{CH4}$, $\delta^{2}H_{CH4}$, and $\delta^{13}C_{C2H6}$), indicate that the gas is bacterial in origin. Comparison of CH_4 data with $\delta^{2}H$ and Cl^- measured as part of this study suggests CH_4 behaves as a conservative tracer.

The compilation of physical and chemistry data from the sediments at the King site presented in this study are in agreement with the parameters previously measured at the site. Therefore, the data presented on the Cretaceous units not encountered in other studies (Ardkenneth and Beechy) can be incorporated with confidence.

Numeric modeling of the $\delta^{2}H$ of the pore waters at the King site produced results that coincide with timing and parameters used in previous studies. A timeframe of 20-30 ka was predicted for the development of the pore water isotope profile over the till-clay interface and a timeframe of 7-9 ka was predicted for the development of the upper portion of the profile. These timeframes are in agreement with climate records of the Holocene, and with previous modeling studies at the King site.

The successful results of the $\delta^{2}H$ modeling using Hydrus-1D software enabled application of those model parameters to simulations of CH_4 transport. Slight modifications to the lower geology were required to incorporate the source for CH_4, presumed to be the Milk River aquifer. The zero-concentration boundary of the CH_4 lies at depth within the Snakebite clay, up to 20 m below the top of that unit, which also differed from the $\delta^{2}H$ profile.

While this was problematic, physical evidence indicates the transport of CH_4 could have been delayed by increased moisture content in the upper Snakebite due to glacial unloading. Modeling of the hydraulics of the system could provide valuable insight into this problem. A first-order reaction was invoked in modeling of the CH_4 to attempt to develop the curvature in the profile, which is suggestive that consumption of the gas occurred. While the solutions developed in this study for defining CH_4 fate and transport were non-unique, they are conclusive in that a reaction impacts the transport of the gas, which does not affect other conservative tracers in the King site sediments. There is a multitude of evidence presented in this study which suggests, however, that CH_4 does show the potential in certain sediments to transport conservatively.

CHAPTER 6

RECOMMENDATIONS FOR FUTURE WORK

This study has introduced valuable new information regarding the geology and pore water geochemistry at the King site. Many avenues of research may be pursued based on this new insight, including:

1. Two-dimensional or three-dimensional modeling of the solute transport within the Ardkenneth aquifer. This would best initially be attempted with one of the well-defined conservative tracers at the King site (e.g. δ^2H or Cl^-). Such modeling could confirm or develop an updated theory on the mode of solute transport within that unit.
2. Additional one-dimensional models of the Cl^- profile developed as part of this study to confirm the δ^2H models in this study and enhance existing Cl^- profiles previously published on the King site.
3. Detailed investigation into the microbiological activity over the Battleford till-Snakebite clay interface. This would provide insight into the geochemical zonations and reactions that occurred within those units which may exert control on CH_4 transport and prohibit its ability to transport as a conservative tracer.
4. Detailed investigation into the hydraulic properties over the Battleford till-Snakebite clay to determine if an influx of glacial water could have impacted the transport of CH_4 in some way.
5. Examination of the relationship between $\delta^{13}C_{CH4}$-CH_4 and $\delta^{13}C_{C2H6}$-C_2H_6 concentrations that were presented in this study. The two data sets showed opposing trends to each other, and the $\delta^{13}C_{CH4}$-CH_4 correlation was contrary to that reported in the literature.
6. The relationship of $\delta^{13}C_{CH4}$ and $\delta^{13}C_{C2H6}$ versus depth presented in this study has potential to be pursued in other or new data sets, considering a few data points which could be outliers.
7. One-dimensional modeling of the $\delta^{13}C_{CH4}$ profile presented in this study may provide additional insight into CH_4 transport and diffusive fractionation effects.

8. Detailed investigation into the CO_2 and $\delta^{13}C_{CO2}$ data that was produced as part of this study, but was beyond the scope of this thesis. Both the concentration and isotope profiles are complete through the entire geologic sequence and may provide unique and valuable insight into the geochemistry of the pore waters and reactions between the pore waters and sediments. Given the completeness of the profiles, one-dimensional modeling could also be conducted with this data set.

9. A great deal of pore water chemistry data was generated as part of, but was beyond the scope of, this study. Examination of this data and correlation with other data sets from these laterally extensive geologic units could offer a regional glimpse of solute transport continuity or otherwise.
10. Experimentation to better constrain the values of k_1 which were applied in the transport modeling of CH_4 as part of this study would contribute to a lack of existing information in the literature.

LIST OF REFERENCES

Abrams, M.A. 1996. Interpretation of methane carbon isotopes extracted from surficial marine sediments for detection of subsurface hydrocarbons. In *Hydrocarbon migration and its near-surface expression, AAPG Memoir* 66: 309-318.

Andrews, J.N., R.J. Drimmie, H.H. Loosli, and M.J. Hendry. 1991. Dissolved gases in the Milk River aquifer, Alberta, Canada. *Applied Geochemistry* 6, no. 4: 393-403.

American Society for Testing Materials (ASTM). 2005. D2216–05: Standard Test Methods for Laboratory Determination of Water (Moisture) Content of Soil and Rock by Mass. *ASTM International*, West Conshohocken, PA.

American Society for Testing Materials (ASTM). 2007. D422–63: Standard Test Method for Particle-Size Analysis of Soils. In *Annual Book of ASTM Standards*, West Conshohocken, PA.

American Society for Testing Materials (ASTM). 2009. D7263–09: Standard Test Methods for Laboratory Determination of Density (Unit Weight) of Soil Specimens. In *Annual Book of ASTM Standards*, West Conshohocken, PA.

Aravena, R., and L.I. Wassenaar. 1993. Dissolved organic carbon and methane in a regional confined aquifer, southern Ontario, Canada: Carbon isotope evidence for associated subsurface sources. *Applied Geochemistry* 8, no. 5: 483-493.

Bangsund, A.L., M.J. Hendry, and A.M Fernández. 2012. Geochemical effects of incremental high-pressure squeezing on pore waters from argillaceous aquitards. Poster presented at 5th International Meeting on Clays in Natural and Engineered Barriers for Radioactive Waste Confinement, Montpellier, FR.

Bárcena, T.G., J.C. Yde, and K.W. Finster. 2010. Methane flux and high-affinity methanotrophic diversity along the chronosequence of a receding glacier in Greenland. *Annals of Glaciology* 51, no. 56: 23-31.

Bárcena, T.G., K.W. Finster, and J.C. Yde. 2011. Spatial patterns of soil development, methane oxidation, and methanotrophic diversity along a receding glacier forefield, southeast Greenland. *Arctic, Antarctic, and Alpine Research* 43, no. 2: 178-188.

Barendregt, R.W., R.J. Enkin, and D.L. Tessler. 2012. Magnetostratigraphy of Late Neogene glacial, interglacial, and preglacial sediments in the Saskatoon and Regina areas, Saskatchewan, Canada. *Studia Geophysica et Geodaetica* 56, no. 3: 705-724.

Barnes, R.O., and E.D. Goldberg. 1976. Methane production and consumption in anoxic marine sediments. *Geology* 4, no. 5: 297-300.

Bear, J., and A.H.-D. Cheng. 2010. *Modeling Groundwater Flow and Contaminant Transport, Theory and Applications of Transport in Porous Media* 23. Springer Science + Business Media B.V.

Bernard, B.B., J.M. Brooks, and W.M. Sackett. 1978. Light hydrocarbons in recent Texas continental shelf and slope sediments. *Journal of Geophysical Research* 83, no. C8: 4053-4061.

Bernard, B.B. 1979. Methane in marine sediments. *Deep Sea Research Part A. Oceanographic Research Papers* 26, no. 4: 429-443.

Berner, U., and E. Faber. 1987. Maturity related mixing model for methane, ethane and propane, based on carbon isotopes. *Advances in Organic Geochemistry* 13, no. 1-3: 67-72.

Birgel, D., J. Peckmann, S. Klautzsch, V. Thiel, and J. Reitner. 2006. Anaerobic and aerobic oxidation of methane at Late Cretaceous seeps in the Western Interior Seaway, USA. *Geomicrobiology Journal* 23, no. 7: 565-577.

Birks, S.J., T.W.D. Edwards, and V.H. Remenda. 2007. Isotopic evolution of Glacial Lake Agassiz: New insights from cellulose and porewater isotopic archives. *Palaeogeography, Palaeoclimatology, Palaeoecology* 246, no. 1: 8-22.

Borowski, W.S., C.K. Paull, and W. Ussler. 1996. Marine pore-water sulfate profiles indicate in situ methane flux from underlying gas hydrate. *Geology* 24, no. 7: 655-658.

Boudreau, B.P. 1996. The diffusive tortuosity of fine-grained unlithified sediments. *Geochimica et Cosmochimica Acta* 60, no. 16: 3139-3142.

Cadrin, A.A.J., T.K. Kyser, W.G.E. Caldwell, and F.J. Longstaffe. 1995. Isotopic and chemical compositions of bentonites as paleoenvironmental indicators of the Cretaceous Western Interior Seaway. *Palaeogeography, Palaeoclimatology, Palaeoecology* 119, no. 3: 301-320.

Caldwell, W.G.E. 1968. *The late Cretaceous Bearpaw formation in the South Saskatchewan River Valley*. Saskatchewan Research Council. Geology Division, Report No. 8.

Chalmers, G.R.L., and R.M. Bustin. 2008. Lower Cretaceous gas shales in northeastern British Columbia, Part I: geological controls on methane sorption capacity. *Bulletin of Canadian Petroleum Geology* 56, no 1: 1-21.

Chanton, J., L. Chaser, P. Glasser, and D. Siegel. 2004. Carbon and hydrogen isotopic effects in microbial methane from terrestrial environments. In *Stable isotopes and biosphere-atmosphere interactions, physiological ecology series*: 85-105.

Christiansen, E.A. 1967. A thin till in West-Central Saskatchewan, Canada. *Canadian Journal of Earth Sciences* 5, no. 2: 329-336.

Christiansen, E.A. 1968. Pleistocene stratigraphy of the Saskatoon area, Saskatchewan, Canada. *Canadian Journal of Earth Sciences* 5, no. 5: 1167-1173.

Christiansen, E.A. 1979. The Wisconsinan deglaciation of southern Saskatchewan and adjacent areas. *Canadian Journal of Earth Sciences* 16, no. 4: 913-938.

Christiansen, E.A. 1990. Geology of the Luck Lake/Lake Bend Irrigation Project. Report 0126-002.

Clark, I., I. Liu, H. Mohammadzadeh, R. Mohapatra, P. Zhang, and M. Wilk. 2010. *Porewater and gas analyses in DGR-3 and DGR-4 Core*. TR-08-19. DGR Site Characterization Document Intera Engineering Project 08-200.

Clark, I.D., D. Ilin, R.E. Jackson, M. Jensen, L. Kennell, H. Mohammadzadeh, A. Poulain, Y.P. Xing, and K.G. Raven. 2015. Paleozoic-aged microbial methane in an Ordovician shale and carbonate aquiclude of the Michigan Basin, southwestern Ontario. *Organic Geochemistry* 83-84: 118-126.

Claypool, G.E., and I.R. Kaplan. 1974. The origin and distribution of methane in marine sediments. In *Natural Gases in Marine Sediments*. Springer US: 99-139.

Coleman, D.D., J.B. Risatti, and M. Schoell. 1981. Fractionation of carbon and hydrogen isotopes by methane-oxidizing bacteria. *Geochimica et Cosmochimica Acta* 45, no. 7: 1033-1037.

Dansgaard, W. 1964. Stable isotopes in precipitation. *Tellus* 16, no. 4: 436-468.

Das, B.M., and K. Sobhan. 2014. *Principles of Geotechnical Engineering*. Cengage Learning.

Dawson, F.M., C.G. Evans, R. Marsh, and R. Richardson. 1994. Uppermost Cretaceous and Tertiary Strata of the Western Canada Sedimentary Basin. In *Geological Atlas of the Western Canada Sedimentary Basin, Canadian Society of Petroleum Geologists and Alberta Research Council*, Calgary: 18.

Desaulniers, D.E., J.A. Cherry, and P. Fritz. 1981. Origin, age and movement of pore water in argillaceous Quaternary deposits at four sites in southwestern Ontario. *Journal of Hydrology* 50: 231-257.

Edwards, J.S. 1991. Potential hazards resulting from the presence of methane dissolved in groundwater. Paper presented at International Mine Water Association, 4th International Mine Water Congress, Ljubljana, Slovenia, Yugoslavia.

Engler, T.W. 2010. *Fluid Flow in Porous Media*. PET 524 Course Notes, New Mexico Institute of Mining and Technology. Socorro, New Mexico.

Faber, E., and W. Stahl. 1984. Geochemical surface exploration for hydrocarbons in North Sea. *AAPG Bulletin* 68, no. 3: 363-386.

Ferguson, G., and S., Jasechko. 2015. The isotopic composition of the Laurentide Ice Sheet and fossil groundwater. *Geophysical Research Letters* 42, no. 12: 4856-4861.

Fetter, C.W. 2001. *Applied Hydrogeology*. Prentice Hall.

Floodgate, G.D., and A.G. Judd. 1992. The origins of shallow gas. *Continental Shelf Research* 12, no. 10: 1145-1156.

Fortin, G., G. Van Der Kamp, and J.A. Cherry. 1991. Hydrogeology and hydrochemistry of an aquifer-aquitard system within glacial deposits, Saskatchewan, Canada. *Journal of Hydrology* 126, no. 3-4: 265-292.

Freeze, A., and J.A. Cherry. 1979. *Groundwater*. Prentice-Hall, Inc.

Fuex, A.N. 1977. The use of stable carbon isotopes in hydrocarbon exploration. *Journal of Geochemical Exploration* 7: 155-188.

Fung, K., B. Berry, M. Wilson, G. Romme, K. Bigelow, and E. Pietroniro. 1999. *Atlas of Saskatchewan*. Saskatoon: University of Saskatchewan.

Gillham, R.W., and J.A. Cherry. 1982. Contaminant migration in saturated unconsolidated geologic deposits. *Geological Society of America Special Papers* 189: 31-62.

Goth, M. 1985. Indication of methane movement from petroleum reservoir to surface, Löningen oilfield, NW-Germany. *Journal of Geochemical Exploration* 23, no. 1: 81-97.

Green, D.W., and R.H. Perry. 2008. *Perry's Chemical Engineer's Handbook*. McGraw-Hill.

Hanson, R.S., and T.E. Hanson. 1996. Methanotrophic Bacteria. *Microbiological Reviews* 60, no. 2: 439-471.

Harrington, G.A., M.J. Hendry, and N.I. Robinson. 2007. Impact of permeable conduits on solute transport in aquitards: Mathematical models and their application. *Water Resources Research* 43, no. 5: W05441. DOI: 10.1029/2005WR004144.

Harris, D., W.R. Horwáth, and C. van Kessel. 2001. Acid fumigation of soils to remove carbonates prior to total organic carbon or carbon-13 isotopic analysis. *Soil Science Society of America Journal* 65, no. 6: 1853-1856.

Hendry, M.J., and L.I. Wassenaar. 1999. Implications of the distribution of δD in pore waters for groundwater flow and the timing of geologic events in a thick aquitard system. *Water Resources Research* 35, no. 6: 1751-1760.

Hendry, M.J., and L.I. Wassenaar. 2000. Controls on the distribution of major ions in pore waters of a thick surficial aquitard. *Water Resources Research* 36, no. 2: 503-513.

Hendry, M.J., L.I. Wassenaar, and T. Kotzer. 2000. Chloride and chlorine isotopes (^{36}Cl and $\delta^{37}Cl$) as tracers of solute migration in a thick, clay-rich aquitard system. *Water Resources Research* 36, no. 1: 285-296.

Hendry, M.J., and L.I. Wassenaar. 2004. Transport and geochemical controls on the distribution of solutes and stable isotopes in a thick clay-rich till aquitard, Canada. *Isotopes in Environmental and Health Studies* 40, no. 1: 3-19.

Hendry, M.J., T.G. Kotzer, and D.K. Solomon. 2005. Sources of radiogenic helium in a clay till aquitard and its use to evaluate the timing of geologic events. *Geochimica et Cosmochimica Acta* 69, no. 2: 475-483.

Hendry, M.J., and A.D. Woodbury. 2007. Clay aquitards as archives of Holocene paleoclimate: $\delta^{18}O$ and thermal profiling. *Groundwater* 45, no. 6: 683-691.

Hendry, M.J., and L.I. Wassenaar. 2009. Inferring heterogeneity in aquitards using high-resolution δD and $\delta^{18}O$ profiles. *Groundwater* 47, no. 5: 639-645.

Hendry, M.J., S.L. Barbour, B.E.J. Boldt-Leppin, L.J. Reifferscheid, and L.I. Wassenaar. 2009. A comparison of laboratory and field based determinations of molecular diffusion coefficients in a low permeability geologic medium. *Environmental Science & Technology* 43, no. 17: 6730-6736.

Hendry, M.J., S.L. Barbour, J. Zettl, V. Chostner, and L.I. Wassenaar. 2011. Controls on the long term downward transport of $\delta^{2}H$ of water in a regionally extensive, two-layered aquitard system. *Water Resources Research* 47, no. 6: W06505. DOI: 10.1029/2010WR010044.

Hendry, M.J., S.L. Barbour, K. Novakowski, and L.I. Wassenaar. 2013. Paleohydrogeology of the Cretaceous sediments of the Williston Basin using stable isotopes of water. *Water Resources Research* 49, no. 8: 4580-4592.

Hendry, M.J., and G.A. Harrington. 2014. Comparing vertical profiles of natural tracers in the Williston Basin to estimate the onset of deep aquifer activation. *Water Resources Research* 50, no. 8: 6496-6506.

Hendry, M.J., S.L. Barbour, E.E. Schmeling, and S.O.C. Mundle. 2016 (a). Measuring concentrations of dissolved methane and ethane and the ^{13}C of methane in shale and till. *Groundwater*. DOI: 10.1111/gwat.12445.

Hendry, M.J., S.L. Barbour, E.E. Schmeling, S.O.C. Mundle, and M. Huang. 2016 (b). Fate and transport of dissolved methane and ethane in Cretaceous shales of the Williston Basin, Canada. *Water Resources Research*, 52. DOI: 10.1002/2016WR019047.

Herzog, B., J. Pennino, and G. Nielsen. 1991. Ground-Water Sampling. In *Practical Handbook of Ground-Water Monitoring*. Lewis Publishers: 449-499.

Hinrichs, K-U., J.M. Hayes, W. Bach, A.J. Spivack, L.R. Hmelo, N.G. Holm, C.G. Johnson, and S.P. Sylva. 2006. Biological formation of ethane and propane in the deep marine subsurface. *Proceedings of the National Academy of Sciences* 103, no. 40: 14684-14689.

Honeywell. 2004. Paraffin Wax Material Safety Data Sheet: ASTOR 0001. Honeywell International.

Horton, R.M., and W.H. Leonard. 2005. Mathematical Modeling in Science. *The Science Teacher* 72, no. 5: 40-45.

Huysmans, M., and A. Dassargues. 2004. Review of the use of the Péclet numbers to determine the relative importance of advection and diffusion in low permeability environments. *Hydrogeology Journal* 13, no. 5-6: 895-904.

Iversen, N., and B.B. Jørgensen. 1993. Diffusion coefficients of sulfate and methane in marine sediments: Influence of porosity. *Geochimica et Cosmochimica Acta* 57, no. 3: 571-578.

Ingebritsen, S.E., and W.E. Sanford. 1999. Groundwater in geologic processes. Cambridge University Press.

Jackson, R.E., A.W. Gorody, B. Mayer, J.W. Roy, M.C. Ryan, and D.R. Van Stempvoort. 2013. Groundwater protection and unconventional gas extraction: The critical need for field-based hydrogeological research. *Groundwater* 51, no. 4: 488-510.

Jacops, E., G. Volckaert, N. Maes, E. Weetjens, and J. Govaerts. 2013. Determination of gas diffusion coefficients in saturated porous media: He and CH_4 diffusion in Boom Clay. *Applied Clay Science* 83: 217-223.

Kampbell, D.H., and S.A. Vandegrift. 1998. Analysis of dissolved methane, ethane, and ethylene in ground water by a standard gas chromatographic technique. *Journal of Chromatographic Science* 36, no. 5: 253-256.

Keller, C.K. 1991. Hydrogeochemistry of a clayey till: 2. Sources of CO_2. *Water Resources Research* 27, no. 10: 2555-2564.

Kendall, C., and E.A. Caldwell. 1998. Fundamentals of isotope geochemistry. In *Isotope Tracers in Catchment Hydrology*. Elsevier Science: 51-86.

Kendall, C., and D.H. Doctor. 2005. Stable isotope applications in hydrologic studies. In *Surface and Groundwater, Weathering, and Soils: Treatise on Geochemistry.* Vol. 5. Elsevier: 319-364.

Kotelnikova, S. 2002. Microbial production and oxidation of methane in deep subsurface. *Earth-Science Reviews* 58, no. 3: 367-395.

Koroleva, M., P. Alt-Epping, and M. Mazurek. 2011. Large-scale tracer profiles in a deep claystone formation (Opalinus Clay at Mont Russelin, Switzerland): implications for solute transport processes and transport properties of the rock. *Chemical Geology* 280, no. 3: 284-296.

Kresic, N. 2006. *Hydrogeology and groundwater modeling*. CRC Press.

Kruse, C.W., P. Moldrup, and N. Iversen. 1996. Modeling diffusion and reaction in soils: II. Atmospheric methane diffusion and consumption in a forest soil. *Soil Science* 161, no. 6: 355-365.

Leckie, D.A., J.P. Bhattacharya, J. Bloch, C.F. Gilboy, and B. Norris. 1994. Cretaceous Colorado/Alberta Group of the Western Canada Sedimentary Basin. In *Geological Atlas of the Western Canada Sedimentary Basin, Canadian Society of Petroleum Geologists and Alberta Research Council,* Calgary: 18.

Lawrence, J.R., M.J. Hendry, L.I. Wassenaar, J.J. Germida, G.M. Wolfaardt, N. Fortin, and C.W. Greer. 2000. Distribution and biogeochemical importance of bacterial populations in a thick clay-rich aquitard system. *Microbial Ecology* 40, no. 4: 273-291.

Leythaeuser, D., R.G. Schaefer, and A. Yukler. 1982. Role of diffusion in primary migration of hydrocarbons. *AAPG Bulletin* 66, no. 4: 408-429.

Libes, S. 2009. *Introduction to Marine Biogeochemistry*. Elsevier.

Lis, G., L.I. Wassenaar, and M.J. Hendry. 2008. High-precision laser spectroscopy D/H and $^{18}O/^{16}O$ measurements of microliter natural water samples. *Analytical Chemistry* 80, no. 1: 287-293.

Maathuis, H., and M. Simpson. 2007. Groundwater Resources of the Swift Current (72J) area, Saskatchewan. SRC Publication No. 12178-1E07.

Martens, C.S., and R.A. Berner. 1977. Interstitial water chemistry of anoxic Long Island Sound sediments. 1. Dissolved gases. *Limnology and Oceanography* 22, no. 1: 10-25.

Martens, C.S. 1982. Methane production, consumption, and transport in the interstitial waters of coastal marine sediments. In *The Dynamic Environment of the Ocean Floor*. Lexington Books: 187-202.

Mazurek, M., P. Alt-Epping, A. Bath, T. Gimmi, H.N. Waber, S. Buschaert, P. De Cannière, M. De Craen, A. Gautschi, S. Savoye, A. Vinsot, I. Wemaere, and L. Wouters. 2011. Natural tracer profiles across argillaceous formations. *Applied Geochemistry* 26, no. 7: 1035-1064.

McQuarrie, D.A., P.A. Rock, and E.B. Gallogly. 2011. *General Chemistry*. University Science Books.

Mechalas, B.J. 1974. Pathways and environmental requirements for biogenic gas production in the ocean. In *Natural Gases in Marine Sediments*. Springer US: 11-25.

Oremland, R.S. 1981. Microbial formation of ethane in anoxic estuarine sediments. *Applied and Environmental Microbiology* 42, no. 1: 122-129.

Oremland, R.S., M.J. Whiticar, F.E. Strohmaier, and R.P. Kiene. 1988. Bacterial ethane formation from reduced, ethylated sulfur compounds in anoxic sediments. *Geochimica et Cosmochimica Acta* 52, no. 7: 1895-1904.

Osborn, S.G., A. Vengosh, N.R. Warner, and R.B. Jackson. 2011. Methane contamination of drinking water accompanying gas-well drilling and hydraulic fracturing. *Proceedings of the National Academy of Sciences* 108, no. 20: 8172-8176.

Patriarche, D., J.L. Michelot, E. Ledoux, and S. Savoye. 2004. Diffusion as the main process for mass transport in very low water content argillites: 1. Chloride as a natural tracer for mass transport – Diffusion coefficient and concentration measurements in interstitial water. *Water Resources Research* 40, no. 1: W01516. DOI: 10.1029/2003WR002600.

Petrucci, R.H., W.S. Harwood, and F.G. Herring. 2002. *General chemistry: principles and modern applications*. Vol. 1. Prentice Hall.

Powell, J.S. 2010. *Geotechnical Characterization of the Bearpaw Shale*. Ph.D. dissertation. Queen's University, Kingston, Ont.

Prinzhofer, A.A., and A.Y. Huc. 1995. Genetic and post-genetic molecular isotopic fractionations in natural gases. *Chemical Geology* 126, no. 3: 218-290.

Prinzhofer, A., and E. Pernaton. 1997. Isotopically light methane in natural gas: bacterial imprint or diffusive fractionation? *Chemical Geology* 142, no. 3: 193-200.

Prinzhofer, A., J.P. Girard, S. Buschaert, Y. Huiban, and S. Noirez. 2009. Chemical and isotopic characterization of hydrocarbon gas traces in porewater of very low permeability rocks: The example of the Callovo-Oxfordian argillites of the eastern part of the Paris Basin. *Chemical Geology* 260, no. 3: 269-277.

Reeburgh, W.S., and D.T. Heggie. 1974. Depth distributions of gases in shallow water sediments. In *Natural Gases in Marine Sediments*. Springer US: 27-45.

Reeburgh, W.S. 1982. A major sink and flux control for methane in marine sediments: Anaerobic consumption. In *The Dynamic Environment of the Ocean Floor*. Lexington Books.

Remenda, V.H., J.A. Cherry, and T.W.D. Edwards. 1994. Isotopic composition of old ground water from Lake Agassiz: implications for Late Pleistocene Climate. *Science* 266, no. 5193: 1975-1978.

Remenda, V.H., G. van der Kamp, and J.A. Cherry. 1996. Use of vertical profiles of $\delta^{18}O$ to constrain estimates of hydraulic conductivity in a thick, unfractured aquitard. *Water Resources Research* 32, no. 10: 2979-2987.

Ricchiuto, T., and M. Schoell. 1987. Origin of natural gases in the Apulian Basin in south Italy: A case history of mixing of gases of deep and shallow origin. *Advances in Organic Geochemistry* 13, no. 1-3: 311-318.

Ridgley, J.L. 1998. Gas geochemistry of Upper Cretaceous Second White Speckled Shale, southern Alberta and western Saskatchewan, Canada – A regional perspective. Williston Basin Symposium.

Riedinger, N., B. Brunner, Y-S. Lin, A. Vossmeyer, T.G. Ferdelman, and B.B. Jørgensen. 2010. Methane at the sediment-water transition in Black Sea sediments. *Chemical Geology* 274, no. 1: 29-37.

Rowe, D., and K. Muehlenbachs. 1999. Isotopic fingerprints of shallow gases in the Western Canadian sedimentary basin: tools for remediation of leaking heavy oil wells. *Organic Geochemistry* 30, no. 8: 861-871.

Saskatchewan Ministry of the Economy. 2014. Stratigraphic Correlation Chart.

Sauchyn, M.A., and D.J. Sauchyn. 1991. A continuous record of Holocene pollen from Harris Lake, southwestern Saskatchewan, Canada. *Palaeogeography, Palaeoclimatology, Palaeoecology* 88, no. 1: 13-23.

Sauer, E.K., L.F. Gareau, and E.A. Christiansen. 1990. Softening of overconsolidated Cretaceous clays by glacial erosion. *Quarterly Journal of Engineering Geology and Hydrogeology* 23, no. 4: 307-324.

Sauer, E.K., and E.A. Christiansen. 1996. Geological site characterization guidelines: A framework for geohydrological and geotechnical applications in Saskatchewan. *Saskatchewan Environment and Resource Management*.

Schloemer, S., and B.M. Krooss. 2004. Molecular transport of methane, ethane and nitrogen and the influence of diffusion on the chemical and isotopic composition of natural gas accumulations. *Geofluids* 4, no. 1: 81-108.

Schloemer, S., J. Elbracht, M. Blumenberg, and C.J. Illing. 2016. Distribution and origin of dissolved methane, ethane and propane in shallow groundwater of Lower Saxony, Germany. *Applied Geochemistry* 67: 118-132.

Schmutz, J.K. 2002. Community Conservation Plan for the Luck Lake Important Bird Area. Important Bird Areas program (http://www.ibacanada.ca), *Nature Saskatchewan*, Regina, SK.

Schoell, M. 1980. The hydrogen and carbon isotopic composition of methane from natural gases of various origins. *Geochimica et Cosmochimica Acta* 44, no. 5: 649-661.

Schoell, M. 1983. Genetic characterization of natural gases. *AAPG Bulletin* 67, no. 12: 2225-2238.

Schoell, M. 1988. Multiple origins of methane in the Earth. *Chemical Geology* 71, no.1: 1-10.

Schulz, H.D., and M. Zabel. 2013. *Marine Geochemistry*. Springer Science & Business Media.

Schwartz, F.W., and H. Zhang. 2003. *Fundamentals of Groundwater*. John Wiley & Sons, Inc.

Shackelford, C.D., and D.E. Daniel. 1991. Diffusion in saturated soil. I: Background. *Journal of Geotechnical Engineering* 117, no. 3: 467-484.

Sharp, Z. 2007. *Principles of Stable Isotope Geochemistry*. Pearson Education.

Shaw, R.J. 1997. *Hydrogeology of a thick clay-rich till and Cretaceous bedrock clay sequence in Saskatchewan, Canada*. Master's thesis. University of Saskatchewan, Saskatoon, SK.

Shaw, R.J., and M.J. Hendry. 1998. Hydrogeology of a thick clay till and Cretaceous clay sequence, Saskatchewan, Canada. *Canadian Geotechnical Journal* 35, no. 6: 1041-1052.

Simpkins, W.W., and T.B. Parkin. 1993. Hydrogeology and redox geochemistry of CH_4 in a Late Wisconsinan till and loess sequence in Central Iowa. *Water Resources Research* 29, no. 11: 3643-3657.

Simpson, M.A. 1998. Geology and Hydrostratigraphy of the Rosetown Area (720), Saskatchewan. Saskatchewan Research Council Publication No. 10416-2C98.

Šimůnek, J., M. Šenja, H. Saito, M. Sakai, and M. Th. van Genuchten. 2013. The Hydrus-1D Software Package for Simulating the One-Dimensional Movement of Water, Heat, and Multiple Solutes in Variably-Saturated Media. Department of Environmental Sciences, University of California, Riverside Research Reports.

Sperazza, M., J.N. Moore, and M.S. Hendrix. 2004. High-resolution particle size analysis of naturally occurring very fine-grained sediment through laser diffractometry. *Journal of Sedimentary Research* 74, no. 5: 736-743.

Stahl, W.J. 1977. Carbon and nitrogen isotopes in hydrocarbon research and exploration. *Chemical Geology* 20: 121-149.

Stumpp, C., and M.J. Hendry. 2012. Spatial and temporal dynamics of water flow and solute transport in a heterogeneous glacial till: The application of high-resolution profiles of $\delta^{18}O$ and $\delta^{2}H$ in pore waters. *Journal of Hydrology* 438: 203-214.

Szatkowski, B., S. Whittaker, B. Johnston, C. Sikstrom, and K. Muehlenbachs. 2001. Identifying the source of dissolved hydrocarbons in aquifers using stable carbon isotopes. Paper presented at 54th Canadian Geotechnical Conference, Oil Sands Hydrogeology, Calgary, Alberta. No. H307.

Taylor, S.W., B.S. Lollar, and L.I. Wassenaar. 2000. Bacteriogenic ethane in near-surface aquifers: Implications for leaking hydrocarbon well bores. *Environmental science & technology* 34, no. 22: 4727-4732.

Van Everdingen, R.O. 1967. Influence of the South Saskatchewan reservoir (Canada) on piezometric levels in underlying bedrock aquifers. *Journal of Hydrology* 5: 351-359.

Vidic, R.D., S.L. Brantley, J.M. Vandenbossche, D. Yoxtheimer, and J.D. Abad. 2013. Impact of shale gas development on regional water quality. *Science* 340, no. 6134: 1235009.

Vengosh, A., and M.J. Hendry. 2001. Chloride-bromide-$\delta^{11}B$ systematics of a thick clay-rich aquitard system. *Water Resources Research* 37, no. 5: 1437-1444.

Wang, D., and D.W. Anderson. 1998. Direct measurement of organic carbon content in soils by the Leco CR-12 carbon analyzer. *Communications in Soil Science and Plant Analysis* 29, no. 1-2: 15-21.

Wassenaar, L.I., M.J. Hendry, V.L. Chostner, and G.P. Lis. 2008. High resolution pore water $\delta^{2}H$ and $\delta^{18}O$ measurements by $H_2O_{(liquid)}$–$H_2O_{(vapor)}$ equilibration laser spectroscopy. *Environmental science & technology* 42, no. 24: 9262-9267.

Wassenaar, L.I., and M.J. Hendry. 1999. Mechanisms controlling the distribution and transport of ^{14}C in a clay-rich till aquitard. *Groundwater* 38, no. 3: 343-349.

Wentworth, C.K. 1922. A scale of grade and class terms for clastic sediments. *The Journal of Geology* 30, no. 5: 377-392.

Whiticar, M.J., E. Faber, and M. Schoell. 1986. Biogenic methane formation in marine and freshwater environments: CO_2 reduction *vs.* acetate fermentation – Isotope evidence. *Geochimica et Cosmochimica Acta* 50, no. 5: 693-709.

Whiticar, M.J. 1999. Carbon and hydrogen isotope systematics of bacterial formation and oxidation of methane. *Chemical Geology* 161, no. 1: 291-314.

Whittaker, S.G., T.K. Kyser, and W.G.E. Caldwell. 1988. Lithic geochemistry of the Claggett marine cyclothem in south-central Saskatchewan. *Canadian Journal of Earth Sciences* 25, no. 10: 1554-1563.

Xia, X., and Y. Tang. 2012. Isotope fractionation of methane during natural gas flow with coupled diffusion and adsorption/desorption. *Geochimica et Cosmochimica Acta* 77: 489-503.

Yan, X. 2009. *Linear Regression Analysis: Theory and Computing.* World Scientific.

Zou, Y-R., Y. Cai, C. Zhang, X. Zhang, and P. Peng. 2007. Variations of natural gas carbon isotope-type curves and their interpretation – A case study. *Organic Geochemistry* 38, no. 8: 1398-1415.

APPENDIX A

Squeezed Pore Water

Chemical Data

Table A1. Anions measured on squeezed pore waters from the 2013 King site core.

Depth (m BGS)	Geologic Unit	F^- (mg/L)	Cl^- (mg/L)	NO_2^- (mg/L)	Br^- (mg/L)	NO_3^- (mg/L)	P^- (mg/L)	SO_4^- (mg/L)
0.8	Battleford Till	< 0.60	50.35	< 0.3	0.16	0.66	< 0.60	11423.58
0.8	Battleford Till	< 0.60	48.58	< 0.3	< 1.5	0.67	< 0.60	11239.23
1	Battleford Till	< 0.05	53.42	< 0.05	0.29	3.19	< 0.05	15196.90
1	Battleford Till	3.49	54.27	< 0.05	< 0.05	4.43	< 0.05	14957.11
2	Battleford Till	< 0.60	42.93	< 0.3	0.62	< 0.60	< 0.60	26087.91
4	Battleford Till	< 0.60	36.60	< 0.3	< 1.5	< 0.60	< 0.60	52851.19
5	Battleford Till	-	57.77	< 0.05	1.50	-	< 0.05	68422.00
5	Battleford Till	< 0.05	46.84	0.81	< 0.05	-	< 0.05	61129.76
6	Battleford Till	< 0.60	69.13	< 0.3	1.67	< 0.60	< 0.60	28191.07
6	Battleford Till	< 0.60	69.63	< 0.3	1.42	< 0.60	< 0.60	28221.94
7	Battleford Till	0.51	76.43	0.50	1.24	0.10	< 0.05	31936.50
7	Battleford Till	-	83.03	< 0.05	2.80	0.16	< 0.05	33434.74
10	Battleford Till	< 0.60	98.28	< 0.3	2.50	0.60	< 0.60	5521.01
11	Battleford Till	0.37	105.90	< 0.05	2.57	0.23	< 0.05	5598.17
12	Battleford Till	< 0.60	113.29	< 0.3	2.17	< 0.60	< 0.60	4834.87
15	Battleford Till	< 0.60	96.25	< 0.3	2.06	1.55	< 0.60	4173.14
15	Battleford Till	< 0.60	95.87	< 0.3	1.91	1.51	< 0.60	4224.83
17	Battleford Till	< 0.60	83.03	< 0.3	1.12	0.60	< 0.60	3355.65
19	Battleford Till	< 0.60	75.94	< 0.3	1.33	< 0.60	< 0.60	3346.55
22	Battleford Till	< 0.60	71.11	< 0.3	1.03	8.82	< 0.60	3544.49
25	Battleford Till	< 0.60	54.65	< 0.3	0.88	< 0.60	< 0.60	3230.36
29	Battleford Till	0.38	48.44	0.08	0.96	0.26	< 0.05	2690.68
31	Battleford Till	< 0.60	49.28	< 0.3	0.65	< 0.60	< 0.60	3116.74
31	Battleford Till	< 0.60	47.52	< 0.3	0.78	5.71	< 0.60	3029.90
31	Battleford Till	< 0.60	47.30	< 0.3	0.72	5.87	< 0.60	3053.81
33	Battleford Till	<1.0	37.28	< 0.05	1.14	9.60	< 0.05	2656.01

Table A1. Anions measured on squeezed pore waters from the 2013 King site core continued.

Depth (m BGS)	Geologic Unit	F^- (mg/L)	Cl^- (mg/L)	NO_2^- (mg/L)	Br^- (mg/L)	NO_3^- (mg/L)	P^- (mg/L)	SO_4^- (mg/L)
36	Battleford Till	< 0.60	46.20	< 0.3	0.47	0.90	< 0.60	3028.57
38	Battleford Till	< 0.05	26.37	< 0.05	0.84	0.06	< 0.05	3170.42
40	Battleford Till	0.43	27.73	< 0.05	< 0.05	0.92	< 0.05	2918.55
42	Battleford Till	< 0.60	41.71	< 0.3	0.50	1.36	< 0.60	3021.08
44	Battleford Till	0.28	22.29	< 0.05	0.66	0.64	< 0.05	3048.01
48	Battleford Till	< 0.60	35.33	< 0.3	0.59	< 0.60	< 0.60	3293.27
51	Battleford Till	< 0.60	36.45	< 0.3	0.61	0.78	< 0.60	3341.43
56	Battleford Till	0.27	52.07	< 0.05	0.40	0.13	< 0.05	3115.78
63	Battleford Till	< 0.60	43.67	< 0.3	0.60	< 0.60	< 0.60	3282.08
63	Battleford Till	< 0.60	42.52	< 0.3	0.72	< 0.60	< 0.60	3264.63
68	Battleford Till	< 0.60	50.49	< 0.3	1.90	< 0.60	< 0.60	3556.29
74	Battleford Till	< 0.60	57.45	< 0.3	0.70	< 0.60	< 0.60	3553.38
78	Battleford Till	< 0.60	75.28	< 0.3	0.89	< 0.60	< 0.60	3326.90
83	Snakebite Clay	< 0.60	69.02	< 0.3	0.70	0.93	< 0.60	2709.03
86	Snakebite Clay	< 0.60	84.88	< 0.3	0.77	< 0.60	< 0.60	4371.95
92	Snakebite Clay	< 0.60	202.72	< 0.3	1.09	1.00	< 0.60	8913.41
98	Snakebite Clay	< 0.60	278.67	< 0.3	1.24	< 0.60	< 0.60	3075.93
102	Snakebite Clay	< 0.60	238.65	< 0.3	1.01	< 0.60	< 0.60	3404.50
102	Snakebite Clay	< 0.60	238.50	< 0.3	1.11	0.62	< 0.60	3375.78
108	Snakebite Clay	< 0.60	263.18	< 0.3	1.43	0.77	< 0.60	6459.01
112	Snakebite Clay	< 0.60	339.18	< 0.3	2.14	1.55	< 0.60	6544.35
119	Snakebite Clay	8.83	738.70	< 0.05	2.60	3.48	< 0.05	8737.06
128	Snakebite Clay	< 0.60	360.27	< 0.3	4.09	0.99	< 0.60	5998.73
129	Snakebite Clay	< 0.60	325.57	< 0.3	4.37	1.34	< 0.60	6206.95
137	Snakebite Clay	0.12	576.28	< 0.05	2.80	1.25	< 0.05	7014.39
143	Snakebite Clay	0.19	634.82	< 0.05	3.12	1.29	< 0.05	9122.54

Table A1. Anions measured on squeezed pore waters from the 2013 King site core continued.

Depth (m BGS)	Geologic Unit	F^- (mg/L)	Cl^- (mg/L)	NO_2^- (mg/L)	Br^- (mg/L)	NO_3^- (mg/L)	P^- (mg/L)	SO_4^- (mg/L)
148	Snakebite Clay	2.46	487.95	< 0.05	1.92	1.59	< 0.05	10326.30
154	Snakebite Clay	0.06	500.06	< 0.05	3.02	2.11	< 0.05	13282.11
159	Ardkenneth Sand	<1.0	1006.09	<1.0	6.52	0.71	< 1.0	18427.67
160	Ardkenneth Sand	0.68	957.99	88.96	8.73	19.41	< 0.60	1395.93
163	Ardkenneth Sand	0.72	859.57	154.13	10.40	12.45	< 0.60	2246.59
163	Ardkenneth Sand	1.35	931.64	< 0.05	5.34	120.84	< 0.05	1191.11
167	Ardkenneth Sand	1.81	1050.07	88.95	11.30	11.55	< 0.60	1532.84
167	Ardkenneth Sand	1.77	1036.71	87.31	10.31	11.21	< 0.60	1501.48
170	Ardkenneth Sand	0.28	1107.72	54.81	5.81	8.12	< 0.05	5715.75
171	Ardkenneth Sand	< 0.05	1048.35	42.29	5.66	16.18	< 0.05	8384.95
172	Ardkenneth Sand	0.77	976.79	< 0.05	6.10	0.18	< 0.05	5582.88
179	Ardkenneth Sand	1.96	982.62	< 0.3	8.62	< 0.60	< 0.60	4017.56
183	Ardkenneth Sand	0.47	943.50	< 0.05	5.56	0.21	< 0.05	5043.15
188	Ardkenneth Sand	< 0.60	847.58	< 0.3	7.63	3.90	< 0.60	10968.73
188	Ardkenneth Sand	< 0.60	835.59	< 0.3	6.75	3.42	< 0.60	10761.30
194	Beechy Sands, Silts & Clay	0.30	887.47	-	6.93	1.04	-	5306.00
198	Beechy Sands, Silts & Clay	< 0.60	744.40	< 0.3	4.98	2.44	< 0.60	5930.55
204	Beechy Sands, Silts & Clay	18.38	1064.64	< 0.05	6.19	0.48	< 0.05	9687.59
208	Beechy Sands, Silts & Clay	< 0.60	1051.22	< 0.3	6.53	< 0.60	< 0.60	4127.34
211	Beechy Sands, Silts & Clay	1.18	1849.41	< 1.0	12.12	< 1.0	< 1.0	3738.59
213	Beechy Sands, Silts & Clay	1.15	1737.99	11.43	9.09	1.03	< 0.05	6026.43
217	Beechy Sands, Silts & Clay	0.78	1121.08	< 1.0	8.41	0.69	< 1.0	2800.07
218	Beechy Sands, Silts & Clay	0.79	940.19	< 0.05	5.07	0.22	< 0.05	753.89
225	Beechy Sands, Silts & Clay	< 1.0	1289.89	< 1.0	4.32	1.83	< 1.0	4367.84
228	Beechy Sands, Silts & Clay	< 0.60	1517.07	< 0.3	10.52	0.87	< 0.60	2162.71
233	Beechy Sands, Silts & Clay	0.33	1353.23	< 0.05	7.06	3.23	< 0.05	4918.90
238	Beechy Sands, Silts & Clay	-	2309.22	< 0.05	13.41	0.92	< 0.05	10813.40

Table A2. Cations measured on squeezed pore waters from the 2013 King site core.

Depth (m BGS)	Li (mg/L)	B (mg/L)	Na (mg/L)	Mg (mg/L)	Al (mg/L)	Si (mg/L)	P (mg/L)	K (mg/L)	Ca (mg/L)	Ti (mg/L)	V (mg/L)	Cr (mg/L)	Mn (mg/L)	Fe (mg/L)	Co (mg/L)
0.8	2.36	2.37	1341.92	1705.35	0.02	6.90	0.32	ud	451.57	0.01	0.01	0.01	1.01	0.85	0.03
1	2.58	1.37	1931.62	2352.55	0.01	4.48	0.09	ud	450.16	0.01	0.01	0.01	1.10	0.01	0.01
2	3.70	1.09	3864.12	4057.67	0.03	6.81	0.57	ud	486.86	0.02	0.03	0.00	0.22	0.11	0.01
2	3.79	1.08	3966.72	4075.40	0.03	7.13	0.58	ud	494.79	0.02	0.03	0.01	0.22	0.12	0.01
4	4.84	0.33	6631.05	9207.33	0.01	8.86	0.31	ud	627.23	0.05	0.01	0.01	3.00	ud	0.02
5	3.65	0.48	5807.42	8180.22	0.03	10.81	0.17	ud	667.22	0.02	0.01	0.01	1.91	0.02	0.03
5	3.83	0.40	5767.74	7743.04	0.02	10.69	0.05	ud	591.30	0.06	0.01	0.01	1.76	ud	0.03
6	3.12	0.44	4131.59	4200.99	0.01	4.41	0.08	ud	577.95	0.03	0.00	0.01	10.66	1.23	0.07
7	2.23	0.48	3399.05	3042.05	0.01	20.10	0.09	ud	629.62	0.01	0.01	0.01	8.86	0.04	0.03
7	2.15	0.49	3934.66	2889.27	0.01	17.67	0.07	ud	610.34	0.02	0.01	0.01	8.69	0.02	0.03
10	0.67	0.63	1391.47	359.85	0.01	5.09	0.10	ud	576.69	0.00	0.01	0.00	2.30	0.08	0.01
11	0.64	0.52	1262.59	361.79	0.02	14.86	0.10	ud	475.32	0.01	0.00	0.00	2.85	ud	0.00
12	0.58	0.56	972.80	340.91	0.03	6.66	0.44	ud	699.70	0.00	0.00	0.01	3.13	0.76	0.03
15	0.50	0.61	668.94	304.31	0.01	7.27	0.07	4.14	739.70	0.00	0.01	0.00	2.99	0.08	0.01
17	0.43	0.62	325.33	261.36	0.02	6.60	0.09	14.51	726.03	0.00	0.00	0.01	2.98	0.08	0.01
19	0.44	0.75	274.54	279.28	0.02	7.32	0.12	14.92	806.62	0.00	0.00	0.00	3.04	0.09	0.01
22	0.43	0.66	258.14	274.88	0.02	10.28	0.16	18.99	845.92	0.00	0.01	0.00	3.12	0.09	0.01
29	0.37	0.59	251.00	211.00	0.01	16.39	0.08	16.84	546.25	0.01	0.00	0.03	1.08	0.66	0.02
31	0.36	0.60	192.57	276.24	0.03	8.74	0.13	11.36	738.66	0.00	0.01	0.00	3.08	0.08	0.01
33	0.34	0.53	193.86	246.54	0.01	16.70	0.08	17.79	669.92	0.00	0.00	0.00	1.85	ud	0.00
36	0.36	0.72	292.13	257.81	0.02	18.33	0.06	13.04	693.54	0.01	0.00	0.02	2.70	0.62	0.03
38	0.32	0.50	170.62	271.16	0.01	10.22	0.06	15.25	740.49	0.00	0.00	0.00	3.51	0.02	0.01
40	0.33	0.51	170.57	255.88	0.00	12.17	0.07	15.77	690.56	0.00	0.00	0.02	3.88	0.25	0.03
42	0.27	0.58	193.68	240.18	0.02	9.08	0.08	15.01	673.26	0.00	0.00	0.00	3.15	0.07	0.01

Table A2. Cations measured on squeezed pore waters from the 2013 King site core continued.

Depth (m BGS)	Ni (mg/L)	Cu (mg/L)	Zn (mg/L)	As (mg/L)	Se (mg/L)	Rb (mg/L)	Sr (mg/L)	Mo (mg/L)	Sb (mg/L)	Ba (mg/L)	W (mg/L)	Hg (mg/L)	Pb (mg/L)	U (mg/L)
0.8	1.77	0.11	2.50	0.01	0.05	0.00	9.71	0.07	0.00	0.03	0.00	ud	0.00	0.10
1	0.09	0.24	0.26	0.02	0.09	0.00	11.02	0.15	0.00	0.04	0.00	ud	0.00	0.09
2	0.44	0.22	0.43	0.03	0.08	0.01	10.03	0.08	0.00	0.02	0.00	0.00	0.00	0.15
2	0.43	0.17	0.42	0.03	0.08	0.01	9.98	0.08	0.00	0.02	0.00	0.00	0.00	0.15
4	0.50	0.37	0.34	0.01	0.08	0.01	20.06	0.17	0.00	0.05	0.00	0.01	0.01	0.21
5	0.42	0.22	0.44	0.03	0.10	0.04	22.31	0.24	0.00	0.07	0.00	ud	0.00	0.07
5	0.38	0.35	0.46	0.02	0.05	0.03	17.65	0.17	0.00	0.07	0.00	ud	0.00	0.06
6	2.00	0.25	0.40	0.02	0.18	0.01	16.01	0.17	0.00	0.02	0.00	0.00	0.00	0.09
7	1.69	0.11	0.40	0.04	0.25	0.02	18.40	0.30	0.00	0.03	0.00	ud	0.00	0.04
7	1.62	0.19	0.48	0.02	0.18	0.02	15.84	0.23	0.00	0.03	0.00	ud	0.00	0.03
11	0.07	0.12	0.54	0.01	0.16	0.01	4.99	0.13	0.00	0.01	0.00	0.01	0.00	0.02
11	0.04	0.05	0.25	0.03	0.23	0.01	5.13	0.08	0.00	0.02	0.00	0.00	0.00	0.02
13	0.96	0.04	0.67	0.01	0.16	0.01	5.21	0.07	0.00	0.05	0.00	0.00	0.00	0.02
15	0.09	0.03	2.07	0.01	0.15	0.01	4.78	0.06	0.00	0.04	0.00	0.01	0.00	0.03
17	0.16	0.05	0.81	0.01	0.16	0.01	4.58	0.05	0.00	0.05	0.00	ud	0.00	0.02
20	0.07	0.07	0.63	0.01	0.15	0.01	4.66	0.07	0.00	0.04	0.00	0.01	0.00	0.02
23	0.20	0.04	7.70	0.01	0.13	0.01	5.05	0.04	0.00	0.03	0.00	0.00	0.00	0.01
29	1.53	0.05	1.50	0.02	0.18	0.02	4.03	0.04	0.00	0.07	0.00	ud	0.00	0.01
32	0.11	0.04	1.53	0.01	0.11	0.00	3.81	0.04	0.00	0.03	0.00	0.00	0.00	0.02
33	0.07	0.03	0.51	0.02	0.16	0.01	3.93	0.04	0.00	0.06	0.00	ud	0.00	0.01
37	1.16	0.02	0.53	0.01	0.09	0.01	3.71	0.03	0.00	0.06	0.00	0.00	0.00	0.01
38	0.08	0.02	0.30	0.02	0.13	0.00	4.07	0.08	0.00	0.02	0.00	0.01	0.00	0.01
40	2.19	0.02	0.60	0.02	0.13	0.01	3.57	0.03	0.00	0.07	0.00	0.01	0.00	0.01
42	0.06	0.02	2.19	0.02	0.10	0.01	4.09	0.04	0.00	0.05	0.00	0.00	0.00	0.02

Table A2. Cations measured on squeezed pore waters from the 2013 King site core continued.

Depth (m BGS)	Li (mg/L)	B (mg/L)	Na (mg/L)	Mg (mg/L)	Al (mg/L)	Si (mg/L)	P (mg/L)	K (mg/L)	Ca (mg/L)	Ti (mg/L)	V (mg/L)	Cr (mg/L)	Mn (mg/L)	Fe (mg/L)	Co (mg/L)
45	0.32	0.58	262.99	231.40	0.02	14.96	0.08	3.68	603.62	0.00	0.00	0.00	2.88	ud	0.02
49	0.32	0.61	211.69	286.60	0.01	11.64	0.08	12.23	842.62	0.00	0.00	0.01	2.12	0.29	0.02
52	0.29	0.48	215.36	265.99	0.01	18.88	0.06	11.32	909.69	0.00	0.00	0.00	2.93	0.05	0.01
56	0.30	0.59	196.80	241.85	0.02	9.82	0.08	12.27	648.85	0.00	0.00	0.00	2.84	0.03	0.00
63	0.29	0.51	251.84	278.84	0.02	15.34	0.09	12.15	701.61	0.00	0.00	0.00	1.06	0.04	0.00
69	0.31	0.53	398.75	262.99	0.04	9.48	0.04	8.74	752.07	ud	0.00	0.00	3.56	0.09	0.01
74	0.27	0.52	739.65	180.23	0.01	11.18	0.08	0.81	513.36	0.00	0.00	0.00	2.12	0.04	0.01
78	0.25	0.70	1185.19	101.57	0.02	4.14	0.06	ud	251.77	ud	0.00	0.00	0.45	0.06	0.00
83	0.27	1.76	1182.16	29.34	0.05	12.90	0.10	ud	66.61	0.00	0.00	0.00	0.31	0.04	0.00
86	0.33	1.64	1773.79	38.44	0.03	16.31	0.08	ud	119.35	0.00	0.00	0.01	0.76	0.06	0.00
92	0.81	2.74	3713.58	120.46	0.02	14.72	0.09	ud	354.64	0.01	0.00	0.01	1.80	0.10	0.03
92	0.86	2.66	4051.82	125.15	0.02	16.02	0.10	ud	351.37	0.01	0.00	0.01	1.72	0.10	0.03
99	0.21	2.64	1491.43	10.76	0.04	8.51	0.11	ud	49.03	0.01	0.00	0.02	0.70	0.16	0.01
103	0.32	2.76	2257.08	15.20	0.02	5.57	0.04	ud	50.81	0.00	0.02	0.01	0.08	0.05	0.00
109	0.57	3.67	4259.50	68.19	0.01	4.92	0.02	ud	183.58	0.00	0.01	0.01	0.73	0.12	0.01
113	0.57	3.93	3017.26	63.37	0.06	9.20	0.09	ud	174.35	0.01	0.01	0.52	0.52	0.95	0.02
120	0.71	3.53	3486.32	94.41	0.02	7.30	0.03	ud	239.36	0.01	0.01	0.01	0.29	0.06	0.00
120	0.74	3.59	3724.46	97.15	0.02	7.48	0.03	ud	241.83	0.01	0.01	0.01	0.30	0.07	0.00
129	0.49	4.49	3051.66	46.50	0.02	11.68	0.08	ud	180.70	0.01	0.00	0.02	0.71	0.25	0.05
130	0.50	3.41	2687.12	56.17	0.03	12.03	0.08	ud	130.98	0.01	ud	0.02	3.39	0.11	0.08
137	0.57	4.22	2952.30	67.98	0.02	19.47	0.04	ud	202.55	0.00	0.00	0.02	1.61	0.05	0.01
144	0.65	3.80	3360.09	99.91	0.01	30.22	0.10	ud	273.13	0.01	0.00	0.02	0.47	0.01	0.01
155	1.13	7.42	4339.91	296.81	0.01	19.83	0.09	ud	489.89	0.01	0.00	0.02	6.40	0.17	0.10
161	0.28	3.64	1587.69	12.50	0.23	13.25	0.14	ud	33.63	0.01	0.01	0.05	0.11	0.32	0.00
164	0.26	2.77	1609.40	10.85	1.40	15.55	0.21	ud	31.92	0.06	0.03	0.07	0.04	1.06	0.00

Table A2. Cations measured on squeezed pore waters from the 2013 King site core continued.

Depth (m BGS)	Ni (mg/L)	Cu (mg/L)	Zn (mg/L)	As (mg/L)	Se (mg/L)	Rb (mg/L)	Sr (mg/L)	Mo (mg/L)	Sb (mg/L)	Ba (mg/L)	W (mg/L)	Hg (mg/L)	Pb (mg/L)	U (mg/L)
45	0.05	0.07	1.02	0.03	0.12	0.01	3.70	0.05	0.00	0.02	0.00	ud	0.00	0.02
49	0.66	0.02	0.68	0.01	0.08	0.01	4.29	0.03	0.00	0.05	0.00	0.01	0.00	0.01
52	0.42	0.09	0.80	0.01	0.09	0.01	5.56	0.06	0.00	0.12	ud	ud	0.00	0.01
56	0.03	0.02	0.26	0.02	0.12	0.01	4.13	0.03	0.00	0.06	0.00	0.00	0.00	0.01
63	0.14	0.02	0.29	0.01	0.07	0.01	3.98	0.05	0.00	0.03	0.00	0.02	0.00	0.02
69	0.06	0.03	0.50	0.01	0.05	0.01	3.99	0.04	0.00	0.02	0.00	0.00	0.00	0.01
74	0.16	0.06	0.54	0.01	0.10	0.00	3.34	0.03	0.00	0.05	0.00	ud	0.00	0.01
78	0.02	0.04	0.14	0.03	0.12	0.02	2.16	0.11	0.00	0.09	0.00	0.00	0.00	0.02
83	0.02	0.04	1.36	0.03	0.10	0.01	0.58	0.20	0.00	0.03	0.00	0.01	0.00	0.01
86	0.15	0.08	0.77	0.05	0.30	0.01	1.11	0.19	0.00	0.05	0.00	0.03	0.00	0.01
92	0.50	0.15	1.03	0.04	0.36	0.02	4.46	0.10	0.00	0.05	0.00	0.02	0.00	0.00
92	0.49	0.17	1.02	0.05	0.36	0.02	4.53	0.10	0.00	0.05	0.00	0.06	0.00	0.00
99	0.46	0.11	0.96	0.03	0.09	0.01	0.50	0.14	0.00	0.02	0.00	0.01	0.00	0.00
103	0.01	0.13	0.78	0.03	0.14	0.01	0.65	0.09	0.00	0.02	0.00	0.00	0.00	0.01
109	0.07	0.09	0.94	0.03	0.14	0.02	2.52	0.05	0.00	0.04	0.00	0.00	0.00	0.00
113	0.60	0.22	1.19	0.03	0.19	0.02	2.56	0.09	0.00	0.04	0.00	0.00	0.00	0.00
120	0.03	0.25	1.52	0.02	0.25	0.03	3.82	0.05	0.00	0.02	0.00	0.02	0.00	0.00
120	0.03	0.24	1.51	0.02	0.24	0.03	3.77	0.06	0.00	0.02	0.00	0.04	0.00	0.00
129	0.07	0.07	0.56	0.02	0.21	0.02	2.15	0.14	0.00	0.02	0.00	0.01	0.00	0.01
130	2.08	0.16	0.61	0.02	0.17	0.01	2.01	0.01	0.00	0.02	ud	0.00	0.00	0.00
137	0.35	0.16	1.22	0.03	0.20	0.02	2.66	0.05	0.00	0.03	0.00	0.01	0.00	0.00
144	0.25	0.31	1.13	0.09	0.40	0.03	4.46	0.11	0.00	0.03	0.00	0.01	0.00	0.01
155	0.35	0.41	1.81	0.07	0.57	0.06	8.83	0.04	0.00	0.02	0.00	0.02	0.00	0.01
161	0.01	0.05	0.55	0.04	0.15	0.01	0.65	0.16	0.01	0.11	0.05	0.01	0.00	0.06
164	0.01	0.02	0.24	0.12	0.09	0.01	0.52	0.20	0.01	0.13	0.05	0.01	0.01	0.02

Table A2. Cations measured on squeezed pore waters from the 2013 King site core continued.

Depth (m BGS)	Li (mg/L)	B (mg/L)	Na (mg/L)	Mg (mg/L)	Al (mg/L)	Si (mg/L)	P (mg/L)	K (mg/L)	Ca (mg/L)	Ti (mg/L)	V (mg/L)	Cr (mg/L)	Mn (mg/L)	Fe (mg/L)	Co (mg/L)
164	0.27	2.75	1708.34	10.70	1.39	15.35	0.21	ud	31.00	0.05	0.03	0.07	0.04	1.19	0.00
164	0.24	2.58	1399.60	8.93	1.31	14.10	0.18	ud	33.87	0.05	0.03	0.05	0.04	1.37	0.00
164	0.32	2.99	1806.94	16.00	2.11	17.20	0.13	ud	53.87	0.09	0.02	0.04	0.13	2.27	0.00
168	0.25	2.18	1605.39	8.60	4.24	18.56	0.30	ud	20.51	0.18	0.03	0.05	0.14	5.15	0.01
171	0.58	2.17	2644.50	48.15	1.22	11.80	0.15	ud	147.94	0.03	0.01	0.05	0.11	1.18	0.00
171	0.57	2.08	2831.00	48.69	1.36	11.82	0.14	ud	148.42	0.06	0.01	0.05	0.11	1.18	0.00
172	0.84	2.34	3324.67	84.94	1.79	11.33	0.11	ud	253.17	0.10	0.02	0.05	0.79	1.79	0.00
173	0.54	1.60	2784.30	37.93	1.00	5.92	0.10	ud	109.65	0.04	0.01	0.04	0.31	0.97	0.00
173	0.55	1.60	2890.39	31.85	1.15	6.77	0.10	ud	117.31	0.04	0.01	0.24	0.35	1.94	0.00
180	0.32	1.26	2560.96	15.78	2.07	12.85	0.17	ud	60.61	0.05	0.02	0.04	0.13	2.63	0.00
184	0.52	1.68	2679.44	29.51	2.91	15.82	0.15	ud	113.14	0.11	0.02	0.04	0.18	3.28	0.00
189	1.22	2.30	4047.44	129.33	0.06	8.27	0.06	ud	438.06	0.01	0.01	0.03	0.57	0.08	0.00
195	0.54	1.86	2829.61	29.67	0.02	3.68	0.04	ud	118.98	0.00	0.00	0.03	0.67	0.06	0.01
199	0.30	2.27	2089.79	15.52	0.06	8.86	0.14	ud	77.96	0.01	0.00	0.07	0.38	0.42	0.01
205	0.71	1.78	3532.69	99.19	0.01	6.89	0.06	ud	367.55	0.01	0.01	0.04	0.72	ud	0.02
209	0.41	2.25	2499.94	24.30	0.02	9.04	0.11	ud	82.01	0.00	0.03	0.04	0.06	0.10	0.00
214	0.31	0.75	3172.79	31.52	0.33	13.87	0.10	ud	171.87	0.01	0.01	0.06	0.08	0.20	0.00
219	0.14	1.91	957.26	3.12	0.03	15.78	0.10	ud	8.93	0.00	0.03	0.05	0.01	ud	0.00
219	0.14	1.88	965.71	3.13	0.03	15.95	0.10	ud	9.02	0.00	0.03	0.05	0.01	ud	0.00
226	0.48	1.83	2693.63	27.97	0.92	13.26	0.13	ud	108.79	0.04	0.02	0.08	0.24	2.40	0.00
229	0.40	1.17	4211.54	24.05	0.03	17.85	0.17	ud	184.87	0.01	0.02	0.09	0.02	0.11	0.00
234	0.43	2.04	2457.42	41.34	0.01	23.31	0.40	ud	146.71	0.01	0.00	0.06	0.17	0.02	0.00
239	2.17	5.10	5476.60	218.11	0.04	3.88	0.08	ud	531.92	0.01	0.01	0.09	5.24	0.02	0.07
239	1.20	2.41	4613.70	145.04	0.03	9.93	0.10	ud	683.57	0.01	0.00	0.08	1.23	0.38	0.02

Table A2. Cations measured on squeezed pore waters from the 2013 King site core continued.

Depth (m BGS)	Ni (mg/L)	Cu (mg/L)	Zn (mg/L)	As (mg/L)	Se (mg/L)	Rb (mg/L)	Sr (mg/L)	Mo (mg/L)	Sb (mg/L)	Ba (mg/L)	W (mg/L)	Hg (mg/L)	Pb (mg/L)	U (mg/L)
164	0.01	0.03	0.24	0.12	0.07	0.01	0.52	0.20	0.01	0.12	0.05	0.01	0.01	0.02
164	0.01	0.08	0.23	0.11	0.08	0.02	0.55	0.20	0.01	0.10	0.04	ud	0.01	0.01
164	0.02	0.08	0.80	0.07	0.14	0.02	0.99	0.62	0.00	0.14	0.03	ud	0.03	0.03
168	0.03	0.06	0.80	0.06	0.09	0.03	0.37	0.63	0.01	0.11	0.01	0.01	0.02	0.02
171	0.02	0.20	0.33	0.04	0.12	0.03	1.65	0.38	0.00	0.09	0.00	0.00	0.00	0.00
171	0.02	0.12	0.33	0.04	0.11	0.03	1.61	0.36	0.00	0.09	0.00	0.01	0.00	0.00
172	0.05	0.35	0.30	0.04	0.18	0.06	2.50	0.09	0.00	0.11	0.00	ud	0.00	0.00
173	0.01	0.06	0.14	0.04	0.09	0.03	1.18	0.31	0.02	0.08	0.00	0.00	0.00	0.01
173	0.03	0.16	0.18	0.04	0.08	0.04	1.35	0.34	0.02	0.08	0.00	ud	0.00	0.01
180	0.01	0.07	0.41	0.05	0.12	0.03	0.93	0.39	0.00	0.10	0.00	ud	0.00	0.01
184	0.01	0.14	0.08	0.04	0.17	0.04	1.20	0.52	0.01	0.13	0.00	ud	0.00	0.01
189	0.03	0.19	2.62	0.03	0.31	0.07	3.66	0.04	0.00	0.07	0.00	0.00	0.00	0.00
195	0.07	0.13	0.89	0.11	0.25	0.03	1.30	0.73	0.00	0.03	0.00	0.04	0.00	0.01
199	0.18	0.12	1.36	0.08	0.20	0.02	0.79	0.43	0.00	0.03	0.00	0.02	0.00	0.00
205	0.10	0.35	0.69	0.10	0.55	0.05	3.57	0.23	0.00	0.04	0.00	0.01	0.00	0.00
209	0.02	0.13	0.80	0.09	0.31	0.02	1.20	0.32	0.00	0.04	0.00	0.01	0.00	0.01
214	0.04	0.13	0.48	0.08	0.24	0.04	2.18	2.70	0.00	0.07	0.01	ud	0.00	0.02
219	0.01	0.03	0.39	0.17	0.06	0.00	0.14	0.74	0.00	0.02	0.01	0.01	0.00	0.00
219	0.01	0.03	0.40	0.17	0.05	0.00	0.14	0.74	0.00	0.02	0.01	0.01	0.00	0.00
226	0.01	0.08	10.44	0.14	0.24	0.02	1.64	1.23	0.00	0.04	0.00	0.00	0.00	0.01
229	0.02	0.14	1.17	0.26	0.62	0.04	3.16	2.91	0.00	0.04	0.00	0.01	0.00	0.00
234	0.03	0.27	1.14	0.07	0.33	0.01	1.92	0.28	0.00	0.03	0.00	ud	0.00	0.00
239	0.74	0.14	1.84	0.12	0.86	0.10	4.07	0.21	0.00	0.04	0.00	0.04	0.00	0.00
239	0.51	0.38	0.83	0.06	0.43	0.06	4.89	0.15	0.00	0.10	0.00	0.01	0.01	0.01

*The following cations were measured but no data is presented because all samples were <0.01 mg L^{-1},or undetected (ud); Sc, Ga, Ge, Y, Zr, Nb, Ho, Ag, Cd, Sn, Cs, La, Ce, Er, Pr, Nd, Sm, Eu, Gd, Tb, Tm, Dy, Yb, Lu, Hf, Ti, and Th.

APPENDIX B

Grain size distribution data

Grain Size Analysis			
Date:	20-May-14		Operator:
Client:	University of Saskatchewan		DA
Sample ID:	BIRI 3 149 23.7m		Checked By:
			AH

Soil Description:	
Shape:	
Specific Gravity:	2.65 (assumed)
Dispersion Device:	Mechanical stirring device (1 minute dispersion time)

Gravel	Coarse Sand	Medium Sand	Fine Sand	Silt	Clay
> 4.75 mm	2 to 4.75 mm	0.425 to 2 mm	0.075 to 0.425 mm	0.005 to 0.075 mm	<0.005 mm
0.0	0.0	4.5	30.8	40.3	24.4

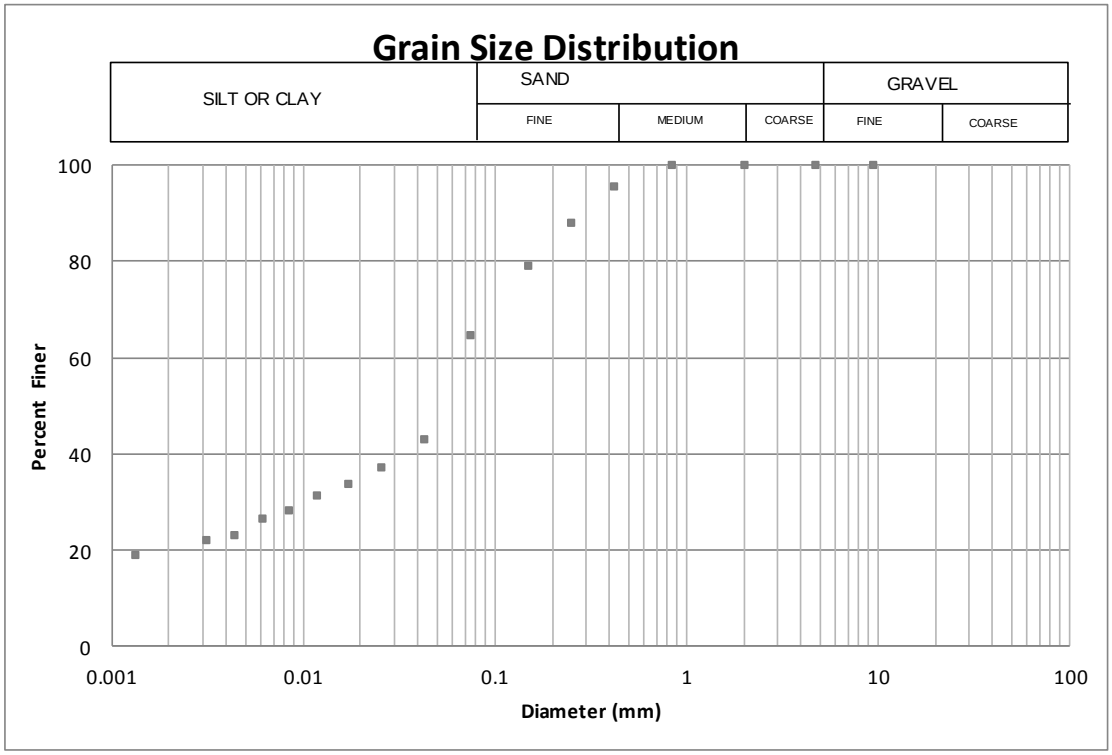

Notes:

Grain Size Analysis			
Date:	20-May-14		Operator:
Client:	University of Saskatchewan		DA
Sample ID:	BIRI 3 14 85.2m		Checked By:
			AH

Soil Description:	
Shape:	
Specific Gravity:	2.65 (assumed)
Dispersion Device:	Mechanical stirring device (1 minute dispersion time)

Gravel	Coarse Sand	Medium Sand	Fine Sand	Silt	Clay
> 4.75 mm	2 to 4.75 mm	0.425 to 2 mm	0.075 to 0.425 mm	0.005 to 0.075 mm	<0.005 mm
0.0	0.0	0.0	0.0	18.2	81.8

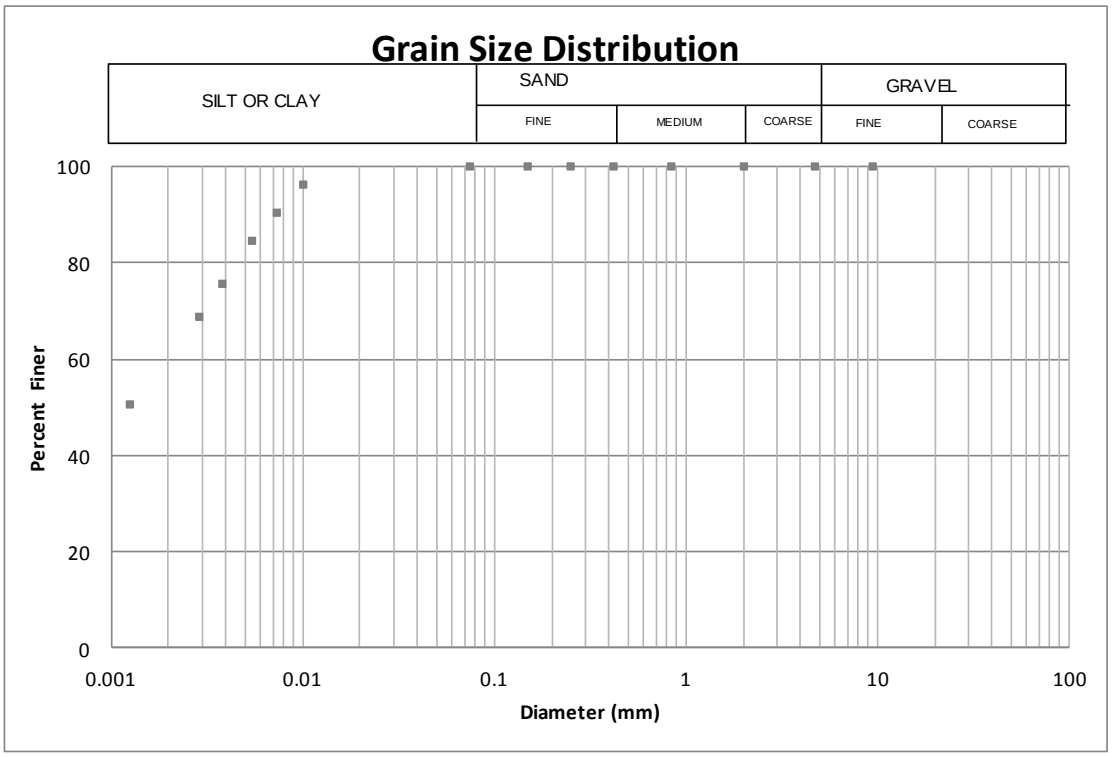

Notes:

Grain Size Analysis			
Date:	20-May-14		Operator:
Client:	University of Saskatchewan		DA
Sample ID:	BIRI 3 14 159.4m		Checked By:
			AH

Soil Description:	
Shape:	
Specific Gravity:	2.65 (assumed)
Dispersion Device:	Mechanical stirring device (1 minute dispersion time)

Gravel	Coarse Sand	Medium Sand	Fine Sand	Silt	Clay
> 4.75 mm	2 to 4.75 mm	0.425 to 2 mm	0.075 to 0.425 mm	0.005 to 0.075 mm	<0.005 mm
0.0	0.0	0.0	66.4	27.1	6.5

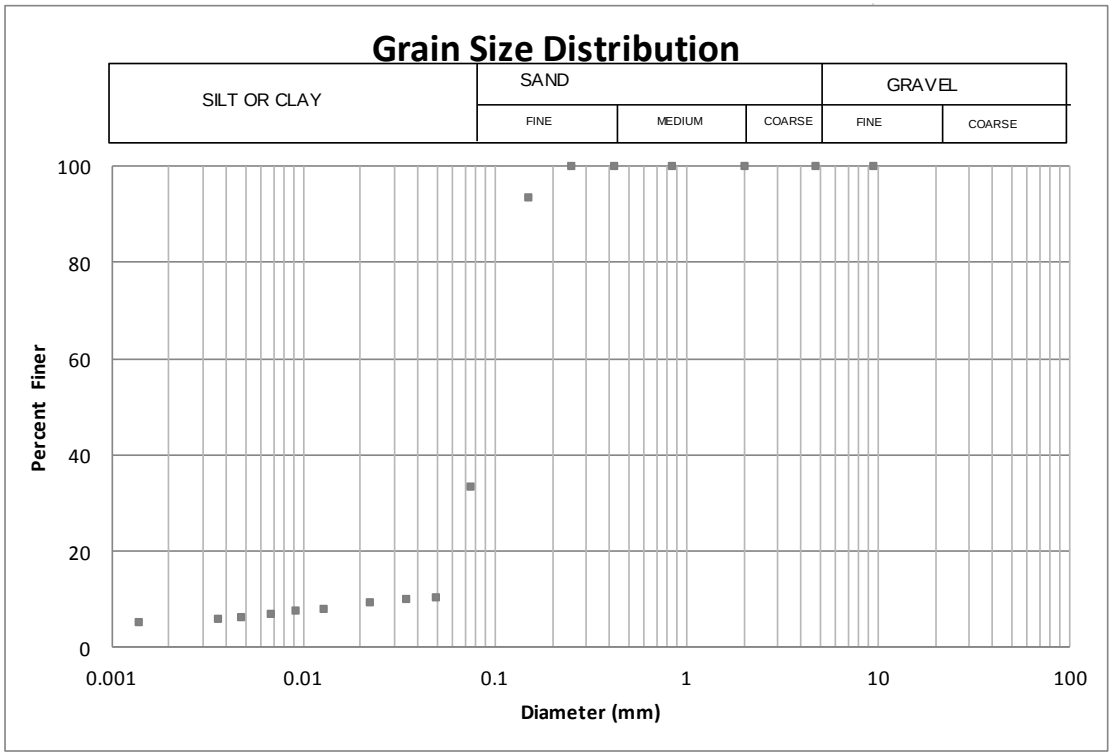

Notes:

Grain Size Analysis			
Date:	20-May-14		Operator:
Client:	University of Saskatchewan		DA
Sample ID:	BIRI 3 10 162.7m		Checked By:
			AH

Soil Description:	
Shape:	
Specific Gravity:	2.65 (assumed)
Dispersion Device:	Mechanical stirring device (1 minute dispersion time)

Gravel	Coarse Sand	Medium Sand	Fine Sand	Silt	Clay
> 4.75 mm	2 to 4.75 mm	0.425 to 2 mm	0.075 to 0.425 mm	0.005 to 0.075 mm	<0.005 mm
0.0	0.0	0.0	84.7	13.3	2.0

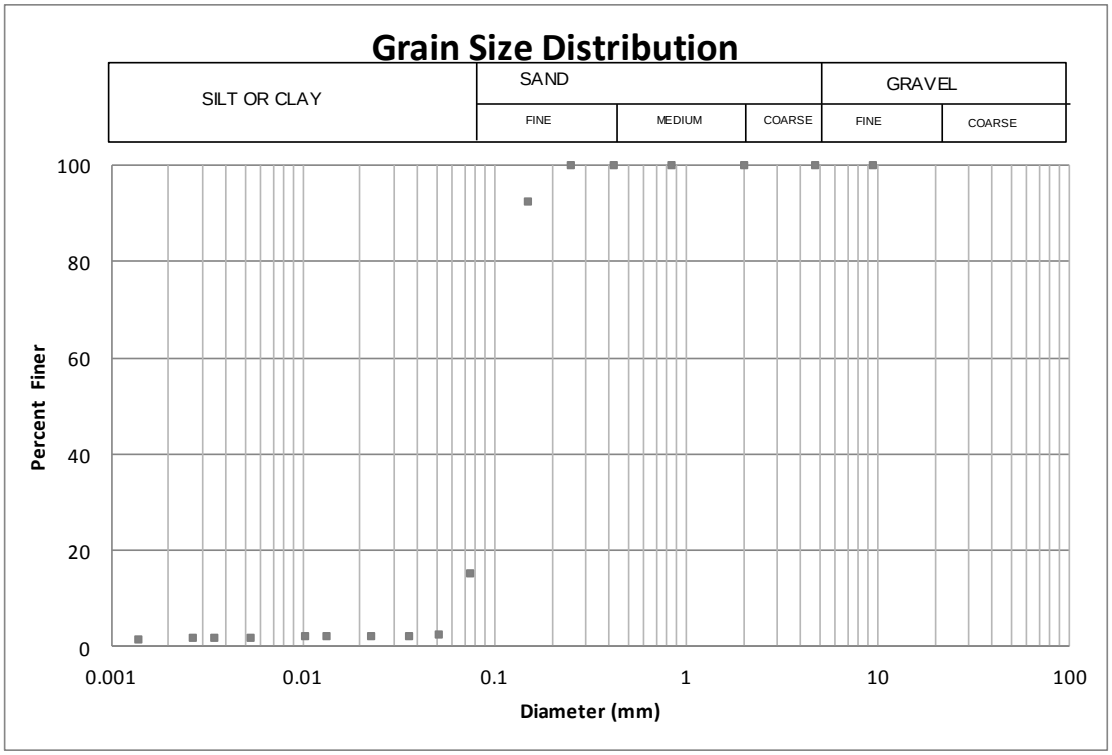

Notes:

Grain Size Analysis			
Date:	20-May-14		Operator:
Client:	University of Saskatchewan		DA
Sample ID:	BIRI 3 11 165.7m		Checked By:
			AH

Soil Description:	
Shape:	
Specific Gravity:	2.65 (assumed)
Dispersion Device:	Mechanical stirring device (1 minute dispersion time)

Gravel	Coarse Sand	Medium Sand	Fine Sand	Silt	Clay
> 4.75 mm	2 to 4.75 mm	0.425 to 2 mm	0.075 to 0.425 mm	0.005 to 0.075 mm	<0.005 mm
0.0	0.0	0.0	93.0	6.5	0.5

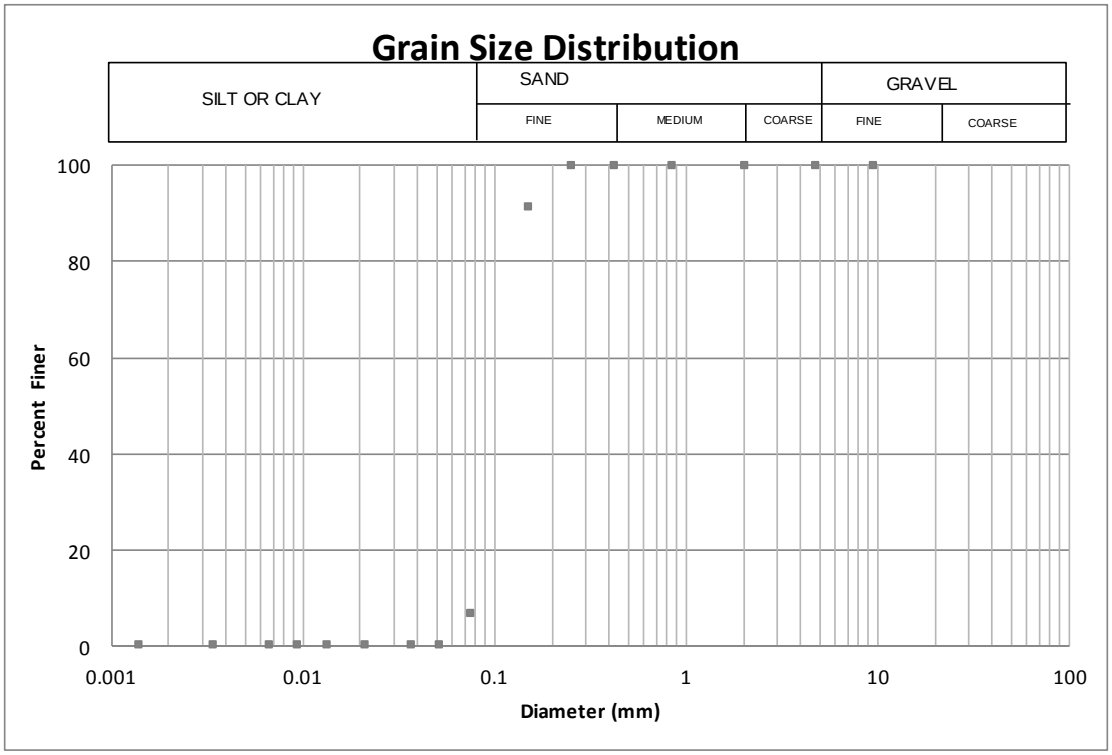

Notes:

Grain Size Analysis			
Date:	20-May-14		Operator:
Client:	University of Saskatchewan		DA
Sample ID:	BIRI 3 at 174.7m		Checked By:
			AH

Soil Description:	
Shape:	
Specific Gravity:	2.65 (assumed)
Dispersion Device:	Mechanical stirring device (1 minute dispersion time)

Gravel	Coarse Sand	Medium Sand	Fine Sand	Silt	Clay
> 4.75 mm	2 to 4.75 mm	0.425 to 2 mm	0.075 to 0.425 mm	0.005 to 0.075 mm	<0.005 mm
0.0	0.0	0.0	51.1	40.0	8.9

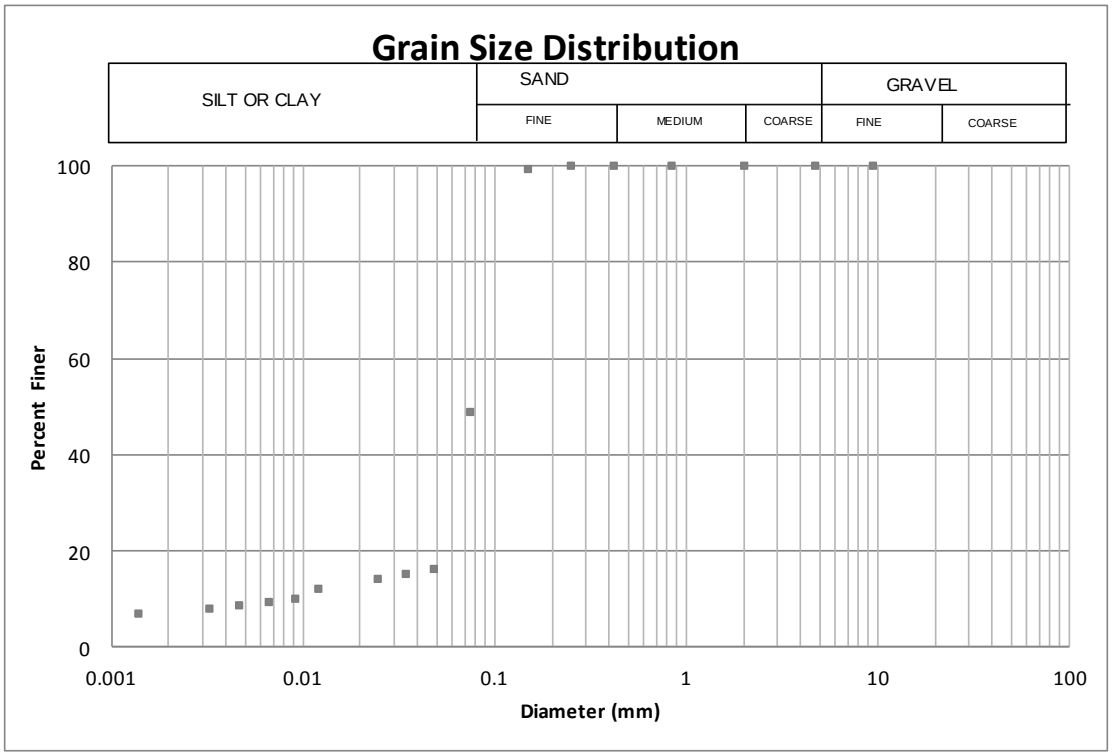

Notes:

Grain Size Analysis			
Date:	20-May-14		Operator:
Client:	University of Saskatchewan		DA
Sample ID:	BIRI 3 at 206.7m		Checked By:
			AH

Soil Description:	
Shape:	
Specific Gravity:	2.65 (assumed)
Dispersion Device:	Mechanical stirring device (1 minute dispersion time)

Gravel	Coarse Sand	Medium Sand	Fine Sand	Silt	Clay
> 4.75 mm	2 to 4.75 mm	0.425 to 2 mm	0.075 to 0.425 mm	0.005 to 0.075 mm	<0.005 mm
0.0	0.0	0.0	3.2	76.3	20.5

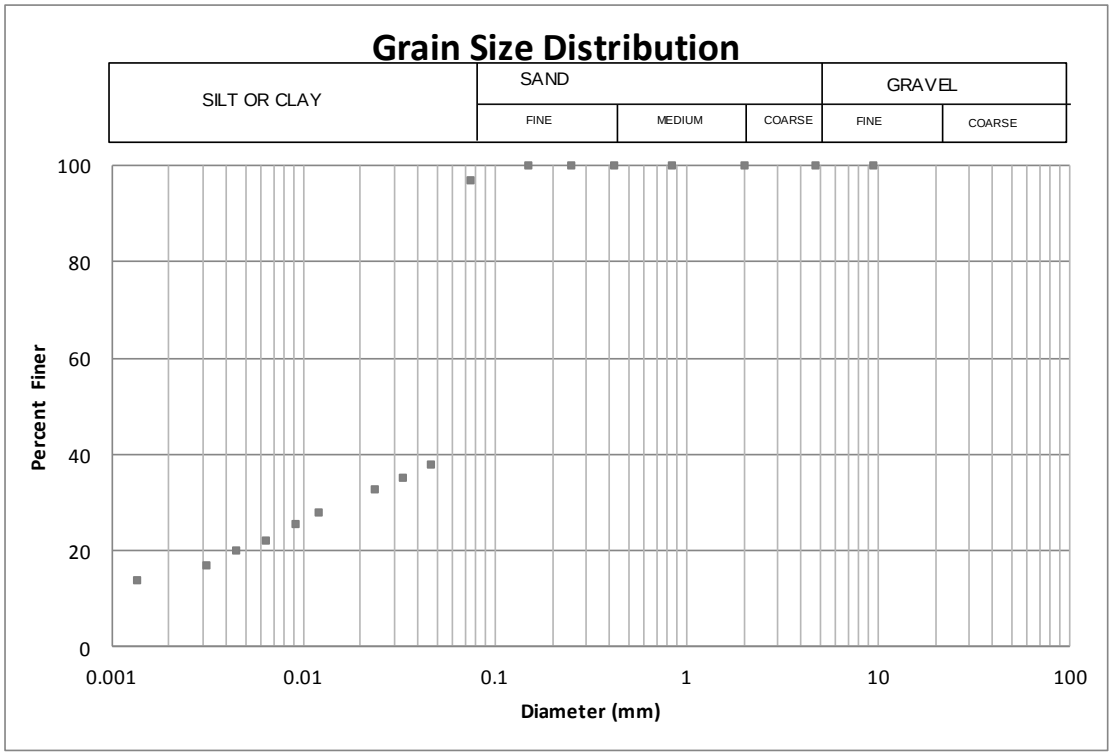

Notes:

Grain Size Analysis			
Date:	20-May-14		Operator:
Client:	University of Saskatchewan		DA
Sample ID:	BIRI 3 at 212.7m		Checked By:
			AH

Soil Description:	
Shape:	
Specific Gravity:	2.65 (assumed)
Dispersion Device:	Mechanical stirring device (1 minute dispersion time)

Gravel	Coarse Sand	Medium Sand	Fine Sand	Silt	Clay
> 4.75 mm	2 to 4.75 mm	0.425 to 2 mm	0.075 to 0.425 mm	0.005 to 0.075 mm	<0.005 mm
0.0	0.0	0.0	7.1	62.3	30.6

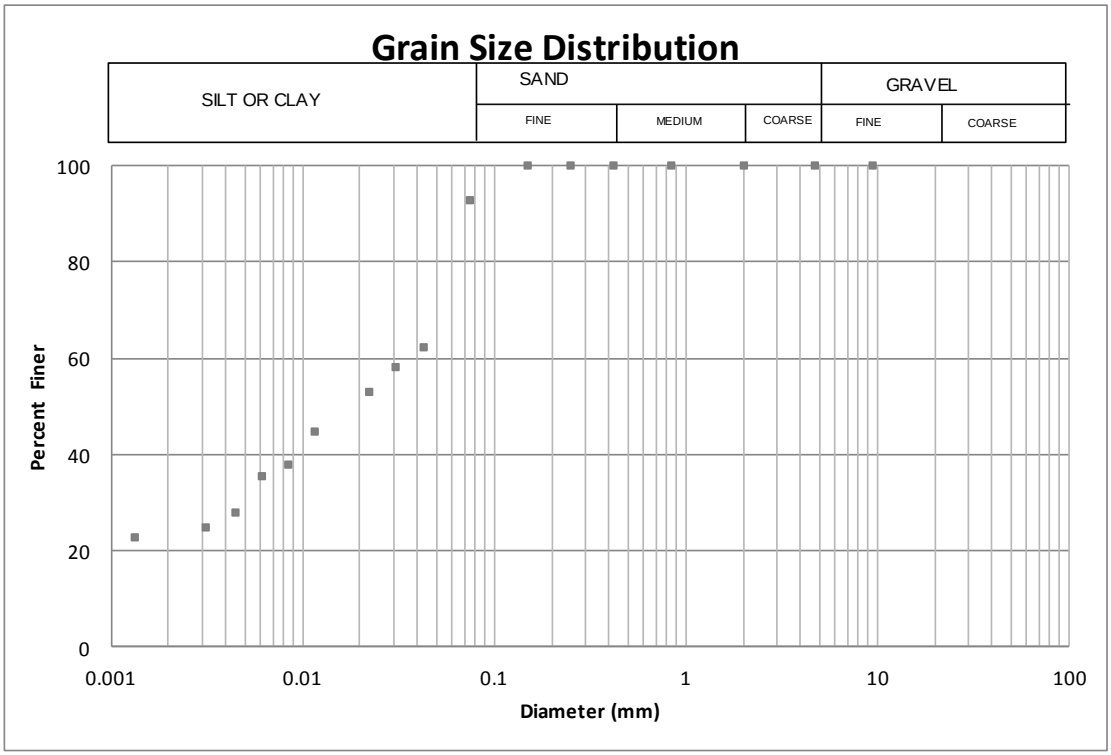

Notes:

Table B1. Grain size distribution data measured on the 2013 King site core samples via the particle size analyzer method.

Depth (m BGS)	**% Gravel** (2-4.75mm)	**% Sand** (0.075-2mm)	**% Silt** (0.005-0.075mm)	**% Clay** (<0.005mm)	**Depth** (m BGS)	**% Gravel** (2-4.75mm)	**% Sand** (0.075-2mm)	**% Silt** (0.005-0.075mm)	**% Clay** (<0.005mm)
6	0	40	43	17	63	3	52	23	22
13	0	32	46	22	69	0	79	11	11
15	1	34	42	23	69	0	58	21	22
16	0	27	48	25	74	6	43	33	18
17	6	26	47	21	83	0	0	11	89
18	0	30	44	26	86	0	0	21	79
19	0	30	41	29	93	0	0	40	60
20	13	27	41	19	99	0	0	38	62
23	12	31	38	19	103	0	0	32	68
24	6	31	39	24	109	0	0	48	52
25	0	32	46	22	113	0	0	21	79
26	3	32	43	23	120	0	0	43	57
30	2	33	36	29	129	0	0	27	72
31	0	23	47	30	130	0	0	33	67
32	0	22	55	23	135	0	0	29	71
36	2	27	50	22	137	0	0	43	57
37	2	32	44	22	150	0	0	20	80
41	0	28	46	27	160	0	73	24	3
42	4	27	48	21	160	0	48	40	11
43	3	25	47	24	161	0	73	23	4
45	3	33	44	20	164	0	81	17	2
48	0	30	46	24	166	0	53	37	10
49	0	30	45	25	167	0	53	37	11
51	0	19	54	27	168	0	73	25	2
59	1	59	21	18	168	0	48	41	11

Table B1. Grain size distribution data measured on the 2013 King site core samples via the particle size analyzer method continued.

Depth (m BGS)	% Gravel (2-4.75mm)	% Sand (0.075-2mm)	% Silt (0.005-0.075mm)	% Clay (<0.005mm)	Depth (m BGS)	% Gravel (2-4.75mm)	% Sand (0.075-2mm)	% Silt (0.005-0.075mm)	% Clay (<0.005mm)
169	0	46	43	12	186	0	38	53	9
170	0	50	38	12	187	0	43	48	9
171	0	58	32	10	189	0	32	61	7
172	0	51	38	11	190	0	29	58	13
174	0	51	39	9	191	0	35	54	10
174	0	46	42	12	192	0	23	63	14
175	0	55	35	10	193	0	32	56	13
176	0	46	42	13	194	0	44	47	9
177	0	34	43	23	195	0	31	65	5
178	0	56	35	9	195	0	33	56	11
180	0	52	39	9	196	0	42	47	11
182	0	57	36	8	197	0	33	54	12
183	0	53	38	10	198	0	36	54	10
184	0	37	57	6	199	0	36	54	10
184	0	44	46	9	229	0	13	64	24
185	0	38	52	10	238	0	40	39	21

Table B2. Grain size distribution data measured on the 2013 King site core samples via the hydrometer method at the Cameco Chair Geochemistry Laboratory.

Depth (m BGS)	% Gravel (2-4.75mm)	% Sand (0.075-2mm)	% Silt (0.005-0.075mm)	% Clay (<0.005mm)	Depth (m BGS)	% Gravel (2-4.75mm)	% Sand (0.075-2mm)	% Silt (0.005-0.075mm)	% Clay (<0.005mm)
59	1	59	22	18	86	0	0	18	82
63	3	52	25	20	104	0	0	37	63
69	0	79	12	10	121	0	4	27	73
74	6	43	28	23	145	0	4	25	75

APPENDIX C

Dissolved CO_2 data

measured on IsoJar® samples

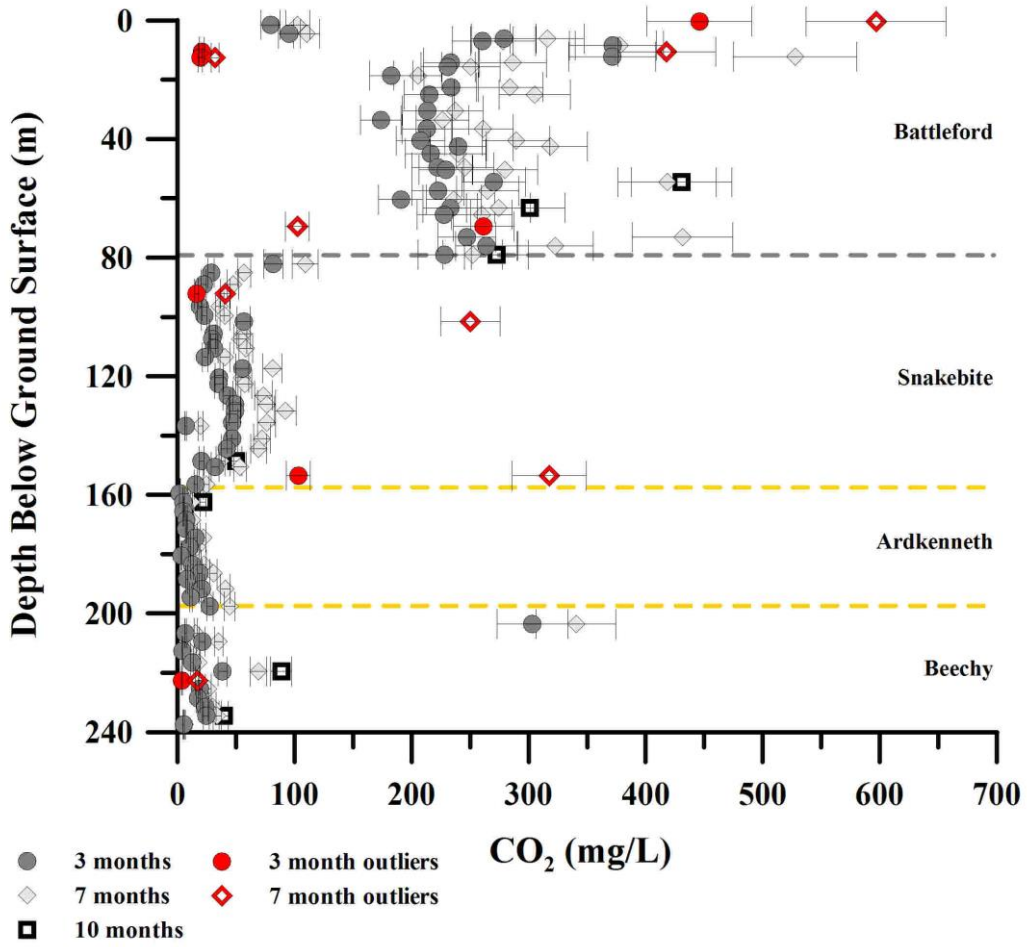

Figure C1. Dissolved CO_2 concentrations of core samples collected at the King site in 2013 versus depth measured at three, seven, and 10 months post-collection.

Table C1. The μ, minimum, and maximum of CO_2 concentrations measured on core samples collected at the King site in 2013. Results of the three month measurements are presented only. Values were converted from headspace concentration to pore water concentration (mg L^{-1}) by the method described in Section 3.4.1.

Formation	n	μ CO_2 (mg L^{-1})*	Min CO_2 (mg L^{-1})*	Max CO_2 (mg L^{-1})*
Battleford	26	226.52	79.49	371.78
Snakebite	24	45.37	6.94	263.91
Ardkenneth	14	11.12	1.71	27.78
Beechy	11	43.35	4.30	303.14

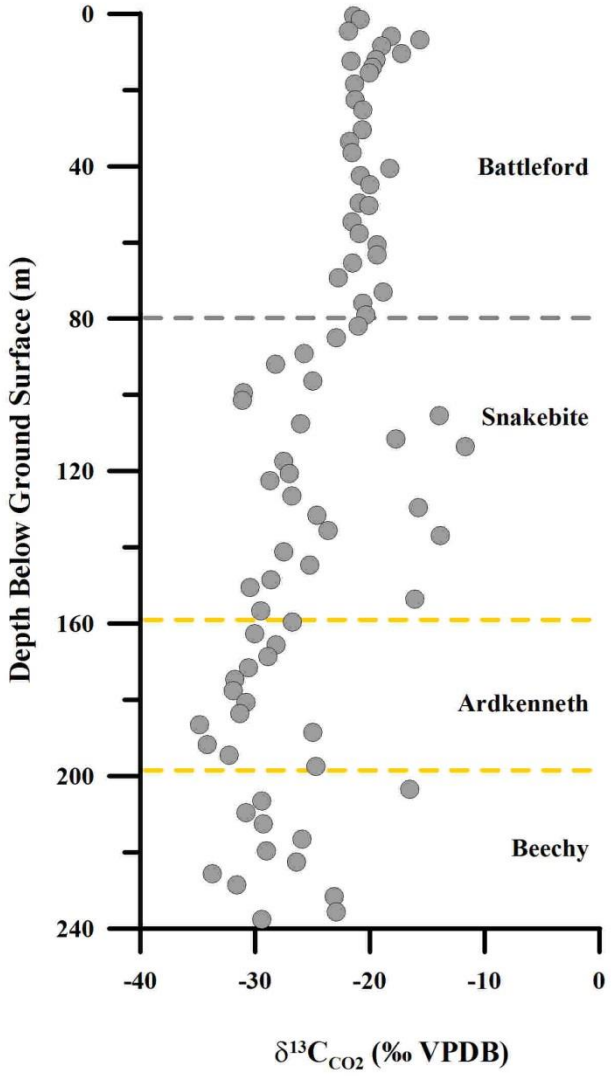

Figure C2. The $\delta^{13}C_{CO2}$ values of core samples collected at the King site in 2013 versus depth.

Table C2. The μ, minimum, and maximum of the $\delta^{13}C_{CO2}$ values measured on core samples collected at the King site in 2013.

Formation	n	μ $\delta^{13}C_{CO2}$ (‰ VPDB)	Min $\delta^{13}C_{CO2}$ (‰ VPDB)	Max $\delta^{13}C_{CO2}$ (‰ VPDB)
Battleford	31	-20.2	-22.7	-15.6
Snakebite	25	-24.0	-31.1	-11.7
Ardkenneth	14	-30.1	-34.8	-24.7
Beechy	12	-27.3	-33.7	-16.5